INSTITUTO POLITÉCNICO DE BRAGANÇA
Escola Superior de Tecnologia e Gestão

Preparation and Ionic Transport Properties of Conductive Polymers for Dye-Sensitized Solar Cells

Amir Bzainia

Thesis report submitted to the **Escola Superior de Tecnologia e Gestão – Instituto Politécnico de Bragança** to the Fulfillment of the Requirements for the Master's Degree in **Chemical Engineering** in the joint double diploma with the **Institut Supérieur Privé Polytechnique – Université Libre de Tunis**

Supervised by:

Dr. Rolando Carlos Pereira Simões Dias (IPB)

Dr. Mohamed Mezni (ULT)

July 2019

Bragança, Portugal

Abstract

This work aims to improve the components of the dye-sensitized solar cells (DSSCs) which are a type of photovoltaics that consist mainly of a photoanode, a counter electrode, a light sensitive molecule (sensitizer) and an electrolyte solution that regenerates the solar cell through a redox system. The improvement of the DSSC focuses on the material used for the counter electrode. Usually, it is made out from platinum sputtered on a conductive glass. However, platinum is an expensive metal that is hard to manipulate and can be corroded by the mediator. In this perspective, an alternative material for the expensive platinum is investigated which is the conductive polymer poly(3,4-ethylenedioxythiophene) (PEDOT). This polymer has a structure that promotes high ionic and electronic conductivities, and it can be doped with different anions (e.g. PSS, perchlorate). PEDOT was synthesized chemically and electrochemically. Its chemical structure was characterized by FTIR. The electrochemical behavior of PEDOT was assessed by cyclic voltammetry (CV). The catalytic activity of PEDOT towards the redox system proved to be higher than the activity of the platinum. In addition to the experimental approach, modelling of the ionic-electronic conductivity of PEDOT was performed based on the Nernst-Planck-Poisson and the Butler-Volmer formalisms, and the simulation outputs were fitted to the experimental data. In the last step, the conductive polymer PEDOT was used as a counter electrode to fabricate DSSCs. The cells were characterized through electrochemical impedance spectroscopy (EIS) and through current-voltage (J-V) curves. The based PEDOT cells demonstrated an efficiency of 8.1%, which was higher than the based-platinum solar cells (6.3%).

Keywords: Conductive polymers; Dye-sensitized solar cells; Cylic voltammetry; Nernst-Planck-Poisson equations.

Résumé

Ce travail vise à améliorer les composants des cellules solaires à pigment photo-sensibles (en anglais dye-sensiztized solar cells, DSSCs). Ce type de cellule photovoltaïque se compose principalement d'une photoanode, d'une contre électrode, d'une molécule sensible à la lumière (pigment) et d'une solution électrolyte qui régénère la cellule solaire à travers un système redox. L'amélioration de la DSSC se concentre sur le matériau utilisé dans la contre électrode. Généralement, cette dernière est faite de platine déposé sur un verre conducteur. Cependant, le platine est un métal coûteux qui est difficile à manipuler et peut être corrodé par le couple redox. Dans cette perspective, un matériau alternatif pour le platine est étudié et qui s'agit du polymère conducteur (3,4-éthylènedioxythiophène) (PEDOT). Ce polymère a une structure qui favorise la conductivité ionique et électronique, et il peut être dopé avec des anions différents (par exemple PSS, perchlorate). Le PEDOT a été synthétisé par la voie chimique ainsi que la voie électrochimique. Sa structure chimique a été caractérisée par FTIR. Le comportement électrochimique du PEDOT a été évalué par la voltamétrie cyclique (CV). L'activité catalytique du PEDOT vis-à-vis du système redox s'est avérée plus élevée que celle du platine. En plus de l'approche expérimentale, la modélisation de la conductivité ionique et électronique du PEDOT a été réalisée en se basant sur les formalismes de Nernst-Planck-Poisson et de Butler-Volmer. Les résultats de la simulation ont été ajustés aux données expérimentales. Dans la dernière étape, le polymère conducteur PEDOT a été utilisé comme une contre électrode pour fabriquer des DSSCs. Les cellules ont été caractérisées par la spectroscopie d'impédance électrochimique (EIS) et par les courbes de courant-tension (J-V). Les cellules à base de PEDOT ont montré une efficacité de 8,1 %, ce qui était plus élevé que les cellules solaires à base de platine (6,3 %).

Mots-clés: Polymères conducteurs; Cellules solaires à pigment photo-sensibles; Voltamétrie cylique; Équations de Nernst-Planck-Poisson.

Resumo

Este trabalho visa melhorar os componentes das células solares sensíveis ao corante (DSSCs) que são um tipo de células fotovoltaicas que consistem principalmente em um foto-ânodo, um contra elétrodo, uma molécula sensível à luz (sensibilizante) e uma solução de eletrólitos que regenera a célula solar através de um sistema redox. A melhoria da DSSC centra-se no material usado para o contra elétrodo. O contra elétrodo é geralmente preparado através da deposição de uma camada fina de platina na superfície de um substrato de vidro condutor. No entanto, a platina é um metal caro que é difícil de manipular, pode ser corroído pelo redox e nessa perspetiva, materiais alternativos (polímeros condutores, grafite, nanotubos de carbono…) para a substituição da platina têm vindo a ser investigados. Nesta investigação foi escolhido o polímero condutor poli (3,4-etilenodioxitiofeno) (PEDOT) para substituir a platina na preparação do contra elétrodo. Este polímero possui uma estrutura que promove altas condutividades iônicas e eletrônicas, podendo ser dopado com diferentes aniões (por exemplo, PSS, perclorato). O PEDOT foi sintetizado quimicamente e electroquimicamente, a sua estrutura química foi caracterizada por espectroscopia de infravermelhos (FTIR) e o comportamento eletroquímico do PEDOT foi avaliado através de voltamétrica cíclica (CV). A atividade catalítica de PEDOT para o sistema redox provou ser maior do que a atividade da platina. Além da abordagem experimental, a modelagem da condutividade iônica-eletrônica do PEDOT foi realizada com base nos formalismos de Nernst-Planck-Poisson e Butler-Volmer, e os resultados da simulação foram ajustados aos dados experimentais. Na última etapa, o polímero condutor PEDOT foi usado como um contra elétrodo para fabricar DSSCs. As células foram caracterizadas por espectroscopia de impedância eletroquímica (EIS) e por curvas de corrente-tensão (J-V) e os resultados obtidos mostram que as DSSCs fabricadas, usando PEDOT como base apresentam uma eficiência de 8,1%, maior do que as células solares baseadas em platina de 6,3%.

Palavras-chave: Polímeros condutores; células solares sensíveis a corantes; Voltamétrica cíclica; Equações de Nernst-Planck-Poisson.

ملخّص

يهدف هذا العمل إلى تحسين مكونات الخلايا الشمسية الصبغية (DSSCs) والتي تعد نوعًا من الخلايا الكهروضوئية التّي تتكون أساسًا من مصعد (أنود)، مهبط (كتود)، صباغ حساس للضوء ومحلول إلكتروليتي لإعادة توليد الخلايا الشمسية من خلال نظام الأكسدة. يركز تحسين الخلايا على المواد المستخدمة في المهبط (كتود)، و الذّي عادةً ما يتم تصنيعه من البلاتين الموضوع على زجاج ناقل للكهرباء. يعد البلاتين معدنًا مكلفًا يصعب معالجته ويمكن تآكله بواسطة الإلكتروليت. لذا، تمت دراسة مادة بديلة للبلاتين باهظ الثمن وهي مبلمر موصل (4.3-إيتيلين ديوكسي تيوفين) (PEDOT). يحتوي هذا المبلمر على هيكل يعززبصفة عالية التوصيلات الأيونية والإلكترونية، ويمكن إشابته بأنيونات مختلفة. تمّ تصنيع PEDOT كيميائيا وكهربائيا ثمّ تشخيصه بواسطةFTIR لمعرفة تركيبته الكيميائية. تمّ تقييم السلوك الكهروكيميائي لـ PEDOT بواسطة قياس الجهد الدوري. تمّ إثبات أنّ النشاط التحفيزي لـ PEDOT تجاه نظام الأكسدة أعلى من نشاط البلاتين. بالإضافة إلى المنهج التجريبي، تمّ نمذجة التوصيلية الأيونية الإلكترونية لـ PEDOT استنادًا على معادلات نرست-بلانك-بواسون وبتلر- فلمر، وتمّ مقارنة النتائج التجريبية بنتائج المحاكاة. أخيرا، تمّ استخدام هذا المبلمر الموصل كمهبط (كتود) لتصنيع خلايا شمسية صبغية. تمّ تقييم الخلايا من خلال مطيافية المعاوقة الكهروكيميائية (EIS) ومن خلال منحنيات التيار-توتر (J-V) . أظهرت الخلايا القائمة على PEDOT كفاءة 8.1 ٪، والتي كانت أعلى من الخلايا الشمسية القائمة على البلاتين (6.3 ٪).

الكلمات المفاتيح: المبلمرات الموصلة، الخلايا الشمسية الصبغية، الجهد الكهربائي الدوري، معادلات نرست-بلانك-بواسون.

Acknowledgments

First and foremost, I am grateful to my supervisor Rolando Carlos Pereira Simões Dias, not only for his huge help in this work but also for his inspiring, encouraging, and supporting personality. He was always willing to give me advice and guide me in my research. Working with him has been a great honor, and I will always consider myself lucky that I had him as an advisor. I am also very thankful to Catarina Pereira Gomes, for her kindness and exciting personality, she was always willing to help, give advice and share a laugh. Also, I am grateful to my supervisor Mohamed Mezni for his valuable aid. Working in the CIMO-LSRE has been a wonderful experience due to the great people in this laboratory, Helder, Mohsen, Diana, Maria, Stephany and of course the awesome person Nadia Pilipenko. I am thankful to all for making this research possible and for the great atmosphere you created.

I would like to thank collaborators from Porto University, for giving me the opportunity to fabricate the solar cells, and especially Carolina Sofia Hora for the effort and time that she dedicated to this work and for her insightful explanations.

Without funding, however I would not have the opportunity to accomplish this work. I gratefully acknowledge funding form the project "AIProcMat@N2020-Advanced Industrial Processes and Materials for a Sustainable Northern Region of Portugal 2020", with the reference NORTE-01-0145-FEDER-000006, supported by "Norte Portugal Regional Operational Programa" (NORTE 2020), under the Portugal 2020 Partnership Agreement, through the European Regional Development Fund (ERDF) and of Project POCI-01-0145-FEDER-006984-Associate Laboratory LSRE-LCM funded by ERDF through COMPETE2020-Programa Operacional Competitividade e Internacionalização (POCI) and by national funds through FCT-Fundação para a Ciência e a Tecnologia.

Of course, none of this could happen without the support and the unconditional love of my adorable family. I am grateful for my beloved mother Monia, for giving me hope and filling me with strength in every step of this work, my great father Hassen for his trust, encouragement and advices in all the steps of my life, my little brother Oussema for his support and for believing in me. Thank you for being there for me, thank you for helping me achieve my dreams !

Contents

List of figures

List of tables

Preface

Energy: it is the word that we hear the most in this era. It has made some countries rise and others fall, it's causing conflicts and wars between nations. This is due to the limited resources that we possess on earth and it is evident that soon we will drain it all. For these reasons, it is compulsory that we switch our view to new energy resources if we wish to maintain a habitable planet. Renewable energy seems to be the answer for the problem, since the renewables are non-exhausting energies that can be used without negatively impacting the environment.

Among these renewables, solar energy appears to be a strong candidate that promises a sustainable and unlimited source of energy (at least for another 5 billion years). Therefore, we use solar cells for the harvesting of the sunlight. They are relatively new devices that can harness sunlight and transform it into electricity. Consequently, solar cells have become the trending subject of many laboratory researches and scientific publications throughout the world.

With that said, we also dive into this subject by treating a specific technology of solar cells named the dye-sensitized-solar-cells (DSSCs) which are a type of photovoltaics that consist mainly of a photoanode, a counter electrode (made of platinum), a light sensitive molecule (sensitizer) and an electrolyte solution that regenerates the solar cell through a redox system. The aim of this work is to utilize the conductive polymer, poly(3,4-ethylenedioxythiophene) (PEDOT) as a substitute for the classically employed platinum in the counter electrode. This choice of PEDOT was based on its mixed ionic-electronic conductivity which is adequate for the DSSCs since they employ an electrolyte as a mediator.

This work is intended to pave the way into this area and give a brief explanation about the different aspects of the conductive polymer PEDOT. Thus, the thesis is organized into six chapters:

Chapter 1 starts with the introduction of the DSSC technology and its main principles. Then some basic chemistry of the conductive polymer PEDOT is given. Finally, a non-

exhaustive review of the state of the art related to the dye-sensitized solar cells based on the conductive polymer PEDOT is made.

Chapter 2 deals with the electrochemical properties of PEDOT, mainly its capacitive behavior revealed by cyclic voltammetry and its relation to the ionic-electronic conductivity of the polymer.

Chapter 3 studies the influence of the used salts on the electro-polymerization of PEDOT. A discussion about the ionic nature of these salts and how they impact the kinetics of the polymerization is made. In addition, the catalytic activity of PEDOT towards the redox system of triiodide-iodide is compared to that of the platinum material.

Chapter 4 examines the ionic-electronic conductivity of PEDOT through modelling approaches by comparing the simulation outputs to the experimental results. This chapter discusses in detail the equations used in the model and the influence of the modelling parameters on the fitting of the experimental data.

Chapter 5 demonstrates the utilization of the conductive polymer PEDOT in the fabrication of dye-sensitized solar cells (DSSCs). The techniques used for their assessments are thoroughly explained and the results obtained are compared to the based platinum DSSC.

Finally, some key points in this thesis have been selected and addressed in the general conclusion, as well as some future perspectives based on this work are suggested.

Chapter 1: Bibliographical review

1.1 Dye-sensitized solar cell

Solar cells can be classified into three different classes depending on the materials and technology used. The first generation is based entirely on the silicon, whereas the second generation relies on thin film technologies, including amorphous silicon, copper indium gallium selenide (CIGS) and cadmium telluride (CdTe) based devices.

The third generation uses novel physical phenomena, materials and structures. Currently, the third generation solar cells mostly include dye-sensitized-solar-cells (DSSCs), organic/polymer solar cells (OSCs), perovskite solar cells (PSCs), and quantum dot (QD) based solar cells **[1.1]**. Energetically speaking, the third generation is a breakthrough in the photovoltaics as it promises to surpass the *Shockley and Queisser* limit of 31% efficiency **[1.2]** which is a limit for the two previous generations that couldn't be exceeded.

Among the latest generation of solar cells, the dye-sensitized-solar-cell (DSSC) has drawn a lot of attention since its emergence from the works of Michael Grätzel in 1991. Its pioneering research led to a jump in power conversion efficiency from 1% to 7% **[1.3]**. In contrast to the traditional photovoltaic devices where a semiconductor carries out both tasks of light absorption and charge transport, in the DSSC these two functions are separated. They are assigned to a sensitizer that absorbs light and a wide band gap semiconductor to separate charges **[1.4]**. Another advantage of this technology is the cheap cost of the materials used in the fabrication process, and it doesn't demand a high purity of reagents **[1.1]**.

1.2 Components of the DSSC

The general architecture of a DSSC comprises a transparent photoanode, an electrolyte solution and a counter electrode, all assembled in series. The photoanode is a three-layered electrode: it is the junction of a large band gap semiconductor (e.g. TiO2) deposited on a transparent conducting oxide (e.g. Fluorine tin oxide) and sensitized with

a dye. The electrolyte solution, containing the redox system (e.g. I_3^-/I^-), is placed between the photoanode and the counter electrode **[1.5].** The DSSC is illustrated by the Figure 1.1.

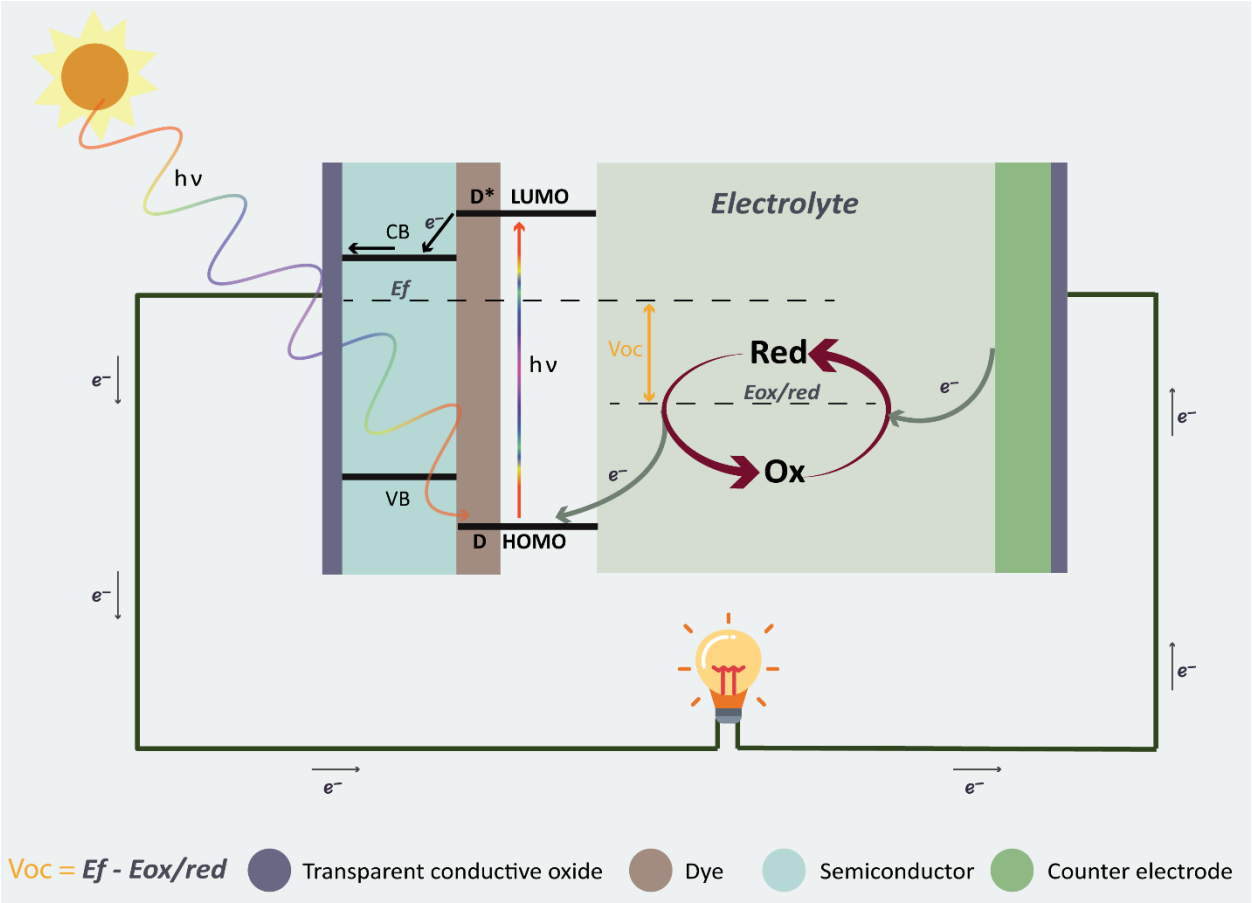

Figure 1.1 Schematic of the dye-sensitized-solar-cell.

1.3 Operating principles of the DSSC

The dye (sensitizer) is photo excited by light, which results in the promotion of an electron from the HOMO level of the dye to its LUMO level. The excited electron is injected into the conduction band of the semiconductor **[1.5]**.

At this stage, the dye is at an oxidized form. To reestablish its neutral state, the dye gains an electron from the electrolyte. The regeneration of the dye is possible by the oxidation of the redox couple. The return of the dye to the ground state is a crucial step because it forbids it from recapturing the excited electron intended to be injected into the conduction band of the semiconductor. As a result, the redox couple is oxidized, and needs also to be regenerated. This is made possible by the reduction at the counter electrode using the electron that migrated through the external load and came back to

the counter electrode **[1.4] [1.6].** The previous passage can be summarized in the following equations that describe a DSSC:

$D + h\nu \rightarrow D^*$ *: Dye excitation* ***(1)***

$D^* + SC \rightarrow D^+ + e^-{}_{CB}\,(SC)$ *: Injection of an electron into the semiconductor (SC)* ***(2)***

$D^* \rightarrow D$ *: Relaxation of the excited dye* ***(2')***

$D^+ + Red \rightarrow D + Ox$ *: Dye regeneration* ***(3)***

$D^+ + e^-{}_{CB}\,(SC) \rightarrow D + SC$ *: Capture of the excited electron by the oxidized dye* ***(3')***

$Ox + n\,e^- \rightarrow Red$ *: Reduction of the redox couple* ***(4)***

$Ox + e^-{}_{CB}\,(SC) \rightarrow D + SC$*: Capture of the excited electron by the oxidized redox couple* ***(4')***

It is important to know that the voltage generated by the cell corresponds to the Nernst potential of the redox couple and the Fermi level of the semiconductor **[1.3]**. This voltage is decreased because of "parasite reactions" that tend to lower the overall current production of the cell. These reactions are demonstrated by the equations ***(2', 3', 4')***: Relaxation of the excited dye, recapture of the excited electron by the oxidized dye or/and the redox couple. The voltage loss is a big hindrance for the power conversion efficiency of the solar cell **[1.7]**, yet it can be overcome by modulating the energy levels of the redox mediator and the sensitizer. For instance, the electron donor in the electrolyte can intercept the recapture of the injected electron: the reduced redox couple reacts with the oxidized dye and thus prevents it from recapturing the injected electron lying on the conduction band of the semiconductor **[1.8]**. Another possibility for the increase of the solar efficiency, is to have a sensitizer that possess an excited state with a barely higher energy than the conduction band of the semiconductor **[1.5]**.

1.4 Solar cell efficiencies

Since solar cells are so diversified, the necessity to establish some parameters is critical to facilitate the evaluation and comparison of a technology to another. These parameters are briefly explained **[1.9]:**

- Short circuit current density (J_{sc}): Density of current measured when the terminals of the solar cell are connected to each other (zero load resistance).

- Open circuit voltage (V_{oc}): It is the maximum voltage that could be generated by the solar cell when the net current through the device is zero.
- Fill factor (FF): It is the ratio of the maximum available power of the solar cell (P_{max}) to the product of V_{oc} and J_{sc}.

$$FF = \frac{P_{max}}{J_{sc}\ \ V_{oc}}$$

- Efficiency (η): It is the ratio of the maximum power of the solar cell (P_{max}) to the incident light power (P_{irr}).

$$\eta = \frac{P_{max}}{P_{irr}} \times 100$$

Table 1.1 displays different efficiencies of different technologies of solar cells (data from the year 2018) **[1.10]**:

Table 1.1 Efficiencies of different technologies of solar cells.

Class	η (%)	Voc (V)	Jsc (mA/cm^2)	Fill Factor (%)	Reference
Si (crystalline cell)	26.7 ± 0.5	0.738	42.65	84.9	**[1.11]**
GaAs (thin film cell)	29.1 ± 0.6	1.127	29.78	86.7	**[1.12]**
CIGS	22.9 ± 0.5	0.744	38.77	79.5	**[1.13]**
CdTe	21.0 ± 0.4	0.875	30.25	79.4	**[1.14]**
Si (amorphous cell)	10.2 ± 0.3	0.896	16.36	69.8	**[1.15]**
Perovskite	20.9 ± 0.7	1.125	24.92	74.5	**[1.16]**
DSSC	11.9 ± 0.4	0.744	22.47	71.2	**[1.17]**
Organic	11.2 ± 0.3	0.780	19.30	74.2	**[1.18]**

1.5 Conductive polymer as a counter electrode

As seen in the previous sections, the dye-sensitized solar cell is mainly composed of a photoanode, an electrolyte solution and a cathode (counter electrode). The latter one is the main theme of this work and it exhibits two main tasks:

- ✓ As a catalyst: the oxidized redox couple is reduced by accepting electrons at the surface of the counter electrode thus allowing the regeneration of the sensitizer (dye) after electron injection **[1.19]**.
- ✓ As a positive electrode: it collects the electrons from the external circuit and transmits them into the cell **[1.19]**.

Typically, the counter electrode in the DSSCs is formed by a transparent conductive oxide as in the case of the doped tin oxide covered with adhered platinum particles. Here the platinum particles catalyze the reaction of the redox's reduction at the cathode's surface. The same catalytic effect was found when a layer of poly(3,4-ethylenedioxythiophene) (PEDOT) deposited onto the transparent conductive oxide is used as counter electrode, and as a consequence it was proposed that the conductive polymer PEDOT can replace platinum for a more cost-effective DSSCs **[1.20].**

1.6 Synthesis of PEDOT

The polymerization of the 3,4-ethylenedioxythiophene (EDOT) monomer is made through two methods: The oxidative polymerization and the electrochemical polymerization. Whether it's the first or the second approach, the polymerization always necessitates the presence of the monomer (EDOT) and a counter ion to maintain the charge neutrality of the conductive polymer. Figure 1.2 presents the monomer EDOT.

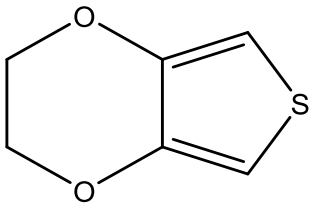

Figure 1.2. Structure of the monomer 3,4-ehtylenedioxythiophene (EDOT).

1.6.1 Oxidative polymerization

Oxidative polymerization of EDOT utilizes iron (III) salts as oxidant agents. Common

oxidants are Fe(III)-p-toluenesulfoante, Fe(III)-sulfonates and Fe(III)-chloride. Sodium persulfate ($Na_2S_2O_8$) is also used to oxidize EDOT in the presence of polystyrene sulfonic acid (PSS) as the counterion to obtain PEDOT:PSS. Other persulfates than the sodium salt can be employed e.g. ammonium or potassium persulfate **[1.21]**.

1.6.2 Electrochemical polymerization

For the electro-polymerization, the oxidation of the EDOT is accomplished on the electrode surface by cyclic voltammetry (most used technique), by constant current or by constant potential. The electro-polymerization is performed in an electrolyte solution in the presence of the monomer and the dopant anion (e.g. PSS to obtain PEDOT:PSS) **[1.22]** .Figure 1.3 shows the conductive polymer poly(3,4-ethylenedioxythiophene):polystyrene sulfonic acid (PEDOT:PSS).

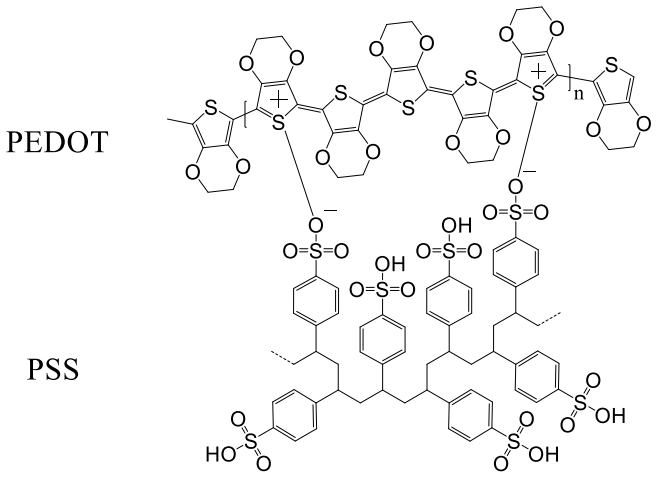

Figure 1.3 Structure of the Poly(3,4-ethylenedioxythiophene): Polystyrene sulfonic acid (PEDOT:PSS) **[1.23].**

1.7 Based PEDOT and PEDOT:PSS hybrid counter electrodes

The idea of mixing a conductive polymer like the PEDOT or PEDOT:PSS with another material arises from their great significance for commercialized applications such as organic light-emitting diode (OLED) and polymer solar cell (PSC) **[1.24]**.

The sole intrinsic polymer conductivity can't meet the needs of these applications, thus a lot of approaches like treating the polymer with dimethyl sulfoxide (DMSO) **[1.25],** tetrahydrofuran (THF) **[1.24]** and ethylene glycol (EG) **[1.26]** are employed.

In addition, based PEDOT and PEDOT:PSS counter electrodes offer higher surface area for the adsorption and reduction of the redox couple. Table 1.2 shows the state of the art of some hybrid counter electrodes. Naturally, a lot of other possibilities for a hybrid counter electrode are found in literature, however this relatively short report can't cover all of them.

Counter electrode	Synthesis method	Characterization	Obtained DSSC				Reference
			η (%)	FF	Jsc (mA/cm^2)	Voc (V)	
PEDOT:PSS/MgO/FTO[a]	MgO powder in PEDOT:PSS aqueous solution coated on the FTO glass by doctor blading method	• XRD[b] • CV[c] • EIS[d]	7.45	0.427	23.80	0.733	**[1.27]**
Graphene/PEDOT:PSS /FTO	In situ polymerization in graphene dispersion drop coated on FTO	• CV • EIS • FT-IR[e] • TEM[f] • XRD	4.66	0.550	11.77	0.726	**[1.28]**
DMSO/PEDOT:PSS/Carbon black/FTO	Dip coating of commercial PEDOT:PSS	• CV • EIS • AFM[g]	5.81	0.530	14.05	0.780	**[1.29]**
PEDOT/ Multi wall carbon nano tube film/ITO[h]	Spin casting of chemically polymerized PEDOT on ITO	• CV • AFM	8.08	0.660	17.00	0.720	**[1.30]**
PEDOT- Ethylene glycol film	Electro-polymerization	• CV • AFM • EIS	8.50	0.640	17.54	0.756	**[1.31]**

Table 1.2 Different technologies of counter electrodes used in the DSSC and their efficiencies. **a** FTO: Fluorine doped tin oxide. **b** XRD: X-ray diffraction. **c** CV: Cyclic voltammetry. **d** EIS: Electrochemical impedance spectroscopy. **e** FT-IR: Fourier transform infrared spectroscopy. **f** TEM: Transmission electron microscopy. **g** AFM: atomic force microscopy. **h** ITO: Indium tin oxide.

1.8 Assessment of the synthesized polymer material: Cyclic voltammetry

As seen in the previous table, basically the same techniques are used to assess the counter electrodes. Here we are going to explain briefly the cyclic voltammetry because of its great utility. Cyclic voltammetry (CV) is an electrochemical analysis widely used to acquire information about the electrochemical properties of a material (e.g. reduction oxidation, capacitance). As shown in Figure 1.4, the setup of the CV encompasses a working electrode, a reference electrode and a counter electrode, all connected to a potentiostat. The three electrodes are emerged in the electrolyte containing the analyte, inside an electrochemical cell. By the means of the potentiostat, the potential of the working electrode is varied from an initial value (Ei) to another value (Ef) in a process called the potential sweeping. Upon reaching the potential (Ef), the scan is switched to return to (Ei). During the potential sweep, the potentiostat measures the resulting current that arises when a certain voltage is applied to the working electrode (where the electrochemical event of interest occurs) **[1.32]**. In addition to the analytical aspect of the cyclic voltammetry technique, it can be also used for the synthesis of a conductive polymer on the working electrode **[1.22].**

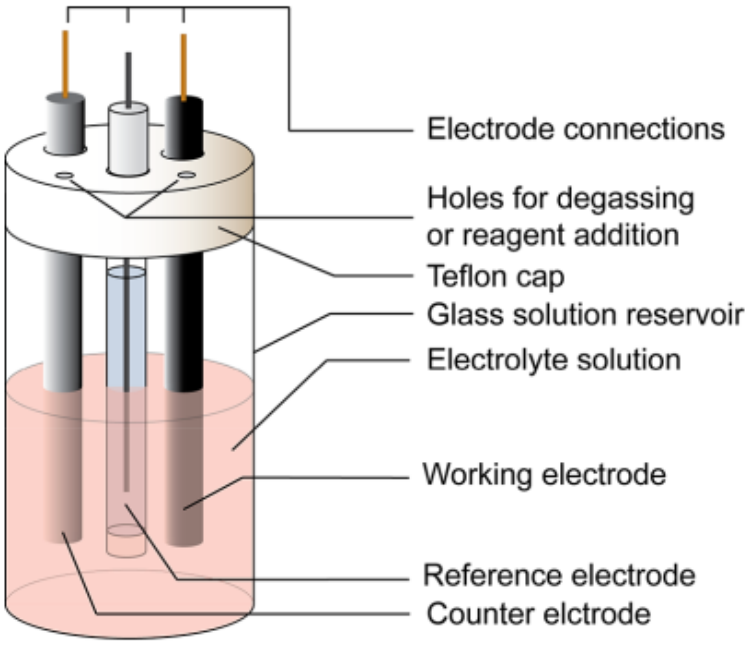

Figure 1.4. Schematic representation of an electrochemical cell for CV experiments **[1.32]**.

1.9 References

[1.1] Z. Pan, H. Rao, I. Mora-Seró, J. Bisquert, and X. Zhong, *Quantum dot-sensitized solar cells*, Chemical Society Reviews, **2018**, 47(20), p. 7659-7702.

[1.2] Fthenakis, V. (**2012**). *Third generation photovoltaics*, Croatia: InTech.

[1.3] B. Oregon and M. Grätzel, *A low-cost, high efficiency solar cell based on dye-sensitized colloidal TiO2 films*, Nature **1991**, 353(6346), p. 737–740.

[1.4] M. Grätzel, *Dye-sensitized solar cells*, Journal of Photochemistry and Photobiology C: Photochemistry Reviews, **2003**, 4(2), p. 145-153.

[1.5] G. Calogero, J. Yum, A. Sinopoli, G. Di Marco, M. Grätzel, and M. Nazeeruddin, *Anthocyanins and betalains as light-harvesting pigments for dye-sensitized solar cells.* Solar Energy, **2012**, 86(5), p. 1563-1575.

[1.6] K. Saranya, M. Rameez, A. Subramania, *Developments in conducting polymer based counter electrodes for dye-sensitized solar cells - An overview.* Eur. Polym. J., **2015**, 66, p. 207–227.

[1.7] W. Zhang, Y. Wu, H. Bahng, Y. Cao, C. Yi, Y. Saygili, J. Luo, Y. Liu, L. Kavan, J. Moser, A. Hagfeldt, H. Tian, S. Zakeeruddin, W. Zhu, W. and M. Grätzel, *Comprehensive control of voltage loss enables 11.7% efficient solid-state dye-sensitized solar cells*. Energy & Environmental Science, **2018**, 11(7), p. 1779-1787.

[1.8] A. Hagfeldt, and M. Grätzel, *Molecular Photovoltaics*, Accounts of Chemical Research, **2000**, 33(5), p. 269-277.

[1.9] P. Kumavat, P. Sonar, and D. Dalal, *An overview on basics of organic and dye sensitized solar cells, their mechanism and recent improvements*, Renewable and Sustainable Energy Reviews, **2017**, 78, p.1262-1287.

[1.10] MA. Green, Y. Hishikawa, ED. Dunlop, DH. Levi, J. Hohl-Ebinger, AWY. Ho-Baillie. *Solar cell efficiency tables (version 52)*. Prog Photovolt Res Appl, **2018**, 26, p. 427–436.

[1.11] K. Yoshikawa, H. Kawasaki, W. Yoshida and al. *Silicon heterojunction solar cell with interdigitated back contacts for a photoconversion efficiency over 26%.* Nature Energy, **2017**, 2(5), 17032.

[1.12] BM. Kayes, H. Nie, R. Twist and al. *27.6% conversion efficiency, a new record for single-junction solar cells under 1 sun illumination*. Proceedings of the 37th IEEE Photovoltaic Specialists Conference, **2011**.

[1.13] Solar Frontier Press Release dated 20 December **2017**, *Solar frontier achieves world record thin-film solar cell efficiency of 22.9%* , retrieved from http://www.solar-frontier.com/eng/news/2017/1220_press.html, accessed 20 February **2019**.

[1.14] First Solar Press Release, First Solar builds the highest efficiency thin film PV cell on record, 5 August **2014**.

[1.15] T. Matsui, K. Maejima, A. Bidiville, H. Sai, T. Koida, T. Suezaki, M. Matsumoto, K. Saito, I. Yoshida, and M. Kondo. *High-efficiency thin-film silicon solar cells realized by integrating stable a-Si:H absorbers into improved device design*. Japanese Journal of Applied Physics, **2015**, 54(8S1), p.08KB10.

[1.16] WS. Yang, JH. Noh, NJ. Jeon, and al. *High-performance photovoltaic perovskite layers fabricated through intramolecular exchange*. Science, **2015**, 348(6240), p. 1234-1237.

[1.17] R. Komiya, A.Fukui, N. Murofushi, N. Koide, R. Yamanaka, and H. Katayama. *Improvement of the conversion efficiency of a monolithic type dye- sensitized solar cell module*. Technical Digest, 21st International Photovoltaic Science and Engineering Conference, Fukuoka, November **2011**, 2C-5O-08.

[1.18] M. Hosoya, H. Oooka, H. Nakao, and al. *Organic thin film photovoltaic modules*. Proceedings of the 93rd Annual Meeting of the Chemical Society of Japan **2013**, 21–37.

[1.19] J. Wu , Y. Li , Q. Tang , G. Yue , J. Lin , M. Huang and L. Meng , *Bifacial dye-sensitized solar cells: A strategy to enhance overall efficiency based on transparent polyaniline electrode*. Sci. Rep, **2014**, 4, 4028.

[1.20] J. Xia and S. Yanagida. *Strategy to improve the performance of dye-sensitized solar cells: Interface engineering principle*. Solar Energy, **2009**, 85(12), p. 3143-3159.

[1.21] A. Elschner, (**2011**). *PEDOT*. Boca Raton, FL: CRC Press.

[1.22] Y. Li, (**2001**). *Organic Electronic Materials*. Berlin Heidelberg Springer-Verlag

[1.23] Kirchmeyer, Stephan, and al **(2007)**. *Poly(3,4-Ethylenedioxythiophene) Scientific Importance, Remarkable Properties, and Applications*. *Handbook of Conducting Polymers*. New York: CRC Press.

[1.24] H. Shi, C. Liu, Q. Jiang, and J. Xu. *Effective Approaches to Improve the Electrical Conductivity of PEDOT:PSS: A Review*. Advanced Electronic Materials, **2015**, 1(4), p. 1500017.

[1.25] S. H. Lee, H. Park, W. Son, H. H. Choi, J. H. Kim, J. Mater. *Novel solution-processable, dedoped semiconductors for application in thermoelectric devices,* Chem. A **2014** 2, 13380.

[1.26] H. Yan , T. Jo , H. Okuzaki. *Highly Conductive and Transparent Poly(3,4-ethylenedioxythiophene)/Poly(4-styrenesulfonate) (PEDOT/PSS) Thin Films,* Polym. J. **2009**, 41, 1028.

[1.27] H. Wang, and Y. Hu. *Electro-catalytic role of insulator/conductor interface in MgO/PEDOT composite electrodes for dye-sensitized solar cells*. Science China Chemistry, **2014**, 58(1), p.101-106.

[1.28] L. Wan, B. Wang, S. Wang, X. Wang, Z. Guo, B. Dong, L. Zhao, J. Li, Q. Zhang, and T. Luo. *Well-dispersed PEDOT:PSS/graphene nanocomposites synthesized by in situ polymerization as counter electrodes for dye-sensitized solar cells*. Journal of Materials Science, **2014**, 50(5), p. 2148-2157.

[1.29] J-G. Chen, H-Y. Wei, K-C. Ho. *Using modified poly(3,4 ethylenedioxythiophene):poly(styrene sulfonate) film as a counter electrode in dye-sensitized solar cells.* Solar Energy Mater Solar Cells, **2007**, 91(15–16), p. 1472–14777.

[1.30] K-M. Lee, W-H. Chiu, H-Y. Wei, C-W. Hu, V. Suryanarayanan, WF. Hsieh, and al. *Effects of mesoscopic poly(3,4-ethylenedioxythiophene) films as counter electrodes for dye-sensitized solar cells*, Thin Solid Films **2010**, 518(6), p. 1716–1721.

[1.31] T-L. Zhang, H-Y. Chen, C-Y. Su, D-B. Kuang. *A novel TCO- and Pt-free counter electrode for high efficiency dye-sensitized solar cells*, J Mater Chem A, **2013**, 1(5), p. 1724

[1.32] N. Elgrishi, K. Rountree, B. McCarthy, E. Rountree, T. Eisenhart, and J. Dempsey. *A Practical Beginner's Guide to Cyclic Voltammetry*. Journal of Chemical Education, **2017**, 95(2), p. 197-206.

[1.33] A. Bard, and L. Faulkner (**2000**). *Electrochemical methods and applications*. New York: Wiley-Interscience.

Chapter 2: Electrochemical properties of PEDOT

2.1 Introduction

Poly(3,4-ethylenedioxythiophene), also known as PEDOT, is a conductive polymer employed in many electronic devices such as the biosensors, fuel cells, capacitors and solar cells **[2.1]**. Therefore, it is natural to investigate its electrical aspects to improve the fabricated devices that contain this polymer.

This chapter deals with an important feature of the PEDOT which is the capacitive behavior. Mainly PEDOT doped ClO_4^- and PEDOT doped with poly(4-styrenesulfonate) (PSS) were studied. The latter was chosen because it was the polymer material used in the fabrication of the dye-sensitized solar cells (DSSCs).

Firstly, it is mandatory to define the capacitance: It is a measure of the ability of a material to store electrons, and by definition it corresponds to the following ratio of $C \equiv {}^{Q}/_{V}$, in which V is the potential within which a number of electrons, are confined (representing the charge Q) **[2.2]**.

The PEDOT belongs to a class of capacitors named the supercapacitors which, based on their charge storage mechanisms, are subdivided into pseudo-capacitors and electrochemical double layer capacitors (EDLC) **[2.3, 2.4]**. In the case of PEDOT, it is classified as pseudo-capacitive polymer. The particularity of this class is that charge storage occurs by fast surface redox reactions **[2.5]**.

To study the capacitance of PEDOT, cyclic voltammetry is used, since it was reported in literature that capacitive materials, like PEDOT, exhibit rectangular shaped voltammograms **[2.5]**.

The interest in the pseudo-capacitance of PEDOT is due to the fact that large amount of information can be extracted, such as the ionic-electronic transport mechanisms of PEDOT, which is the main theme of this thesis.

2.2 Experimental section

Two experiments were conducted:

- The first one was the preparation of PEDOT:ClO_4/graphite electrodes by electro-polymerization and it is a quantitative experiment to show some factors affecting the capacitance of the PEDOT:ClO_4.
- The second one was the preparation a PEDOT:PSS/FTO electrode by electro-polymerization and a PEDOT:PSS/GC (glassy carbon)electrode by oxidative polymerization. This experiment is a qualitative and was intended to show the capacitance of PEDOT:PSS.

2.2.1 Chemicals

For the preparation of the electrodes, the following chemicals were used: The monomer 3,4-ethylenedioxythiophene (EDOT) 99%, lithium perchlorate salt ($LiClO_4$) were purchased from Acros Organics. Sodium persulfate ($Na_2S_2O_8$) 98%, iron(III) sulfate hydrate ($Fe_2(SO_4)_3$) 97% and poly(4-styrenesulfonic acid) (PSS) 18% in water were purchased from Sigma-Aldrich. The solvent acetonitrile, CH_3CN 99.9%, was purchased from Fisher Chemical. Deionized water (DI) was used throughout the experiences and all the chemicals were used directly without further purification or treatment.

2.2.2 Instruments

For both experiments, the same electrochemical set up was used to perform the cyclic voltammetry measurements. The working electrodes used were graphite (provided by the university laboratory) and fluorine tin oxide (FTO) glass (provided by the university of Porto, FEUP). The reference electrode was an Ag/AgCl 3M KCl and the counter electrode was a glassy carbon electrode with a diameter of 2 mm. Both were Metrohm electrodes. The potentiostat used was a ZAHNER XPot, and the cyclic voltammograms were collected using the software package Power-Potentiostats Inspector V 8.1. Fourier transform infrared spectroscopy (FT-IR) was used to characterize the electro-deposited PEDOT on graphite. The FT-IR spectrometer was a PerkinElmer Spectrum two.

2.2.3 Electro-polymerization of PEDOT:ClO_4

Graphite sheets pretreatment:

Before proceeding with the electro-deposition of PEDOT on the graphite, a pre-treatment is necessary. Four sheets of graphite (Figure 2.1) were used to perform the electro-polymerization of PEDOT. The surface area of the deposition of PEDOT was 1.28 cm^2 (using the adhesive tape to limit the surface). Subsequently, the graphite sheets were cleaned with abrasive paper and DI water. After cleaning, they were dried in an oven for 4 hours at 70°C . Afterwards the graphite sheets were weighed on a precise balance to obtain their masses without PEDOT.

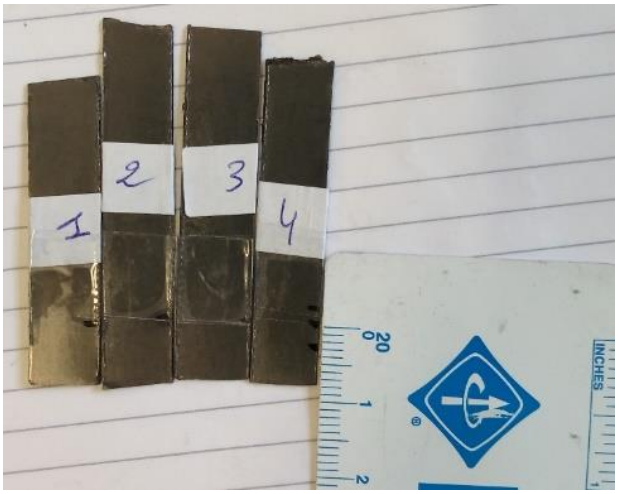

Figure 2.1. Graphite sheets used for the electro-deposition of PEDOT.

Solution preparation:

PEDOT was synthesized in an aqueous solution of 10% Acetonitrile (v/v) and in the presence of 0.1M of lithium perchlorate ($LiClO_4$) and 0.01 M of EDOT. The solution was immersed in a sonic bath for 20 min to homogenize the mixture.

Electro-deposition of PEDOT:ClO_4^-:

The synthesis was carried out with the cyclic voltammetry using a three-electrode system dipped in the prepared solution. The reference electrode used was Ag/AgCl (3M KCl) and the counter electrode was a glassy carbon electrode. The working electrodes were the graphite sheets on which the deposition of the PEDOT took place. The electro-polymerization was conducted in an interval that varied from -0.3 V to 1.5 V at a scan rate of 100mV/s, but for each graphite sheet the number of cycles was changed from 20 to 40 cycles in order to obtain different mases of electrodeposited PEDOT.

2.2.4 Determination of the PEDOT:ClO_4 mass

Following the electro-polymerization, the mass of the PEDOT was determined by gravimetric weight difference method using a sensitive microbalance. The graphite sheets were dried at room temperature for two days and then weighed. By subtracting the mass of the graphite sheets from those of PEDOT/graphite, the mass of deposited PEDOT was determined.

2.2.5 Electrochemical assessment of the PEDOT:ClO_4/graphite electrodes

The electrochemical performances of the four prepared PEDOT:ClO_4/graphite electrodes were measured at room temperature using the three-electrode set-up. The reference electrode was an Ag/AgCl (3M KCl) electrode and the counter electrode was a platinum electrode while the working electrode was the prepared PEDOT:ClO_4/graphite electrode. The electrolyte solution was an aqueous solution of 10% Acetonitrile (v/v) with 0.1M of lithium perchlorate ($LiClO_4$). For each PEDOT:ClO_4/graphite electrode, a series of cyclic voltammograms were performed by changing the scan rate from 5 mV/s to 200 mV. The obtained voltammograms were integrated to extract the mass specific capacitance of the PEDOT by applying the equation **[2.6]**:

$$C = \frac{1}{2\,m\,(Vmax - Vmin)\,v} \int_{Vmin}^{Vmax} I\,dV \qquad (1)$$

where *m* is the mass of the deposited PEDOT film , *Vmax* and *Vmin* are respectively the maximum and the minimum applied potential of the scan window and *v* is the scan rate.

2.2.6 Electro-polymerization of PEDOT:PSS on FTO and its assessment

FTO glass pretreatment:

The FTO glass substrate was cleaned using an ultrasonic bath in detergent, ethanol, deionized water, and isopropanol (2-propanol) for 15 min, respectively. The surface area of the deposition of PEDOT was 2.47 cm^2.

Solution preparation:

PEDOT:PSS was synthesized in an aqueous solution (DI water) containing 0.1M PSS and 0.01 M of EDOT. The solution was put in a sonic bath for 30 min for homogenization.

Electro-deposition of PEDOT:PSS on FTO:

PEDOT:PSS was electro-deposited on the FTO glass by the same electrochemical set-up previously used for the PEDOT/Graphite electrodes. The working electrode was the prepared PEDOT:PSS/FTO electrode.

Electrochemical assessment of PEDOT:PSS/FTO:

Using cyclic voltammetry, the prepared PEDOT:PSS/FTO was tested in a 0.1 M of $LiClO_4$ in acetonitrile in an interval of -1.5 V to 1.5 V.

2.2.7 Coating of PEDOT:PSS on glassy carbon and its assessment

PEDOT:PSS was polymerized through the oxidative chemical way and then pasted on the glassy carbon (GC) electrode.

Solution preparation:

PEDOT:PSS was synthesized in an aqueous solution containing the monomer EDOT and the dopant PSS in the proportion of 1:2.5 (w/w). The initiators used were $Na_2S_2O_8$ and $Fe_2(SO_4)_3$ **[2.7]**.

Pasting of PEDOT:PSS on the glassy carbon

The obtained PEDOT:PSS was dried in oven at 50°C. Before it becomes fully dry, it was pulled out and pasted on the surface of the glassy carbon electrode. The moisture that was left in the PEDOT:PSS helped to form an adhesive paste of PEDOT:PSS.

Electrochemical assessment of the PEDOT:PSS/GC electrode

PEDOT:PSS/GC electrode was used as a working electrode with an Ag/AgCl (3M KCl) electrode as a reference electrode and platinum electrode as a counter electrode. The solution used was an aqueous solution of 10% Acetonitrile (v/v) with 0.1M of lithium perchlorate ($LiClO_4$). The interval of the scan was from -1 V to 1.5 V.

2.3 Results and discussion

2.3.1 PEDOT:ClO_4 investigation

2.3.1.1 Electro-polymerization of PEDOT

The obtained electrodes are shown in Figure 2.2. The shapes of the cyclic voltammograms of the deposition of the PEDOT on graphite are the same for all the prepared electrodes. To demonstrate this typical shape, the voltammograms of 20 cycles of deposition are shown in Figure 2.3. This deposition yielded the first electrode of PEDOT/Graphite. These

voltammograms show the increase of the current intensity with each cycle indicating the film growth of PEDOT on the surface of graphite. What is important to notice in this voltammograms is the region of the potential before the oxidation peak of EDOT (which is around 0.9 V). This region is characterized by a plateau shape where the current is not varying so much with the applied potential. This is caused by the capacitive character of the deposited polymer PEDOT that starts to manifest from the first cycles of the deposition.

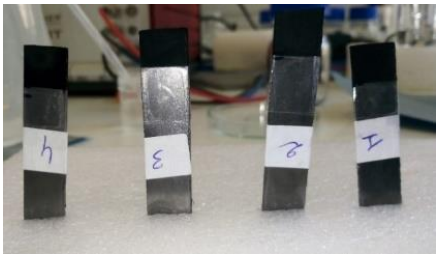

Figure 2.2. PEDOT/Graphite electrodes after the electro-polymerization of PEDOT.

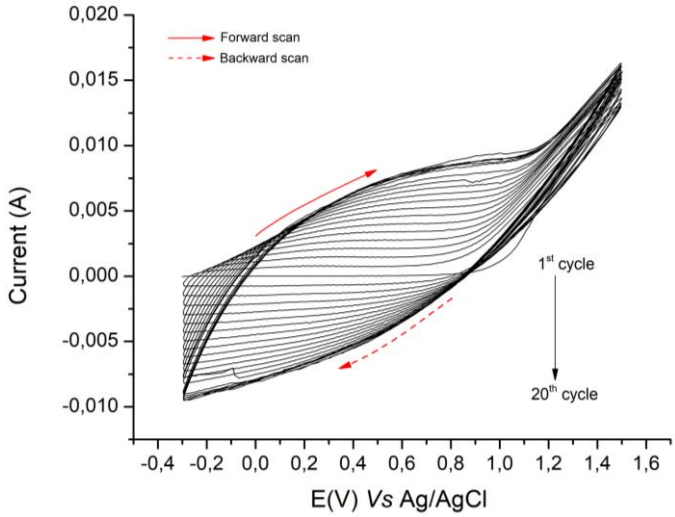

Figure 2.3. Cyclic voltammograms of 0.01M EDOT in aqueous solution of 10% acetonitrile with 0.1M $LiClO_4$. 20 cycles at a 100 mV/s.

2.3.1.2 FT-IR characterization of PEDOT

The electro-deposited PEDOT was scratched from the graphite surface and analyzed by FT-IR spectroscopy. The spectra obtained is shown in Figure 2.4. Characteristic peaks of PEDOT are below 1600 cm^{-1} **[2.8]**. The mentioned peaks are as follows: 1503, 1296, 1168, 1134, 1073, 1030, 961 and 894 cm^{-1}. The peaks at approximately 1503 and 1296 cm^{-1} are assigned to asymmetric stretching mode of C = C and inter-ring stretching mode of C-C, respectively. The peaks appearing at around 1168, 1134, 1073 and 1030 cm^{-1} are attributed to the C-O-C bending vibration in the ethylenedioxy group, while the peaks at

961 and 894 cm^{-1} are the characteristic bands of stretching vibrations of the C-S-C bond in thiophene ring, which suggests the successful formation of the PEDOT in this electro-polymerization reaction **[2.9]**.The peak at 1611 cm^{-1} is considered to be the characteristic peak of the PEDOT-doped state, indicating that ClO_4^- has been doped into the PEDOT **[2.10]**.

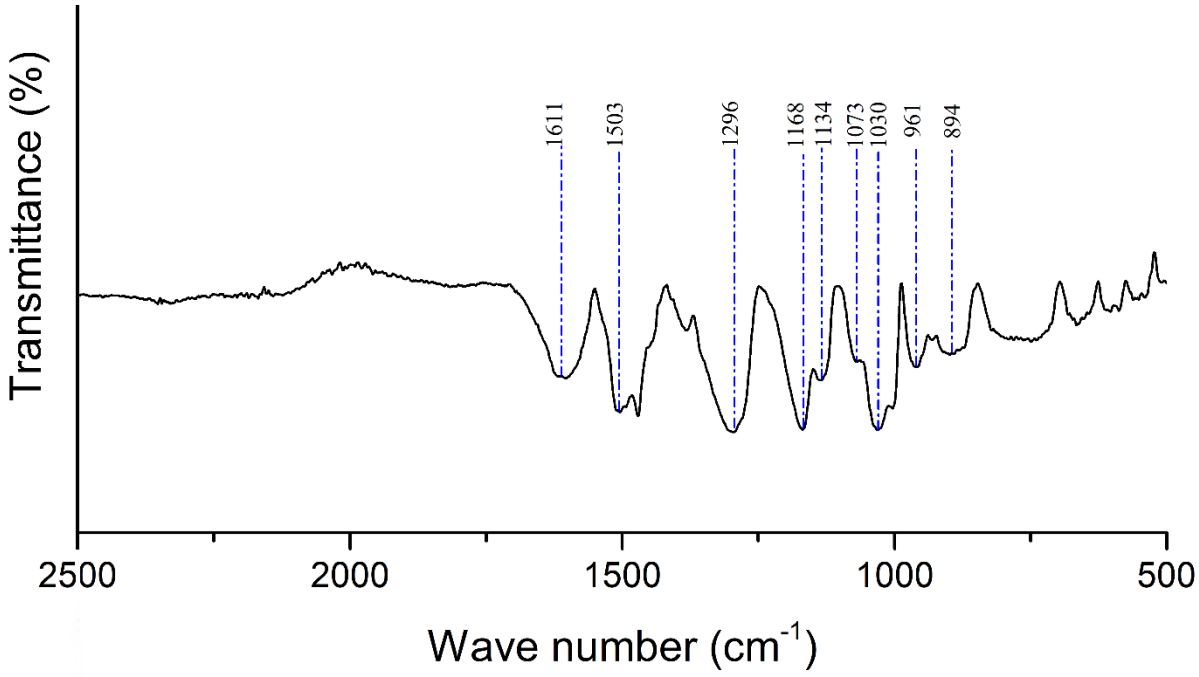

Figure 2.4. FT-IR spectrum of PEDOT deposited on graphite.

2.3.1.3 Electrochemical behavior of PEDOT/graphite electrodes

After the preparation of the PEDOT/Graphite electrodes, they were electrochemically evaluated by cyclic voltammetry in a solution containing only the support electrolyte of $LiClO_4$ (consult the experimental part for detail). For each of the prepared PEDOT/Graphite electrode, a series of cyclic voltammograms were conducted. In Figure 2.5, voltammograms of the four prepared PEDOT/Graphite electrodes with different masses are plotted at 5 mV/s (corresponds to the stable state **[2.11]**). The voltammograms are nearly rectangular without any peak of a faradaic current, the only observed current is capacitive. The voltammogram of the bare graphite electrode was also plotted with the graphs of the PEDOT/Graphite electrode in order to show that this capacitive current is due to the PEDOT. Another indicator about the capacitive character of PEDOT is that the area of the voltammograms is increasing with the amount of the

electro-deposited polymer, meaning that the capacitance is mainly ascribed to the PEDOT.

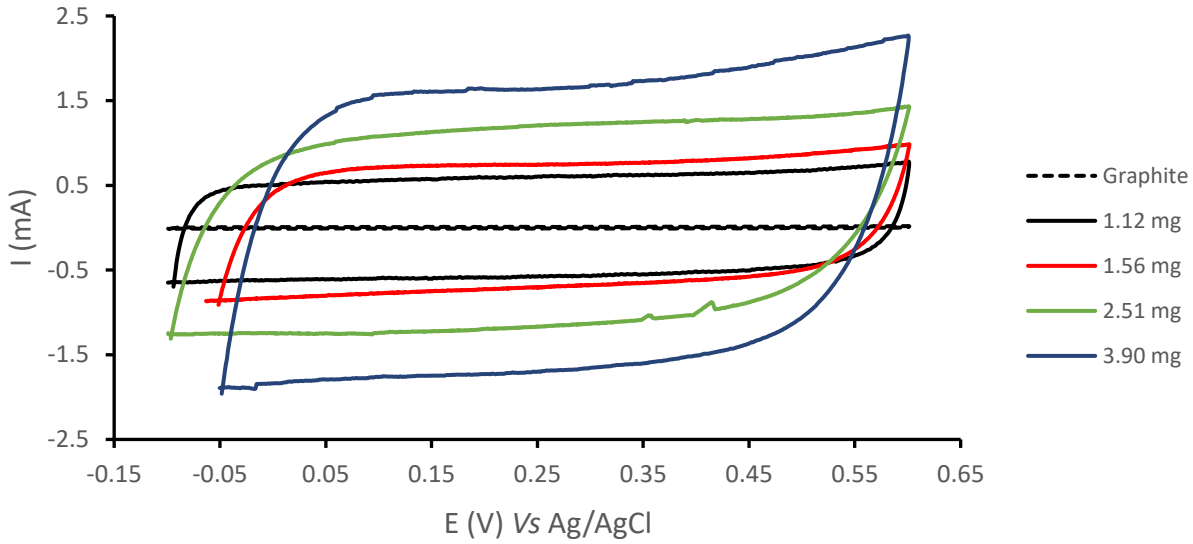

Figure 2.5. Voltammograms of the four prepared PEDOT/graphite electrodes compared with the bare graphite at a scan rate of 5mV/s.

2.3.1.3.1 Specific capacitance results

From the voltammograms obtained (shown in Figure 2.5 and in **Appendix A**), it is possible to quantify the capacitance of the PEDOT. The idea is to integrate the area of the voltammograms and then apply equation (1):

$$C = \frac{1}{2\ m\ (Vmax - Vmin)\ v} \int_{Vmin}^{Vmax} I\ dV$$

By doing so for the four PEDOT/Graphite prepared electrodes, one can estimate the value of the specific capacitance of PEDOT. It is important to notice that the integrated area (green-colored in the formula) is divided by two, because the shape of the voltammograms correspond to charge (from *Vmin* to *Vmax*)/discharge (from *Vmax* to *Vmin*) cycle, thus to find out the correct capacitance it is necessary to take only one part either the charge or the discharge. At the same time, the mass of PEDOT on each graphite sheet was calculated, as described in the experimental part, by weighing the graphite sheet before and after the electro-deposition of PEDOT. Table 2.1 shows the obtained results for the four prepared PEDOT/graphite electrodes. This mass was used to calculate the specific capacitance of PEDOT in F/g as stated in equation (1).

Table 2.1 Mass of the PEDOT electrodeposited on each of the four graphite electrodes.

Electrodes	1	2	3	4
Number of cycles	20	30	35	40
Initial mass of graphite (mg)	906.55	887.46	1014.16	1049.55
Final mass of graphite (mg)	907.67	889.02	1016.67	1053.45
Mass of PEDOT (mg)	1.12	1.56	2.51	3.90

The obtained specific capacitances were plotted in function of the scan rate in Figure 2.6. Theoretically, the specific capacitance (per mass) shouldn't change since it's an inherent character of the material, however experimentally, dispersed values were obtained forming ranges of values. At 5mV/s, the specific capacitance of PEDOT is between 73 F/g and 100 F/g . Also, at 10mV/s, the value of the capacitance is between 70 F/g and 90F/g. These results agree with the values reported in literature **[2.12]**. The main advantage of this method of calculation of the specific capacitance is that by doing many experiments (e.g. 20 PEDOT/Graphite electrodes with different masses of PEDOT) and following the same protocol used here, it can yield more accurate results. What is noticeable about figure 2.6, is that the capacitance is decreasing with the scan rate (extrinsic perturbance), this suggests that the capacitance of PEDOT is influenced by the thickness of the diffusion layer formed between the electrode and the electrolyte. This means that PEDOT is relying on ions that diffuse into and out of the surface/bulk of PEDOT to store charges **[2.10]**.

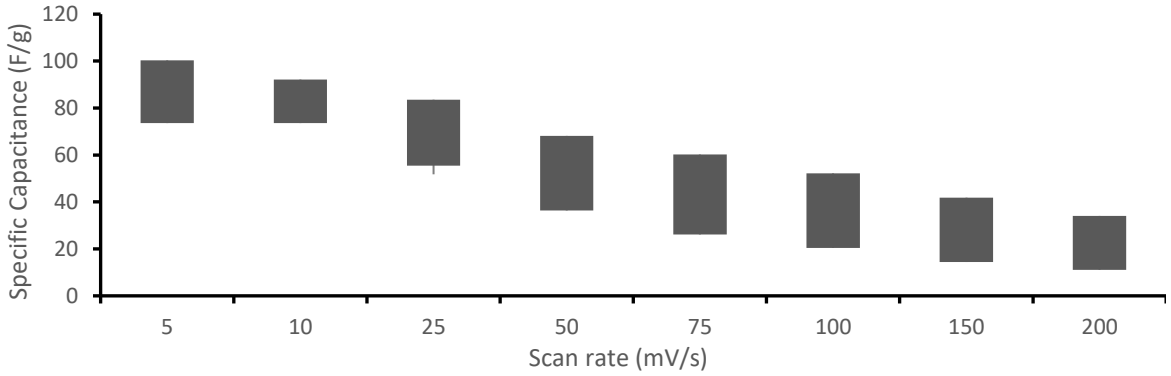

Figure 2.6. Variation of the specific capacitance of PEDOT in function of the applied scan rate.

2.3.1.3.2 Mechanism of the pseudo-capacitance of PEDOT:ClO_4

To describe the charge storage mechanism of PEDOT:ClO_4^- material, a schematic representation of the phenomenon is shown in Figure 2.7**.** This scheme demonstrates the sequences of the charge storage in the PEDOT bulk material. Depending on the applied voltage, electrons are inserted into the PEDOT or extracted from it via the graphite

material. If the applied voltage is negative, electrons migrate through the graphite to the PEDOT bulk triggering the intercalation mechanism of the lithium (Li^+) cations (since the supporting electrolyte used was lithium perchlorate). On the other hand, when the applied potential is positive, electrons migrate from PEDOT to the graphite electrode triggering the de-intercalation of Li^+. This description justifies the shapes of the obtained voltammograms: in the forward scan, fast charging of holes occurs and Li^+ cations are de-intercalated, whereas in the backward scan, electrons are charged in the PEDOT bulk and Li^+ cations are intercalated. The lithium cations are compensating the charge created on the PEDOT by the applied voltage, thus using different electrolytes can yield higher or lower capacitance of PEDOT depending on the diffusivity of the intercalated/de-intercalated species.

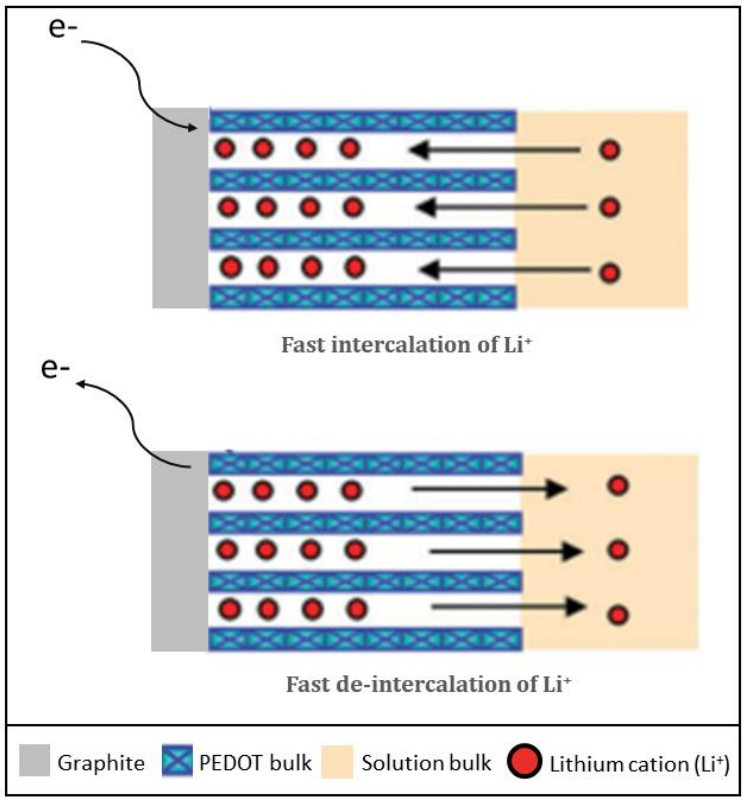

Figure 2.7. Intercalation and de-intercalation of Li^+ cations into and out of the bulk of PEDOT **[2.3]**.

2.3.2 PEDOT:PSS investigation

2.3.2.1 Electrochemical assessment of the PEDOT:PSS/FTO

After the electro-deposition of PEDOT:PSS on the surface of the FTO glass, it was tested in a solution containing only $LiClO_4$ as a supporting electrolyte. Figure 2.8 shows the voltammograms of PEDOT:PSS/FTO compared with the bare FTO glass (to ensure that

the observed current is due only to PEDOT:PSS). Although, there is no redox couple in the solution, the voltammograms show anodic and cathodic peaks. At 10 mV/s, the cathodic peak appears at around 0 V and the anodic one at 0.4 V. At 25mV/s, the cathodic peak shifts to -0.23 V and the anodic peak shifts to 0.6 V. The peaks are ascribed to the doping and de-doping of the PEDOT:PSS with the lithium cations (Li^+)**.**The shifting of the peaks in cyclic voltammetry, indicates a slow process of cation intercalation/de-intercalation. **[2.1]**. After each peak, the current tends to stabilize forming a plateau shape, which reflects the capacitance of PEDOT:PSS.

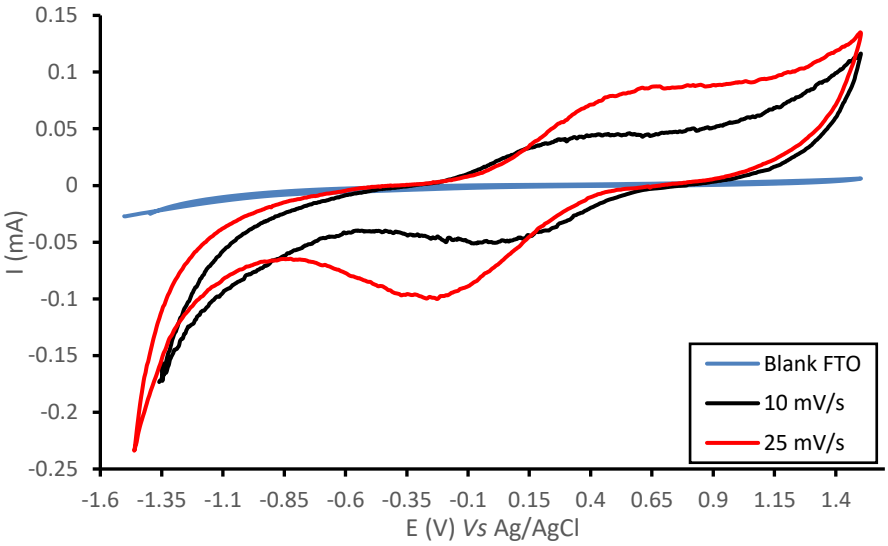

Figure 2.8. Cyclic voltammetry of PEDOT:PSS/FTO electrode in 0.1 M $LiClO_4$.

Interestingly, when the PEDOT:PSS was under the cyclic voltammetry test, it switched colors from dark blue to light blue. The two colors correspond respectively, to the reduced state and the oxidized state of PEDOT:PSS **[2.13]**. Figure 2.9 shows the electrochromic character of PEDOT:PSS.

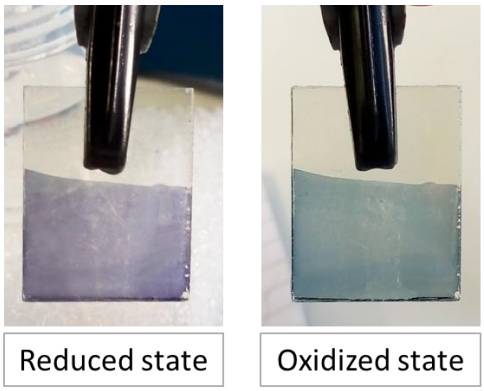

Figure 2.9. Electrochromic states of PEDOT:PSS.

2.3.2.2 Electrochemical assessment of the PEDOT:PSS/GC

The PEDOT:PSS obtained through chemical oxidative polymerization was placed on the active surface of the glassy carbon electrode (GC) to form a film as shown in Figure 2.10.

Figure 2.10. PEDOT:PSS on glassy carbon electrode.

The PEDOT:PSS/GC electrode was tested in the lithium perchlorate solution (0.1 M) and the obtained voltammogram is shown in Figure 2.11. It shows the response of the prepared PEDOT:PSS/GC electrode towards a potential sweep from -1V to 1.4V. At the starting potential of -1 V , the current is low (in the order of -0.1 mA), then when the potential increases to higher voltages, the current begins to increase until reaching the potential of 0.5 V where it jumps to 0.65 mA. This jump is associated to the oxidation of the PEDOT:PSS accompanied with the de-doping of Li^+ cations. After the oxidation of the polymer, the current remains stable at the value of 0.65 mA forming a plateau. This flat shape is explained by the capacitive current accumulated by the PEDOT:PSS. In fact, after the maximal quantity of oxidized polymer has formed, the current becomes entirely capacitive **[2.14]**. In the reverse scan, from 1.12 V, current starts to drop out from the stable value of 0.65 mA to more negative values. Between 0.2 V and -0.4V, a broad cathodic peak appears of an amplitude of -0.57 mA. This peak represents the reduction of the oxidized PEDOT:PSS, and it is due to the incorporation of the Li^+ cations and the electron injection into the polymer bulk **[2.1]**.

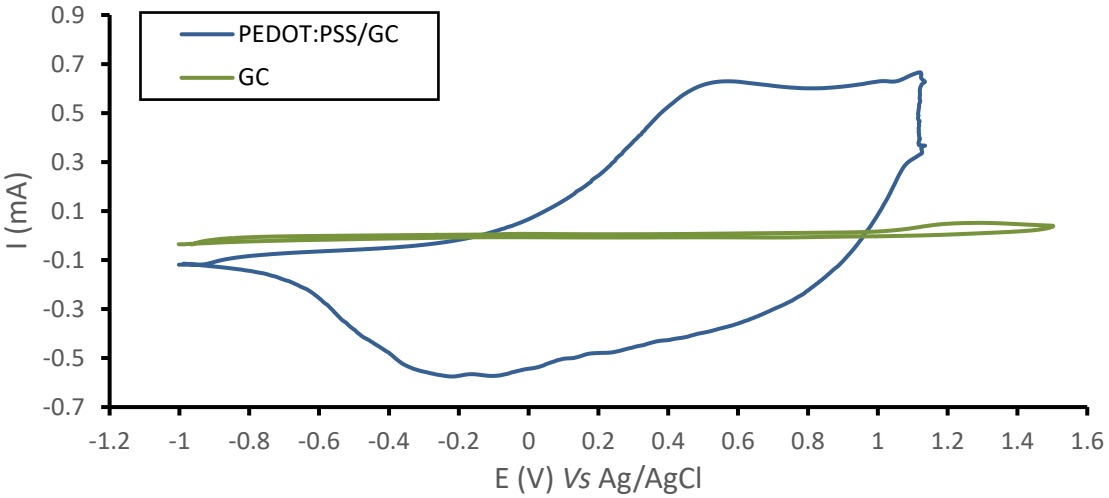

Figure 2.11. Cyclic voltammetry of the PEDOT:PSS/GC electrode at 50 mV/s in 0.1 M of $LiClO_4$.

2.4 Conclusions

PEDOT is a pseudocapacitor that can store charges via cations like Li^+ that exist in the electrolyte solution . Its capacitance is high and can be enhanced by using more suitable cations (electrolyte solution).

Under an applied voltage, cations are either doping or de-doping the PEDOT. This happens because at a sufficiently positive voltage, PEDOT oxidizes (loses electrons) gaining more positive charges on its chain, thus cations de-intercalate out of the PEDOT bulk to maintain the charge neutrality of the polymer. On the other hand, at a sufficiently negative voltage, PEDOT reduces (gaining electrons) and cations intercalate into the PEDOT bulk. This elucidates the mechanisms of the ionic transport in the PEDOT and show its high ionic conductivity.

It was demonstrated that both electro-polymerized and chemical polymerized PEDOT:PSS have capacitive currents and same oxidation peaks (around 0.4 to 0.5 V) indicating similar mechanisms of oxidation. Also, the oxidation and the reduction of the PEDOT material is accompanied by an electrochromic shift from dark blue (reduced) to light blue (oxidized). This aspect can be exploited to fabricate organic optoelectronics such as organic light-emitting diodes, sensors or even smart windows.

2.5 References

[2.1] A. Volkov, K. Wijeratne, E. Mitraka, et al. *Understanding the Capacitance of PEDOT:PSS*. Advanced Functional Materials, **2017**, 27(28), p. 1700329.

[2.2] LaFave, T., & Tsu, R. *Capacitance: A property of nanoscale materials based on spatial symmetry of discrete electrons*. Microelectronics Journal, **2008**, 39(3-4), 617-623.

[2.3] Wang, Y., Song, Y., & Xia, Y. *Electrochemical capacitors: mechanism, materials, systems, characterization and applications*. Chemical Society Reviews, **2016**. 45(21), 5925-5950.

[2.4] Skotheim, T., & Reynolds, J. (**2007**). *Handbook of conducting polymers*. Boca Raton (Fla.): CRC Press.

[2.5] Yin, C., Zhou, H., & Li, J. *Facile one-step hydrothermal synthesis of PEDOT:PSS/MnO2 nanorod hybrids for high-rate supercapacitor electrode materials*. Ionics, **2018**, 25(2), 685-695.

[2.6] Zhang, Z., Xie, D., Cui, P., & Chen, X. *Conversion of a zinc salicylate complex into porous carbons through a template carbonization process as a superior electrode material for supercapacitors*. RSC Advances, **2014**, 4(13), 6664.

[2.7] Wang, J., Cai, G., Zhu, X., & Zhou, X. *Oxidative chemical polymerization of 3, 4-ethylenedioxythiophene and its applications in antistatic coatings*. Journal Of Applied Polymer Science, **2011**, 124(1), 109-115.

[2.8] Du, H., Liu, X., Ren, Z., & Liu, P. *Capacitance characteristic of PEDOT electrodeposited on different substrates*. Journal Of Solid State Electrochemistry, **2018**, 22(12), 3947-3954.

[2.9] Zhao, Q., Jamal, R., Zhang, L., Wang, M., & Abdiryim, T. *The structure and properties of PEDOT synthesized by template-free solution method*. Nanoscale Research Letters, **2014**, 9(1), 557.

[2.10] Pandey, G., Rastogi, A., & Westgate, C. *All-solid-state supercapacitors with poly(3,4-ethylenedioxythiophene)-coated carbon fiber paper electrodes and ionic liquid gel polymer electrolyte*. Journal Of Power Sources, **2014**, 245, 857-865.

[2.11] Wang, H., & Pilon, L. *Physical interpretation of cyclic voltammetry for measuring electric double layer capacitances*. Electrochimica Acta, **2012**, 64, 130-139.

[2.12] Xu, Y., Wang, J., Sun, W., & Wang, S. *Capacitance properties of poly(3,4-ethylenedioxythiophene)/polypyrrole composites*. Journal Of Power Sources, **2006**, 159(1), 370-373.

[2.13] Singh, R., Tharion, J., Murugan, S., & Kumar, A. *ITO-Free Solution-Processed Flexible Electrochromic Devices Based on PEDOT:PSS as Transparent Conducting Electrode.* ACS Applied Materials & Interfaces, **2016**, 9(23), 19427-19435.

[2.14] Feldberg, S. *Reinterpretation of polypyrrole electrochemistry. Consideration of capacitive currents in redox switching of conducting polymers*. Journal of the American Chemical Society, **1984**, 106(17), pp.4671-4674.

Chapter 3: Catalytic activity of PEDOT

3.1 Introduction

The intended Dye-Sensitized Solar Cell (DSSC) employs a redox couple as a mediator that receives the electrons from the counter electrode and regenerates the sensitizer, which by extension regenerates the DSSC. This redox couple is reduced on the counter electrode of the DSSC. Conventionally, the material of the counter electrode is mainly a conductive glass like the fluorine tin oxide (FTO) or the indium tin oxide (ITO) with a sprayed layer of platinum particles that plays the role of the catalyst for the redox mediator. Ideally, the reaction with the redox couple should be fast on the counter electrode which means that this electrode must have a high catalytic activity towards the mediator **[3.1]**.

Herein we demonstrate that the conductive polymer poly(3,4-ethylenedioxythiophene) (PEDOT) can be a substitute for the platinum particles to catalyze the reduction of the redox couple. Therefore, the study of the electrochemical reduction of the mediator on the PEDOT polymer is fundamental to understand and confer insightful results regarding the catalytic activity and the ionic-electronic conductivity of PEDOT.

For this aim, two different redox couples were chosen. The first redox couple was the Iron(III)/Iron(II) (Fe^{3+}/Fe^{2+}), it was chosen because of its simplicity to get a first view on the catalytic effect of the PEDOT compared to that of the platinum material. The second redox couple was the Triiodide/Iodide (I_3^-/I^-) and was chosen owing to its use as a mediator in a classical DSSC.

It is known that the catalytic activity of PEDOT for the reduction of I_3^- is sensitive to the electro-polymerization conditions of the PEDOT, such as the type of the solvent, type of the supporting electrolyte and monomer concentration. Among these factors, the supporting electrolyte plays an important role as it affects the kinetics of the electro-polymerization as well as the doping of the polymer which leads to different catalytic properties of the prepared PEDOT film.

3.2 Experimental section

3.2.1 Catalytic activity of PEDOT towards the Fe^{3+}/Fe^{2+}

3.2.1.1 Chemicals

The monomer 3,4-ethylenedioxythiophene (EDOT) 99%, lithium perchlorate salt ($LiClO_4$) and iron (III) chloride ($FeCl_3$), 98% pure anhydrous were purchased from Acros Organics. Iron(II) chloride tetrahydrate ($FeCl_2{,}4H_2O$) 99% was purchased from Sigma-Aldrich. Hydrochloric acid (HCl) 37% was purchased from PanReac, while the solvent acetonitrile, CH_3CN 99.9%, was purchased from Fisher Chemical. Deionized water (DI) was used throughout the experiments and all the chemicals were used directly without further purification or treatment.

3.2.1.2 Instruments

The electrodeposition of the PEDOT films as well as the electrochemical measurements were all realized in a three-electrode system in an electrochemical cell. The working electrodes used were platinum (2 mm of diameter) and graphite. The reference electrode was an Ag/AgCl 3M KCl and the counter electrode was a glassy carbon electrode with a diameter of 2 mm. All the electrodes (except the graphite sheet) were provided by Metrohm. The potentiostat used was a ZAHNER XPot, and the cyclic voltammograms were collected using the software package Power-Potentiostats Inspector V 8.1. Figure 3.1 shows the electrochemical set-up used.

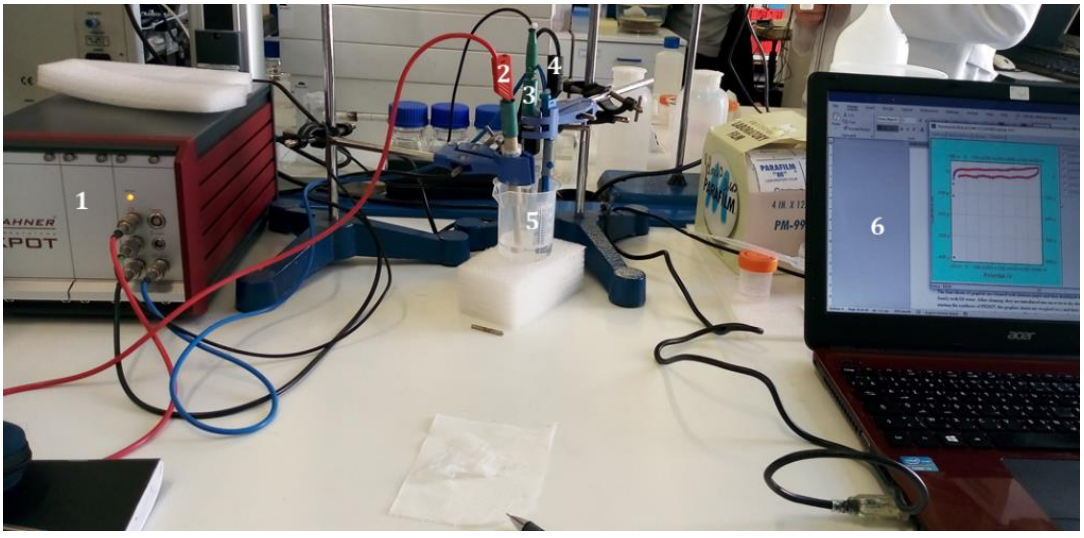

Figure 3.1. 1-Potentiostat. 2-Counter electrode. 3-Reference electrode. 4-Working electrode. 5-Electrochemical cell. 6-Computer collecting data.

3.2.1.3 Electrochemical deposition of PEDOT

PEDOT was potentiodynamically deposited on a graphite sheet and on platinum electrode (separately). The solution used was aqueous and contained 10% Acetonitrile (v/v) in the presence of 0.01 mol/L of EDOT and 0.1 mol/L of lithium perchlorate ($LiClO_4$) **[3.2]**. The reference electrode used was Ag/AgCl and the counter electrode was a glassy carbon electrode. As for the working electrodes, graphite sheet and platinum were used. The interval of the scan was from -0.6 V to 1.6 V at a scan rate of 100mV/s, and the number of cycles was 12.

3.2.1.4 Cyclic voltammetry assessment

The bare graphite electrode, the platinum electrode and the PEDOT/Graphite electrode were all assessed using cyclic voltammetry (CV) in a solution containing 0.05 mol/L of $FeCl_3$ and 0.05 mol/L of $FeCl_2$,$4H_2O$ with 0.5 mol/l of HCl as a buffer. The reference and the counter electrodes were respectively Ag/AgCl 3 M KCl and glassy carbon which were cleaned before and after every measurement. The cyclic voltammograms were recorded between -300 mV and 1200 mV at a scan rate of 25 mV/s. To make sure that the analyses were carried out under the same conditions, the same set of electrodes (reference and counter electrodes), and the same redox solution (Fe^{3+}/Fe^{2+}) were employed. Since platinum and graphite don't have the same area, the collected voltammograms were normalized to the surface area of the employed electrode.

3.2.2 Catalytic activity of PEDOT towards the I_3^-/I^- system

3.2.2.1 Chemicals

The monomer 3,4-ethylenedioxythiophene (EDOT) 99% and the lithium perchlorate salt ($LiClO_4$) were purchased from Acros Organics. Tetrabutylammonium perchlorate salt (TBAP) and bis(trifluoromethane)sulfonimide lithium salt (LiTFS) were purchased from Sigma-Aldrich. The tetrabutylammonium bromide salt (TBAB) was purchased from Fluka analytical. For the Triiodide/Iodide solution, potassium iodide was purchased from Fisher Chemical and the metallic iodine was supplied by the IPB laboratory. While the solvent acetonitrile, CH_3CN 99.9%, was purchased from Fisher Chemical. All the chemicals were used directly without further purification or treatment.

3.2.2.2 Instruments

Cyclic voltammetry experiments in the I_3^-/I^- system and the electrodeposition of PEDOT films were all realized in a three-electrode classical system in an electrochemical cell. The working electrode was platinum with an area of 0.0314cm^2, the reference electrode was an Ag/AgCl 3M KCl and the counter electrode was a glassy carbon electrode with an area of 0.0314 cm^2. All the electrodes were provided by Metrohm. The potentiostat used was a ZAHNER XPot, and the cyclic voltammograms were collected using the software package Power-Potentiostats Inspector V 8.1.

3.2.2.3 Electrochemical deposition of PEDOT on platinum electrode

Four solutions with different salts were prepared to electropolymerize EDOT on the platinum electrode (Pt) potentiodynamically. The used salts were $LiClO_4$, LiTFS, TBAB and TBAP **[3.3, 3.4]**. Each salt confers a different dopant (anion) to the PEDOT film on the platinum (consult Figure 3.2). Thus, the electrodeposited films on the Pt electrode were PEDOT:ClO_4^-, PEDOT:TFS^-, and PEDOT:Br^-. Each solution contained a salt at a concentration of 0.1 mol/L with the EDOT monomer at a concentration of 0.01 mol/L in acetonitrile. For all the prepared solutions, the conditions of the electro-polymerization were the same. A three-electrode system was used with a Pt electrode as a working electrode and a glassy carbon as a counter electrode, while the reference electrode was an Ag/AgCl. The scan rate was 50 mV/s and the applied potential was from -500 mV to 1400 mV, whereas the number of cycles was 5 cycles. Before each electro-polymerization, all the electrodes were cleaned thoroughly: The platinum electrode was cleaned by DI water and sandpaper p1500, the glassy carbon electrode was cleaned by DI water and sandpaper p2000 and the reference electrode was rinsed by DI water. Finally, all the employed electrodes were rinsed by acetonitrile to avoid water in the electrochemical system.

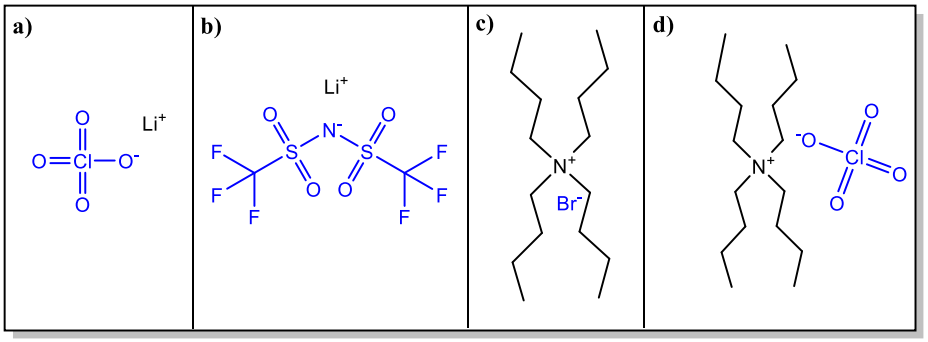

Figure 3.2. Salts used to electrodeposit PEDOT **a)** $LiClO_4$, **b)** LiTFS, **c)** TBAB, **d)** TBAP.

3.2.2.4 Cyclic voltammetry assessment

Electrocatalytic activity for the I_3^-/I^- redox couple of the PEDOT films prepared with $LiClO_4$, LiTFS, TBAB and TBAP were evaluated by using cyclic voltammetry (CV) in an acetonitrile solution containing 10 mmol/L of KI, 1 mmol/L of I_2 and 0.1 mol/L of $LiClO_4$ **[3.3, 3.4]**. The reference and counter electrodes were respectively Ag/AgCl 3 M KCl and glassy carbon which were cleaned every time before and after the use. For each PEDOT film, cyclic voltammograms were recorded between -500 mV and 1500 mV at different scan rates: 10, 25, 50 and 100 mV/s. To ensure that the analyses were carried out under the same conditions, all the prepared PEDOT films were assessed using the same set of electrodes and the same redox solution of (I_3^-/I^-).

3.3 Results and discussion

3.3.1 Catalytic activity of PEDOT towards the Fe^{3+}/Fe^{2+} system

3.3.1.1 Electrodeposition of PEDOT on graphite

The electro-polymerization of EDOT took place on the working electrode surface (graphite sheet) for 12 cycles. The graph of Figure 3.3 shows the evolution of the current intensity as the number of cycles increases, implying that with each cycle the PEDOT is growing layer by layer on the graphite sheet.

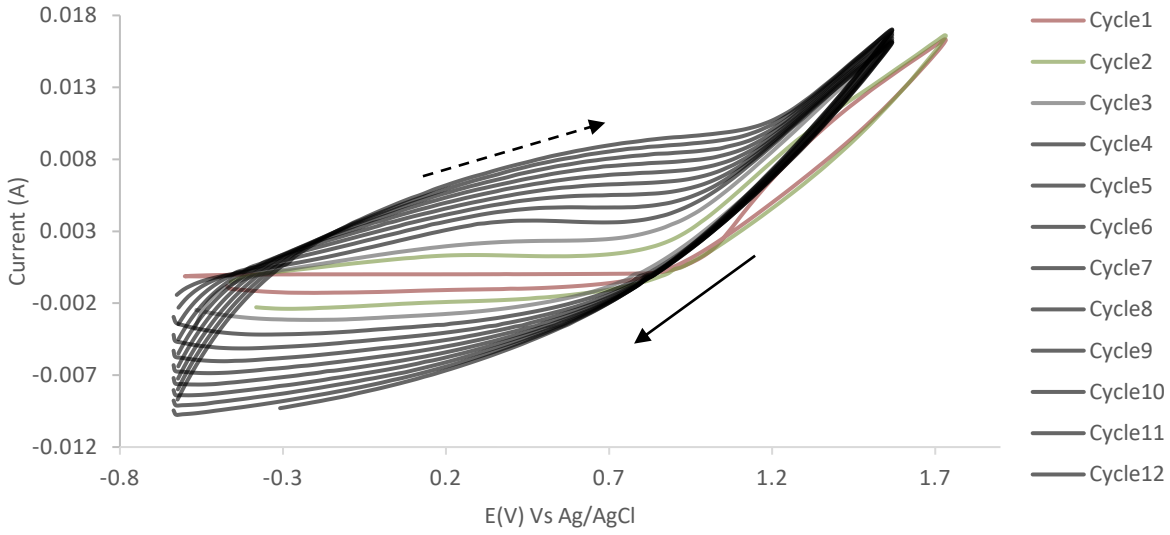

Figure 3.3. Electropolymerization of EDOT in 0.1 mol/L of $LiClO_4$ in 10% ACN/water solution. Scan rate = 100mV/s.

3.3.1.2 Electrocatalytic activity of PEDOT

Figure 3.4 shows the cyclic voltammograms of the Fe^{3+}/Fe^{2+} redox couple on the platinum, bare graphite and PEDOT/graphite working electrodes. Typically, two peaks are observed corresponding to an anodic peak attributed to the oxidation of Iron(II) and a cathodic peak attributed to the reduction of Iron(III). The redox reaction is the following $Fe^{3+} + e^{-} \leftrightharpoons Fe^{2+}$.

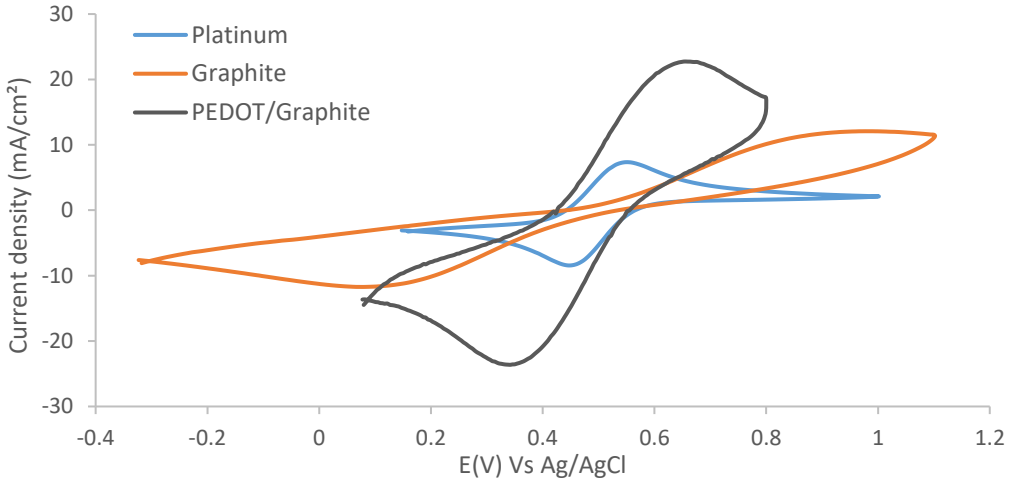

Figure 3.4. Comparison of the Graphite, PEDOT/graphite and platinum working electrodes at 25mV/s.

Table 3.1 shows the current density peaks of each voltammogram. The bare graphite electrode has the lowest values of the anodic peak (J_{pa}) and the cathodic peak (J_{pc}), whereas the PEDOT/graphite electrode has the highest values, even higher than the current density peaks of the bare platinum electrode. This preliminary result demonstrates that the conductive polymer PEDOT has a better catalytic effect towards the oxidation and the reduction of the Fe^{3+}/Fe^{2+} redox system. Therefore, further experiments were made to prove and verify this result by comparing the catalytic effect of PEDOT films made with different dopants to the bare platinum electrode.

Table 3.1. Values of oxidation and reduction current peaks for three electrodes: Platinum, graphite, PEDOT/graphite.

Working electrodes	J_{pa} (mA/cm^2)	J_{pc} (mA/cm^2)
Bare graphite	5.7514	-5.5829
Bare Pt	8.1711	-9.2117
PEDOT/graphite	17.1405	-15.6741

3.3.2 Catalytic activity of PEDOT towards the I_3^-/I^- system

3.3.2.1 Electro-polymerization of PEDOT in different salts

The cyclic voltammograms of the electro-polymerization of EDOT with different salts are shown in Figures 3.5 to 3.7. The four figures show the succession of 5 cycles of electro-polymerization indicating the film growth of PEDOT. However, each figure shows also some dissimilarities that can be resumed in two parameters: The oxidation peaks (I_{peak}) of the EDOT and the oxidation potentials (E_{onset}) of the EDOT **[3.5]**. Therefore, for each salt, these two parameters were extracted.

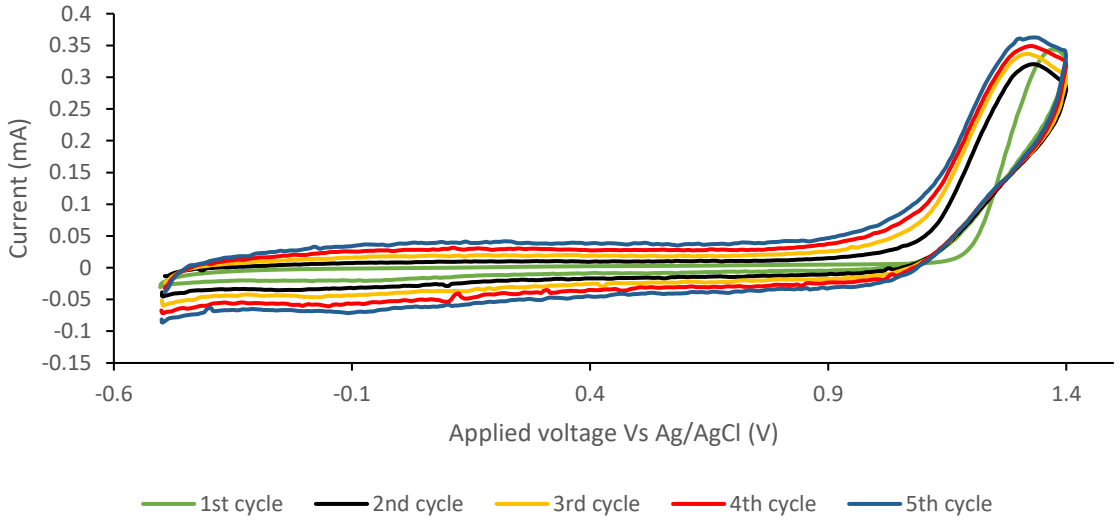

Figure 3.5 Electro-polymerization of EDOT (0.01M) with LiClO4 (0.1M) in ACN.

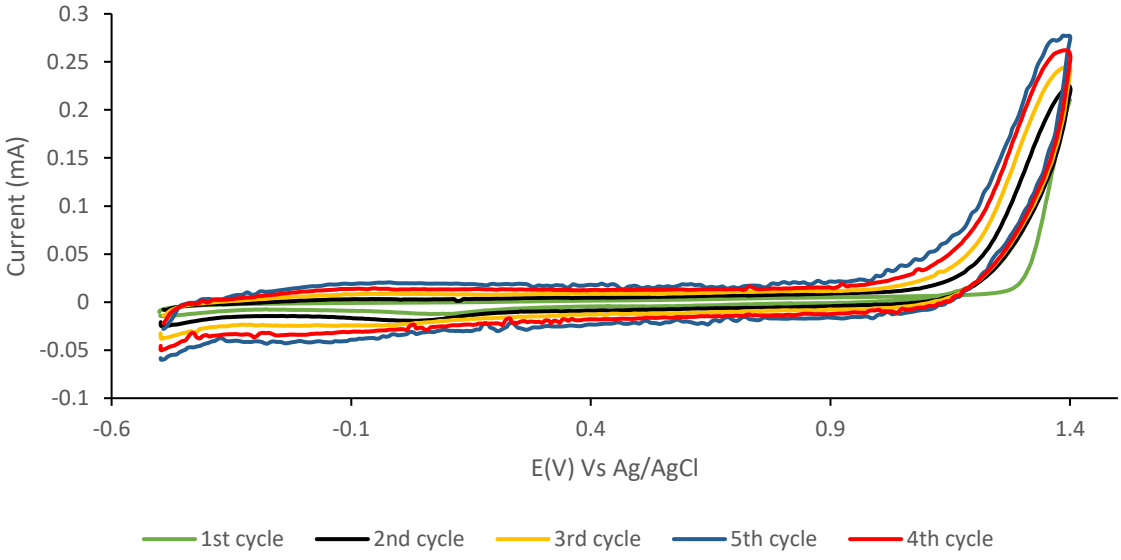

Figure 3.6: Electro-polymerization of EDOT (0.01M) with LiTFS (0.1M) in ACN.

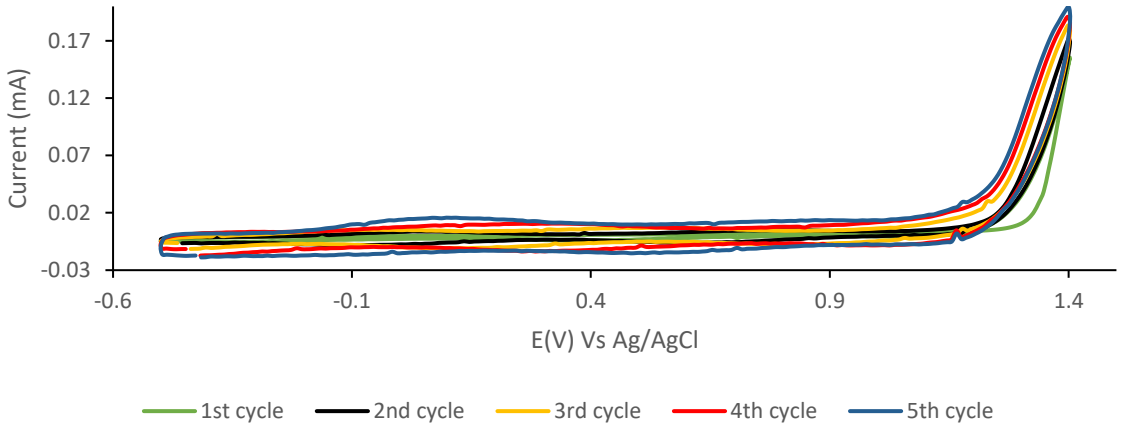

Figure 3.7. Electro-polymerization of EDOT (0.01M) with TBAB (0.1M) in ACN.

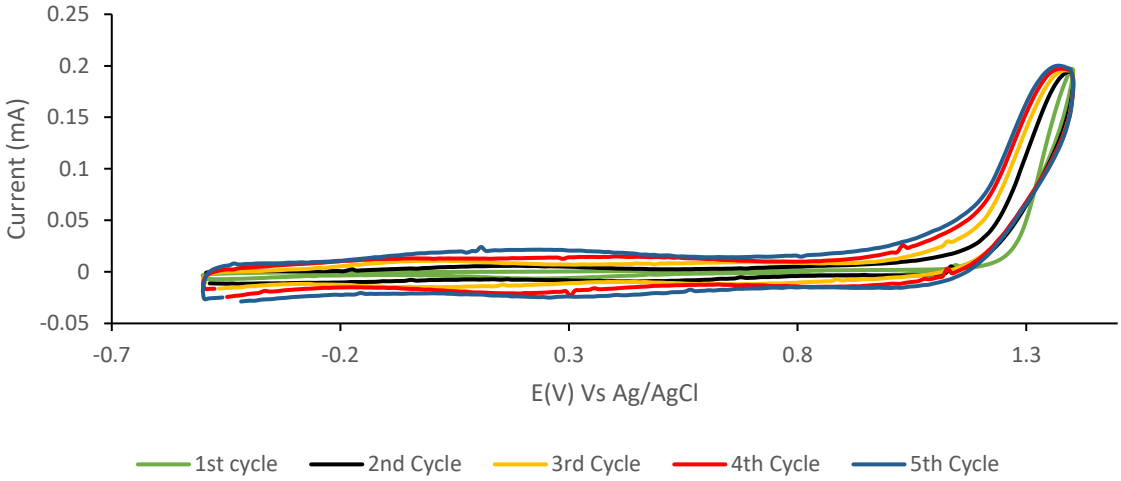

Figure 3.8. Electro-polymerization of EDOT (0.01M) with TBAP (0.1M) in ACN.

The oxidation peak was extracted from the fifth cycle to account for all the polymer film deposited on the platinum electrode. Whereas the oxidation potential was determined by tracing the onset of the first cycle of the electro-polymerization. The results are summarized in Table 3.2 and the detail of the graphical method used to extract I_{peak} and E_{onset} are in **Appendix B and C.**

Table 3.2. Effect of the used salt on the current peak and onset potential of EDOT oxidation

Salt	I_{peak} (mA)	E_{onest} (V)
$LiClO_4$	0.3281	1.1020
LiTFS	0.2597	1.2253
TBAB	0.1886	1.2384
TBAP	0.1846	1.1658

As shown by the data of the Table 3.2, each salt affects the polymerization of the EDOT either by altering the oxidation potential of EDOT or by altering the oxidation peak.
Before starting to analyze the numbers, a brief explanation of the two parameters is necessary:

- The current peak intensity of the oxidation (I_{peak}) is a direct measure of the quantity of EDOT monomers that were oxidized into PEDOT. Since EDOT is an electro-active monomer, it undergoes an oxidation, and the higher is the number of oxidized monomers, the higher is the I_{peak}.
- On the other hand, the oxidation onset of EDOT (E_{onset}) is an indicator of the ease of the oxidation of EDOT in the presence of a given salt. Thus, the lower is the value of E_{onset}, the easier (faster) is the oxidation of EDOT.

Now looking again at the data of Table 3.2 and Figure 3.9 and keeping in mind that the salt is an ionic molecule that decomposes into a pair of an anion and a cation, the analyses can be resumed.
At first glance, two voltammograms are remarkable: the electro-polymerization of EDOT in the presence of lithium perchlorate salt ($LiClO_4$) and the electro-polymerization of EDOT in the presence of tetrabutylammonium bromide salt (TBAB).

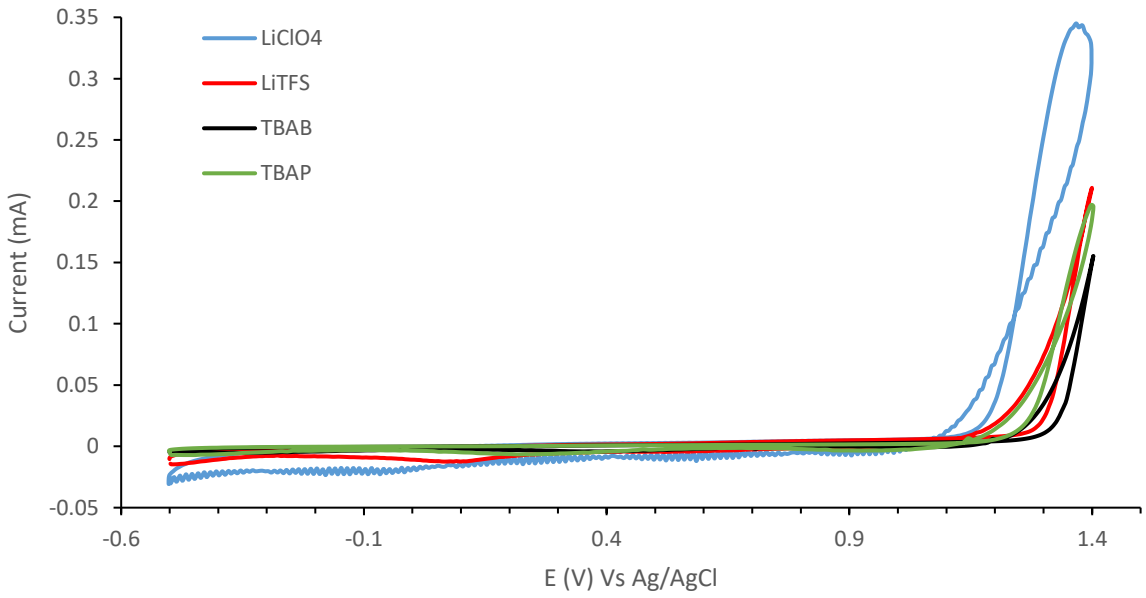

Figure 3.9. First cycle of the electro-polymerization of EDOT in different salts: [EDOT]=0.01 M, [salt]=0.1 M, counter electrode is glassy carbon, working electrode is platinum.

The $LiClO_4$ salt yields the best results with a current oxidation peak of I_{peak} = 0.3281 mA and an oxidation onset of E_{onset} = 1.102 V. However, the TBAB salt yields poor results with an onset potential of E_{onset} =1.2384 V and a current peak intensity of I_{peak} = 0.1886 mA. This comparison suggests that the type of anions and cations present at the moment of the formation of PEDOT films influences the process of the electro-polymerization.

3.3.2.1.1 Effect of the anion of the salt on the electro-polymerization

To study the effect of the anions, it is important to exclude the effect of cations. This is done through comparing two salts that have the same cation but differ in the anion. By inspecting the $LiClO_4$ and LiTFS voltammograms, it is clear that the $LiClO_4$ promotes the oxidation of EDOT better than the LiTFS. This is proved by the values of the current peaks, $I_{peak}(LiClO_4)$ = 0.3281 mA and I_{peak}(LiTFS) = 0.2597 mA , and the oxidation onsets , $E_{onest}(LiClO_4)$ = 1.102 V and E_{onest}(LiTFS) = 1.2253 V. This result can be explained by the Van der Waals volume of the two anions which are 57.09 $Å^3$ for the ClO_4^- and 156.68 $Å^3$ for the TFS^- **[3.6b]**. This implies a higher diffusion coefficient for ClO_4^- that gave rise to the fastest electro-polymerization of EDOT. In fact, the anion plays the role of a compensator of charge for the oxidized EDOT, therefore the faster it diffuses to the electrode surface and dope the EDOT, the quicker the reaction of the electro-polymerization would happen. In the case of a "heavy anion", EDOT oxidation will be delayed as well as the growth of the next polymer layer **[3.13]**.

The same logical approach can be applied to compare TBAB and TBAP salts. The former salt has a bromide anion (Br^-) with a diffusion coefficient of $2.08*10^{-5}$ cm^2/s **[3.6a]**. On the other hand, TBAP salt has a perchlorate anion (ClO_4^-) with a diffusion coefficient of $1.792*10^{-5}$ cm^2/s **[3.6a]**. As a consequence of these values, the TBAP salt yields a faster and better electro-polymerization of EDOT.

3.3.2.1.2 Effect of the cation of the salt on the electro-polymerization

$LiClO_4$ and TBAP salts share the same anion, perchlorate (ClO_4^-) , thus they can be compared to draw out the effect of the cations on the PEDOT formation. For the first salt $I_{peak}(LiClO_4)$= 0.3281 mA and $E_{onest}(LiClO_4)$ = 1.102 V, whereas for the second one I_{peak}(TBAP) = 0.1846 mA and E_{onest}(TBAP) = 1.1658 V. Although both salts have the same anion, they don't exhibit the same behaviors for the oxidation of EDOT. TBA^+ and Li^+ are different cations that have different Van der Waals volumes of 300.40 $Å^3$ and 25.25 $Å^3$

respectively **[3.6]**. Because of its volume, TBA^+ cations exercise a hindrance effect and impede the diffusion of the monomer and the dopant (anion) to the electrode surface resulting in a slow electro-polymerization.

3.3.2.2 Electrocatalytic activity of PEDOT

The four obtained PEDOT-dopant films (electro-polymerized with different salts) were tested in the triiodide/iodide redox system to evaluate their catalytic activity for the I_3^- reduction.

Figure 3.10 shows the cyclic voltammograms (CVs) curves of the different PEDOT-dopant films and the bare platinum at 50mV/s (consult **Appendix D** for the CVs at different scan rates). These curves present two characteristic pairs of oxidation and reduction peaks ascribed to the triiodide/iodide redox reaction and the iodine/triiodide redox reaction **[3.7, 3.8]**. The redox reaction occurring at lower potentials (between 0 and 0.3V *vs* Ag/AgCl) corresponds to the reaction of $I_3^- + 2e^- \rightleftarrows 3I^-$, whereas the redox reaction occurring at higher potentials (between 0.4 and 0.9V *vs* Ag/AgCl) corresponds to the reaction of $3I_2 + 2e^- \rightleftarrows 2I_3^-$.

It is noteworthy to point out the peak that is occurring between 1.3V and 1.5V in the PEDOT films but not in the platinum electrode. It represents the overoxidation of the PEDOT film and corresponds to the same potential window reported by previous works **[3.9, 3.10]**. Normally, in the DSSC, only the reduction of I_3^- occurs on the surface of the counter electrode, thus in our analyses of the voltammograms only the peaks corresponding to the I_3^-/I^- redox couple are deciphered. The parameters extracted from the CVs are the cathodic peak current (I_{pc}), the anodic peak current (I_{pa}), the oxidation potential (E_{ox}), the reduction potential (E_{red}) and the peak-to-peak separation (ΔE_{pp}). Through these parameters it is possible to estimate the catalytic activity of the prepared PEDOT films **[3.11]**. All the mentioned parameters and how to extract them from a voltammogram are illustrated in **Appendix E**.

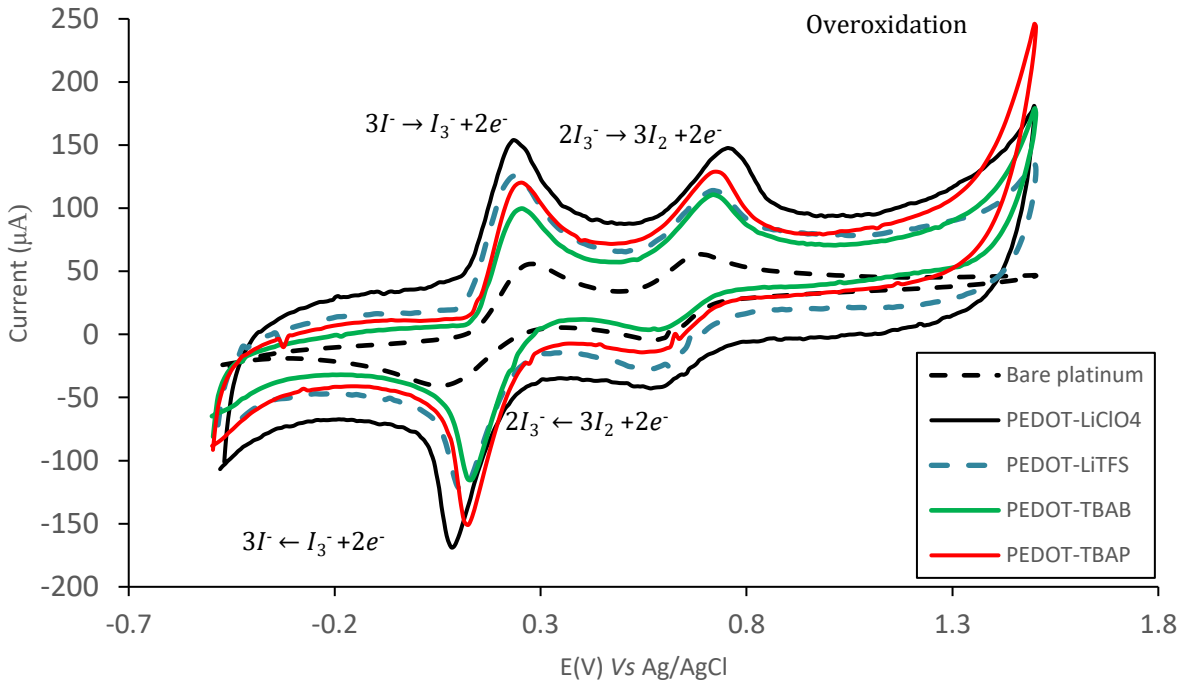

Figure 3.10. Cyclic voltammograms of the triiodide/iodide redox couple for the prepared PEDOT films and the platinum electrode at 50 mV/s.

From Figure 3.10, it is shown the different CVs for the different PEDOT films electrodes and compared with the bare platinum electrode. Furthermore, significant information is drawn out from those CVs and stored in Table 3.7. Through this data, it is demonstrated that all the PEDOT films prepared with various salts exhibit better results than the platinum. For the PEDOT-salt/Pt electrodes, the cathodic current peaks (I_c) vary from -101.24 μA to -141.49 μA, whereas the bare platinum electrode has an I_c of -40.534 μA. This reflects the quantity of the reduced I_3^- ions on the surface of each electrode. Another parameter is the cathodic to anodic current peaks ratio ($|Ic/Ia|$) that reflects the reversibility of the redox reaction on the electrode and by extension its kinetics. Ideally it is equal to 1 **[3.12]**, which means that the system is 100% reversible. The results show that this ratio is deviated from the unit which implies that the reduction and oxidation of the triiodide/iodide redox system is a quasi-reversible system. However, the platinum electrode and the PEDOT-TBAP/Pt electrode have a large deviation from the unit (0.2585 and 0.3021 respectively). At the same time the other three PEDOT-salt electrodes have a small deviation from the unit which means that they reduce and oxidize the triiodide/iodide anions in a more reversible process. Another parameter for the reversibility is the peak to peak separation (ΔEpp) **[3.12]**. The bare platinum has a value of 224.7 mV, but at the same time the PEDOT-salt/Pt electrodes have nearly half of that

value (around 127mV to 140mV). This affirms that PEDOT electrodes confer more reversibility to the redox system. Gathering all these parameters together, it is obvious that PEDOT modified electrodes have a better catalytic activity than the bare platinum.

Table 3.3. Parameters of CVs at 50mV/s for the prepared electrodes.

Electrodes	Ic (µA)	Ia (µA)	Ic/Ia	Ered (mV)	Eox (mV)	ΔEpp (mV)
Bare Pt	-40.534	54.6657	0.7415	56.3	281.0	224.7
PEDOT-$LiClO_4$/Pt	-135.270	121.3150	1.1150	88.2	227.5	139.3
PEDOT-LiTFS/Pt	-107.470	104.4470	1.0289	110.2	239.7	129.5
PEDOT-TBAB/Pt	-101.240	91.0219	1.1122	129.8	256.8	127.0
PEDOT-TBAP/Pt	-141.490	108.6650	1.3021	123.7	0.252.0	128.3

3.3.2.2.1 Reaction mechanism of the I_3^-/I^- redox couple on the modified PEDOT electrodes

In order to enhance the performances of the counter electrodes of the DSSC, it is mandatory to understand the mechanism of the reduction of I_3^- ions on the surface of the PEDOT. Two models are proposed for the reduction of the I_3^-. The first model suggests that the reduction is controlled by the adsorption of the anions on the electrode surface. The second model proposes that the diffusion is the prevailing step in reduction of the I_3^- ions. It is noteworthy to know that the two mechanisms exist all the time but depending on the conditions of the reduction, one of them will be the rate-determining step of the reaction **[3.13, 3.14]**. Through cyclic voltammetry, it is possible to tell whether the mechanism of the reduction of I_3^- ions is diffusion or adsorption controlled. Each model is described by an empirical equation. The diffusion control mechanism can be revealed using the Randles-Sevcik equation **[3.15]**:

$$Ip = 0.4463nF\sqrt{\frac{nFD}{RT}}AC\sqrt{v} \qquad (1)$$

where I_p is the peak current, n is the number of electrons, F is the Faraday constant, T is the temperature in Kelvin, R is the gas constant, A is the surface area of the working electrode, D is the diffusion coefficient of the electroactive species, C is the bulk concentration of the electroactive species, and ν is the scan rate employed in the CV

measurements. On the other hand, the adsorption control mechanism is described by the equation **[3.12]**:

$$Ip = \frac{n^2F^2}{4RT} vA\Gamma \qquad (2)$$

where Γ is the surface coverage of the adsorbed species in mol cm^{-2}.

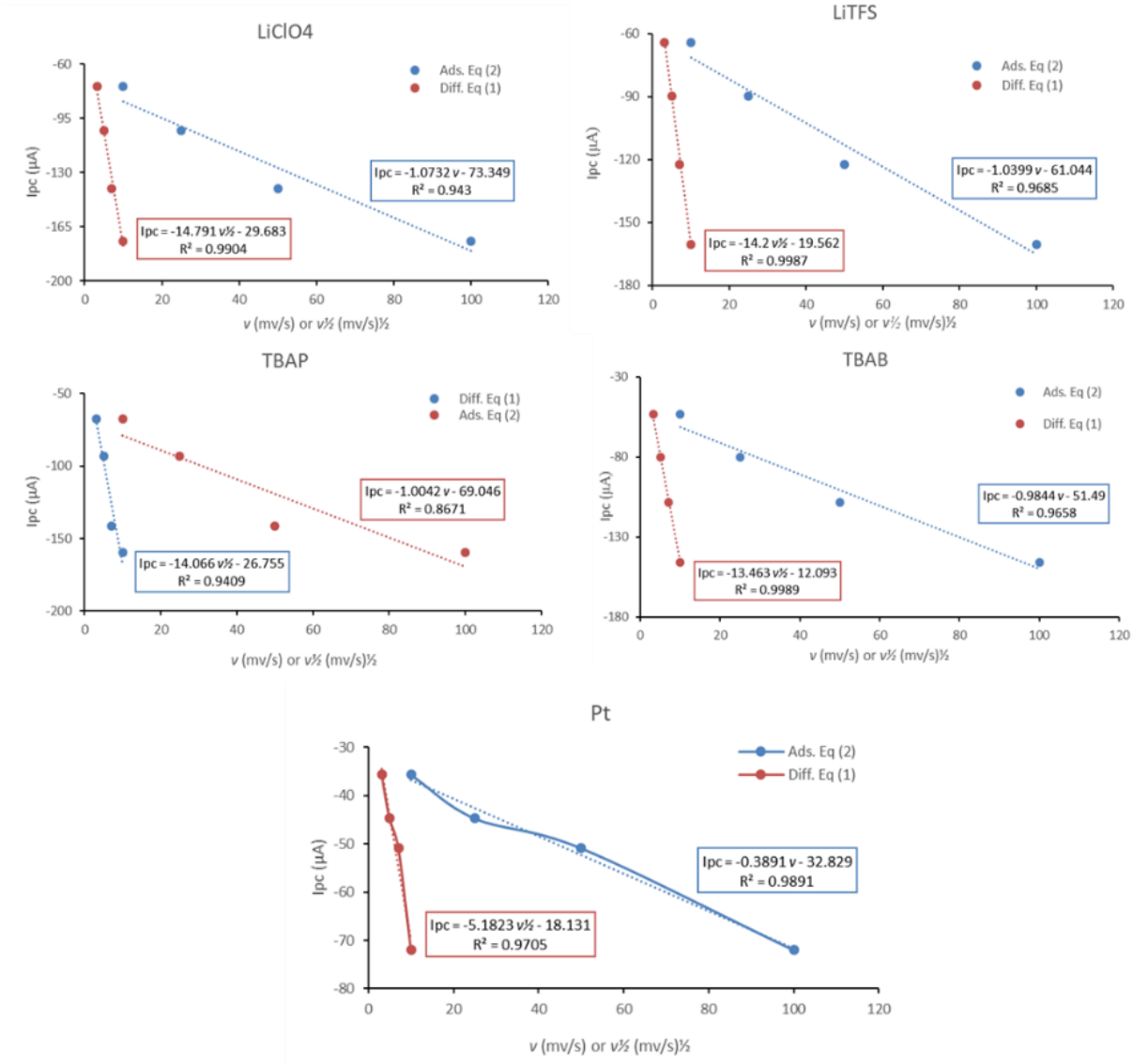

Figure 3.11. Data fitting of the based PEDOT-salt electrodes and the platinum electrode.

From equation (1), the current response for a freely diffusing redox species should vary linearly with the square root of the scan rate. And from equation (2), adsorbed species should have a linear relation between the current peak and the scan rate. These two model equations were employed to plot the data collected from the CVs. For each electrode (PEDOT modified or bare platinum), both equations were used to plot the

corresponding data. The obtained curves are displayed in Figure 3.11. By comparing the coefficient of determination (R^2), it is concluded that the model that best fits the PEDOT modified electrodes is the diffusion model. At the same time, the bare platinum electrode exhibits a better linearity through the adsorption model. From these two observations, an important feature of the PEDOT is revealed: It changes the kinetics of the reduction of the I_3^- anion from an adsorption-controlled reaction to a diffusion-controlled reaction

3.4 Conclusions

This chapter showed to a certain extent, the effect of the electro-polymerization on the catalytic behavior of the PEDOT towards the redox couple of triiodide/iodide. Regarding the electrochemical formation of PEDOT, we can draw a conclusion that using smaller anions for the doping is more suitable to have fast kinetics of electro-polymerization. Another fact is that cations can affect heavily the kinetics of the electro-polymerization by blocking the diffusion flux of the dopants or the monomer to the surface electrode. Thus, choosing the right salt is decisive for the PEDOT film formation.

The fact that PEDOT changes the mechanism of the reduction of I_3^- ions from an adsorption control to a diffusion control is critical, because by changing the synthesis process of PEDOT, it is possible to tailor its catalytic behavior as a counter electrode in the DSSC. Also, it is important to know that the obtained results for the triiodide/iodide redox system are purely specific to this work and can change by changing the conditions under which the experience is conducted. Among these conditions, there are the concentration of triiodide/iodide, the solvent used, the thickness of the polymer film, the pH of the solution and the support electrolyte which they can all alter the mechanism of the reduction of the triiodide on the PEDOT film. This issue requires more investigation especially when the technology of the Dye-Sensitized Solar Cells is advancing at a high pace and the redox systems used are shifting to new modern ones with better efficiencies.

3.5 References

[3.1] L. Bay, K. West, B. Wintherjensen and T. Jacobsen. *Electrochemical reaction rates in a dye-sensitised solar cell—the iodide/tri-iodide redox system*, Solar Energy Materials and Solar Cells **2006**, 90(3), pp.341-351.

[3.2] H. Karaosmanoglua, J. Travas-Sejdica and P.A. Kilmartina. *Comparison of Organic and Aqueous Polymerized PEDOT Sensors,* Molecular Crystals and Liquid Crystals **2014**, 604(1), p. 233-239

[3.3] Xia, J., Masaki, N., Jiang, K. and Yanagida, S. *The influence of doping ions on poly(3,4-ethylenedioxythiophene) as a counter electrode of a dye-sensitized solar cell*. Journal of Materials Chemistry, **2007**, 17(27), p.2845.

[3.4] A. del Valle, M. *Influence of the Supporting Electrolyte on the Electrochemical Polymerization of 3,4-Ethylenedioxythiophene. Effect on p- and n-Doping/Undoping, Conductivity and Morphology*. International Journal of Electrochemical Science, **2016**, pp.7048-7065.

[3.5] Del-Oso, J., Frontana-Uribe, B., Maldonado, J., Rivera, M., Tapia-Tapia, M. and Roa-Morales, G. *Electrochemical deposition of poly[ethylene-dioxythiophene] (PEDOT) films on ITO electrodes for organic photovoltaic cells: control of morphology, thickness, and electronic properties*. Journal of Solid State Electrochemistry, **2018**, 22(7), pp.2025-2037.

[3.6] **a)** CRC Handbook of Chemistry and Physics, 93rd Edition. (**2016**). **b)** Chemicalize.org.

[3.7] Wang, H., Wei, W. and Hu, Y. *Efficient ZnO-based counter electrodes for dye-sensitized solar cells.* Journal of Materials Chemistry *A*, **2013**, 1(22), p.6622.

[3.8] Guo, J., Liang, S., Shi, Y., Hao, C., Wang, X. and Ma, T. *Transition metal selenides as efficient counter-electrode materials for dye-sensitized solar cells.* Physical Chemistry Chemical Physics, **2015**, 17(43), pp.28985-28992.

[3.9] Hui, Y., Bian, C., Wang, J., Tong, J. and Xia, S. *Comparison of Two Types of Overoxidized PEDOT Films and Their Application in Sensor Fabrication*. Sensors, **2017**, 17(3), p.628.

[3.10] Zykwinska, A., Domagala, W., Pilawa, B. and Lapkowski, M. *Electrochemical overoxidation of poly(3,4-ethylenedioxythiophene)—PEDOT studied by*

means of in situ ESR spectroelectrochemistry. Electrochimica Acta, **2005** ,50(7-8), pp.1625-1633.

[3.11] F. Gong, H. Wang, X. Xu, G. Zhou and Z. S. Wang, J. *In Situ Growth of Co0.85Se and Ni0.85Se on Conductive Substrates as High-Performance Counter Electrodes for Dye-Sensitized Solar*. CellsAm.Chem. Soc., **2012**, 134, 10953

[3.12] **a)** A. Bard, and L. Faulkner (**2000**). *Electrochemical methods and applications*. New York: Wiley-Interscience. **b)** N. Elgrishi, K. Rountree, B. McCarthy, E. Rountree, T. Eisenhart, and J. Dempsey. *A Practical Beginner's Guide to Cyclic Voltammetry*. Journal of Chemical Education, **2017**, 95(2), p. 197-206.

[3.13] Tang, Y., & Pan, X. *Influence of Different Electrolytes on the Reaction Mechanism of a Triiodide/Iodide Redox Couple on the Platinized FTO Glass Electrode in Dye-Sensitized Solar Cells*. The Journal of Physical Chemistry, **2010**, *C,114*(9), 4160-4167.

[3.14] Levenspiel, O. (**1999**). *Chemical reaction engineering*. New York: Wiley.

[3.15] Lee, J., Lee, J., Ahn, Y., & Kang, G. *Efficient Recovery of Silver from Crystalline Silicon Solar Cells by Controlling the Viscosity of Electrolyte Solvent in an Electrochemical Process.* Applied Sciences, **2018**, 8(11), 2131.

Chapter 4: Mathematical modelling

4.1 Introduction

Describing physical and chemical phenomena mathematically is the essence of the scientific research. In fact, interpreting the experimental results through specific theories and equations allows to decipher the parameters that influence the phenomena and at the same time to rectify the employed theories. Herein a model for the potentiodynamic and potentiostatic responses of poly(3,4-ehtylenedioxythiophene) (PEDOT) and poly(3,4-ehtylenedioxythiophene):poly(styrene sulfonate) (PEDOT:PSS) were developed. The model is essentially based on the Nernst-Planck-Poisson formalism.

Moreover, from the previous chapters and their discussions, it was shown that the voltammograms of the PEDOT exhibit both faradaic and non-faradaic currents, therefore a model to predict faradaic processes was also developed based on the Butler-Volmer equations.

This chapter is divided into two main parts: The Butler-Volmer model for faradaic processes and the Nernst-Planck-Poisson model for the ionic-electronic conductivity in the conducting polymers (PEDOT and PEDOT:PSS). In each part, the theoretical model is explained, and the results obtained were compared with experimental data. The importance of this comparison resides in the need to understand the parameters controlling the observed phenomena.

4.2 Butler-Volmer model

In faradaic processes, charge is transferred across the electrode-solution interface and causes an oxidation or a reduction to occur. This type of processes is described by the Butler-Volmer equations **[4.1]**. The model presented here is for predicting the cyclic voltammograms of the oxidation/reduction of the Fe^{3+}/Fe^{2+} redox couple on an electrode surface.

4.2.1 Experimental description

The experimental environment of the investigated reaction takes place in an electrochemical cell that encompasses a reference electrode (Ag/AgCl), a counter electrode and a working electrode, all immersed in the F^{3+}/Fe^{2+} solution in the presence

of 0.5 mol/L of hydrochloric acid. The solution was purged by argon to eliminate the interference of the dioxygen molecules. Cyclic voltammetry measurements were carried out by sweeping from the negative potential -0.6 V to the positive potential +0.6 V.

4.2.2 Model descriptions

The heterogeneous reaction of the oxidation and reduction of the F^{3+}/Fe^{2+} is represented by the scheme of Figure 4.1. Depending on the applied voltage at the working electrode, Fe^{3+} or Fe^{2+} will diffuse from the bulk solution to the electrode surface where reduction or oxidation takes place. Consequently, the species that appear by oxidation or reduction on the surface electrode will diffuse back to the bulk solution. Two paths are shown, the oxidation path of Fe^{2+} labeled by red color and the green-labeled path of the Fe^{3+} reduction.

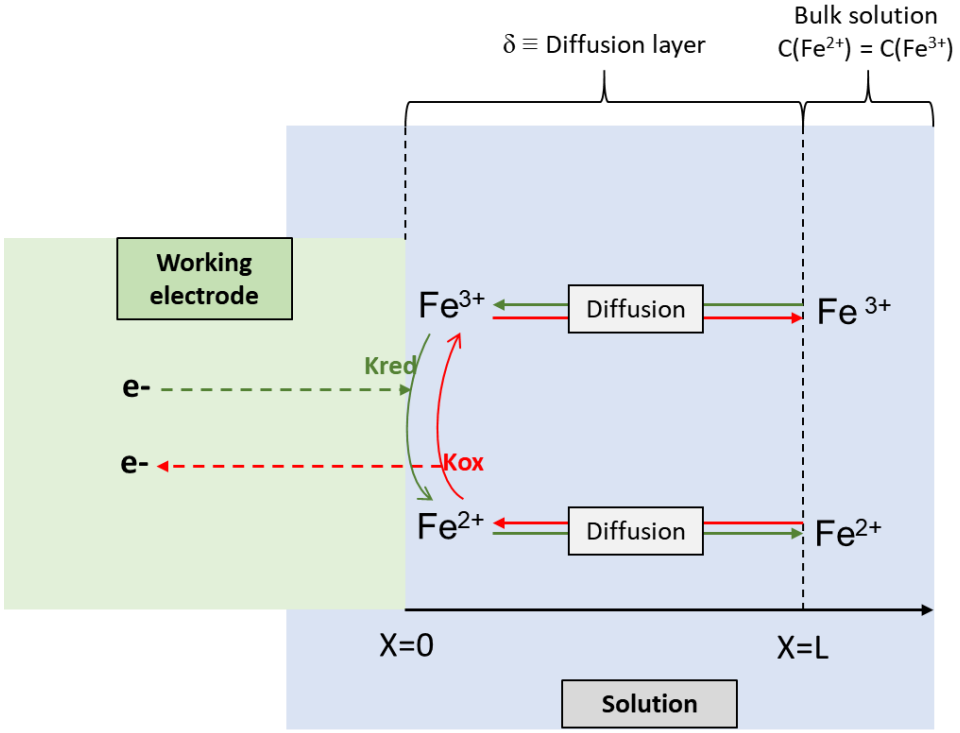

Figure 4.1. Scheme of the electrochemical system: The red arrows indicate the direction of the oxidation and the green arrow indicate the direction of the reduction.

4.2.3 Assumptions

The assumptions used to develop this model were as follows:

1) No homogenous reactions are occurring in the bulk reaction (omitted in this case of Fe^{3+}/Fe^{2+}, however, the developed model can consider a homogenous reaction in the bulk).

2) The transport of Fe^{3+} and Fe^{2+} by diffusion occurs only in the normal direction to the surface electrode (i.e., *x* direction).

3) The diffusion coefficients of Fe^{3+} and Fe^{2+} are equal.

4) The rates of the electrochemical reactions occurring on the surface electrode are based on the Butler-Volmer equations.

4.2.4 Governing equations

Conservation laws

By combining Fick's first law of diffusion and the mass balance, the following equations can be derived for both Fe^{2+} and Fe^{3+}:

$$\frac{\partial C_{Fe^{2+}}}{\partial t} = D_{Fe^{2+}} \frac{\partial^2 C_{Fe^{2+}}}{\partial^2 x} \quad \text{and} \quad \frac{\partial C_{Fe^{3+}}}{\partial t} = D_{Fe^{3+}} \frac{\partial^2 C_{Fe^{3+}}}{\partial^2 x}$$

where $D_{Fe^{2+}}$ and $D_{Fe^{3+}}$ are respectively the diffusion coefficients of Fe^{2+} and Fe^{3+}.

Initial conditions

When the system is at equilibrium (no voltage is applied to the working electrode), the concentrations of both species Fe^{2+} and Fe^{3+} are set equal to their bulk concentrations:

$$C_{Fe^{2+}}(x, 0) = C_{Fe^{3+}}(x, 0) = C_0$$

Boundary conditions

- *Boundary conditions at the electrode/solution interface, $x = 0$:*

At the surface of the working electrode, heterogenous reactions will be held. The process begins with the diffusion of species (Fe^{2+} or Fe^{3+}) from the bulk to the surface and then get oxidized or reduced on that surface. It is assumed that the rate of the diffusion of the species is equal to the rate of the reaction on the surface: the species that diffuse to the surface are immediately consumed by the redox reaction. This condition is described by the following equation:

$$J_{Fe^{3+}} = -D_{Fe^{3+}} \frac{\partial C_{Fe^{3+}}}{\partial x} = k_{ox} C_{Fe^{3+}}(0, t) - k_{red} C_{Fe^{2+}}(0, t)$$

From the stoichiometry of the heterogenous reaction, the flux of Fe^{2+} can be written as:

$$J_{Fe^{2+}} = -D_{Fe^{2+}} \frac{\partial C_{Fe^{2+}}}{\partial x} = -J_{Fe^{3+}}$$

Coefficients of the Butler-Volmer equation

$$k_{red} = k_0 \exp\left(-\alpha \frac{F}{RT}(E - E_0)\right) \qquad k_{ox} = k_0 \exp\left((1-\alpha) \frac{F}{RT}(E - E_0)\right)$$

- K_0 is the standard constant rate that infers about the rapidity of a system to reach the equilibrium **[4.1]**.
- α is the transfer coefficient defined as the fraction of the electrostatic potential energy affecting the reduction rate in an electrode reaction, with the remaining fraction $(1 - \alpha)$ affecting the corresponding oxidation rate **[4.2]**.
- F is the Faraday constant and it is equal to 96 485.33289 C mol^{-1}.
- R is the ideal gas constant and it is equal to 8.3144598 J mol^{-1} K^{-1}.
- T is the temperature and its set to 298.15 K.
- E_0 is the formal potential of Fe^{3+}/Fe^{2+} redox couple and E is the applied potential.

❖ *Boundary condition in the solution at* $x = L$:

At the position $x=L$, the diffusion layer and the bulk solution form an interface on which the concentration of a species is the same on both sides. This applies for the Fe^{2+} as well as the Fe^{3+}:

$$C_{Fe^{2+}}(L, t) = C_{Fe^{3+}}(L, t) = C_0$$

4.2.5 Results

The governing equations were implemented in *MATLAB* and solved through the *PEDPE* function (partial differential equation parabolic and elliptic). The partial differential equations were discretized in space to give ordinary differential equations (ODEs). These ODEs were integrated in time. The resulting model allowed to determine the cyclic voltammograms of the Fe^{3+}/Fe^{2+} redox couple. In addition, the model permitted to calculate the current intensity and the molar fluxes on the surface electrode. It was also possible through this model to predict the concentrations of the species (Fe^{3+} and Fe^{2+}) along the time and space. Besides, the thickness of the diffusion layer (δ) was estimated by employing the following equations **[4.1]**:

$$\delta = 6\sqrt{D\ t_f} \quad \text{and} \quad t_f = \frac{E_2 - E_1}{v}$$

where D is the diffusion coefficient of both Fe^{3+} and Fe^{2+} in cm^2/s and t_f is the time needed to sweep from the lowest voltage E_1 to the highest voltage E_2 at a defined scan rate v. Figure 4.2a shows the experimental and the predicted cyclic voltammograms at 25mV/s. Figure 4.2b shows the corresponding current-time graphs, which describe the variation of the current on the surface electrode. Both a and b plots show qualitative and quantitative agreement between the experimental data and the predictions.

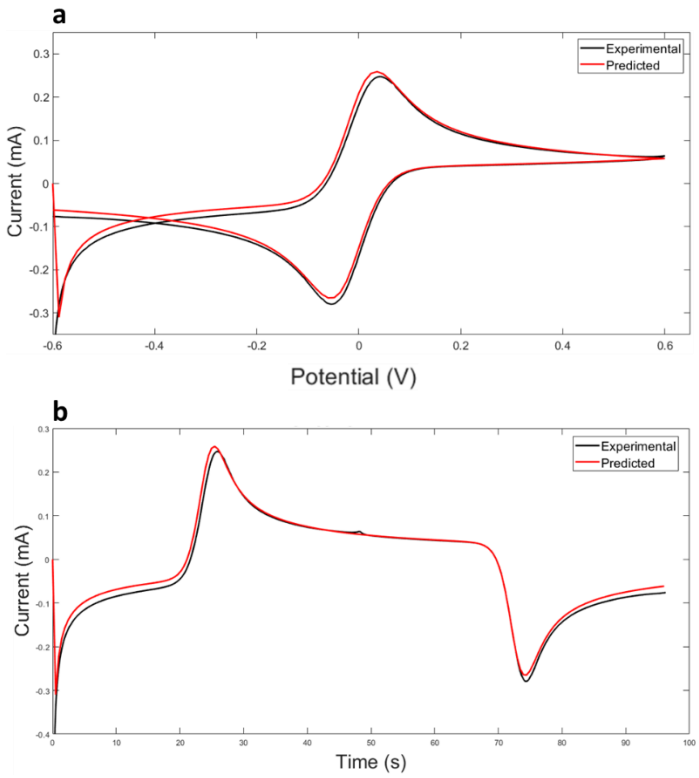

Figure 4.2. Predicted and experimental results at 25 mV/s for the solution of $[Fe^{3+}]= [Fe^{2+}]=0.05$ M. **a,** Predicted and experimental voltammograms. **b,** Predicted and experimental current-time curves.

Fitting of the experimental data with the prediction was carried out by changing three main parameters: The diffusion coefficient of the species (D), the standard constant rate (K_0) and the formal potential of the redox couple (E_0). Eventually, the parameters of the model that best fit the experimental data were chosen and they are shown in Table 4.1, as well as the estimated thickness of the diffusion layer.

Table 4.1. Simulation parameters at 25mV/s

D (cm^2 s^{-1})	**E_0 (V)**	**K_0 (cm s^{-1})**	**δ (cm)**
$\mathbf{0.65 \times 10^{-5}}$	-0.01	5×10^{-3}	0.15

Figure 4.3 shows the distribution of the concentrations of Fe^{3+} and Fe^{2+} along the time and the space. At *x*=0.15 cm, which corresponds to the thickness of the diffusion layer, the concentration is equal to 0.05 M which is the same concentration as the bulk (boundary condition). By approaching the electrode surface, *x*=0, the concentrations of Fe^{3+} and Fe^{2+} begin to change inversely: When $[Fe^{3+}]=0$, $[Fe^{2+}]=0.1$ mol L^{-1} , and when $[Fe^{2+}]=0$, $[Fe^{3+}]=0.1$ mol L^{-1}. These values agree with the cyclic voltammetry principles, because at t=0 , a sufficiently negative potential is applied that reduces all the Fe^{3+}.resulting in the production of Fe^{2+}. Afterwards, and through the course of the cyclic voltammetry, a sufficiently positive voltage is applied and the Fe^{2+} species oxidize to Fe^{3+}.

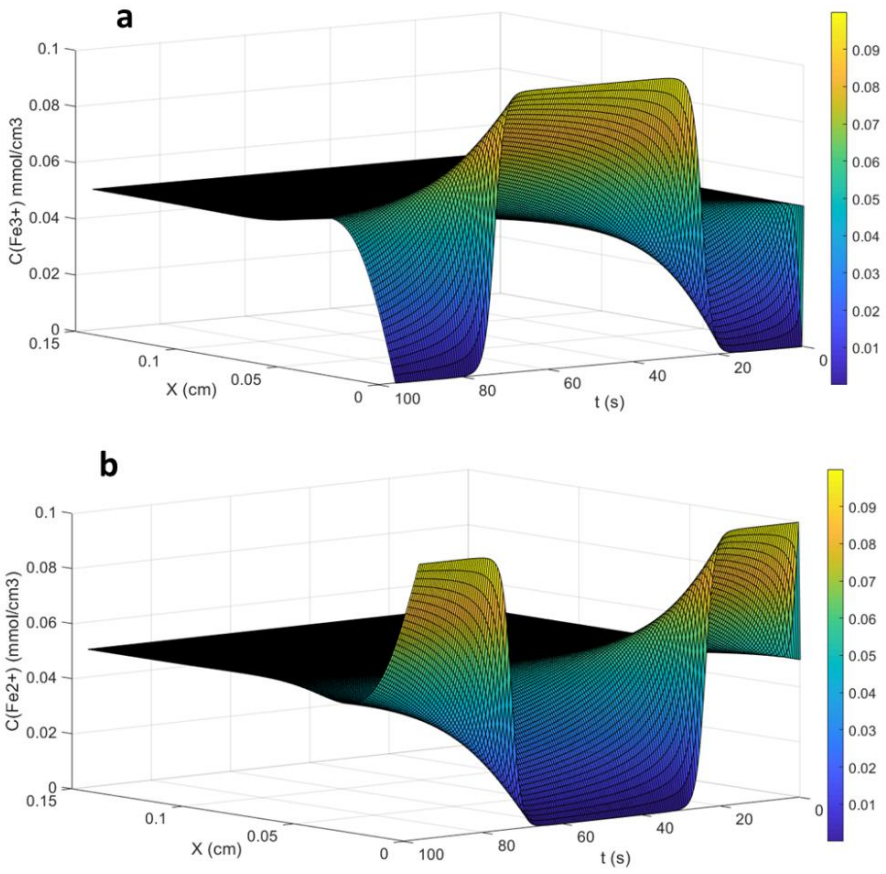

Figure 4.3. Predicted concentrations profiles of the redox species. a, Fe^{3+} and b, Fe^{2+} at 25mV/s.

The same results can be obtained for any desired scan rate, Figure 4.4 shows the predicted and the experimental voltammograms of Fe^{3+}/Fe^{2+} at 50mV/s. The predicted curve fits exactly with the experimental data, which indicates that the model describes accurately the faradaic current produced by the oxidation or the reduction of the Fe^{3+}/Fe^{2+} couple.

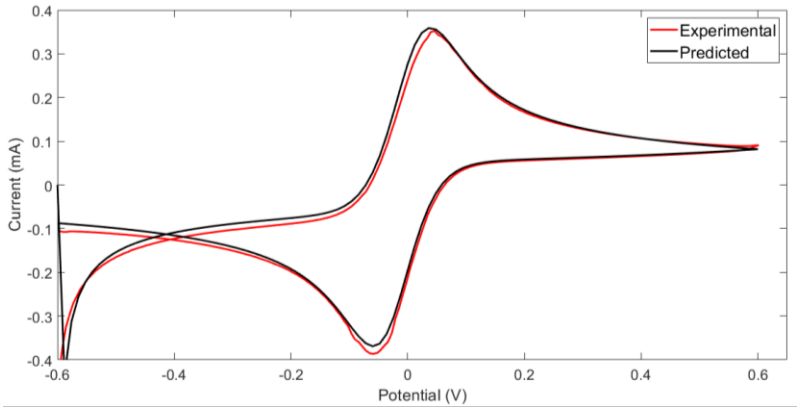

Figure 4.4. Predicted and experimental voltammograms of the Fe^{3+}/Fe^{2+} at 50mV/s

4.3 Nernst-Planck-Poisson model

This model describes the ionic and electronic transport mechanisms in PEDOT and PEDOT:PSS. These polymers exhibit a mixed ionic-electronic conductivity and their chemical structures are shown is Figure 4.5. The difference between the two polymers is that PEDOT has no fixed anions on its chains, whereas PEDOT:PSS does. In fact, PSS have sulfonate anions that are linked to the polystyrene backbone, hence they are not mobile. As a consequence of this structural difference, it is suspected that the ionic-electronic conductivity is influenced. Therefore, the model developed here tries to give a simple analytical description of the ionic and electronic transport within the polymers. The model is treated within the Nernst–Planck–Poisson formalism as outlined below.

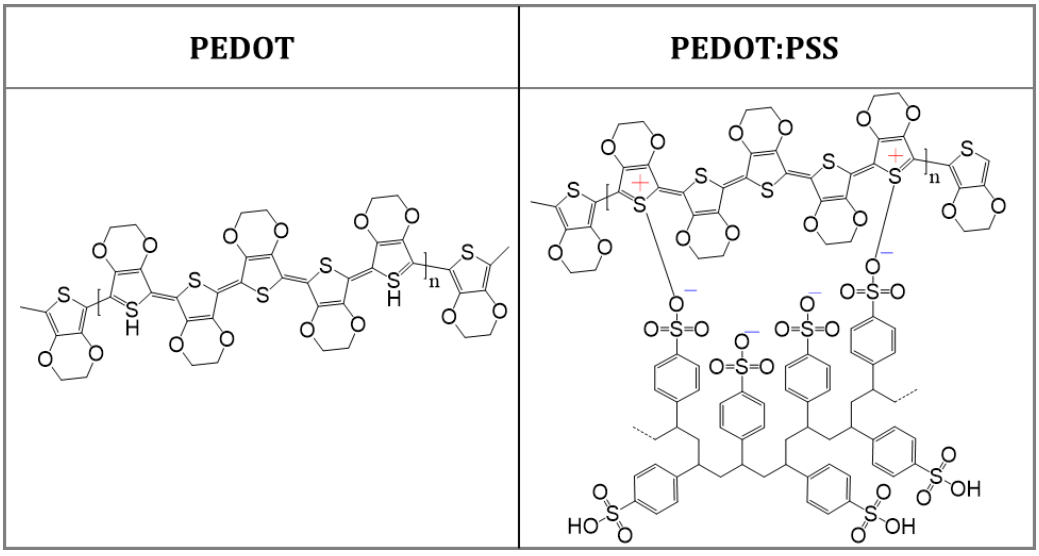

Figure 4.5. Chemical structures of PEDOT and PEDOT:PSS.

4.3.1 Experimental description

PEDOT:PSS was electro-polymerized by cyclic voltammetry on the working electrode that consisted of fluorine doped tin oxide glass (FTO). The reference electrode was the Ag/AgCl used through all over the experiments. The solution used for the electro-deposition contained 0.01 mol L^{-1} of EDOT (monomer), 0.1 mol L^{-1} of PSS and 0.1 mol L^{-1} $LiClO_4$. PEDOT was also prepared by electro-polymerization on top of graphite electrode by cyclic voltammetry. The solution used for the electro-deposition of PEDOT was 0.01 mol L^{-1} of EDOT with 0.1 mol L^{-1} $LiClO_4$. After the electro-polymerization, both of the PEDOT/graphite and PEDOT:PSS/FTO electrodes were assessed by applying a fixed voltage and then measuring the resulting current in function of time. Two experiences were carried out: Oxidation and reduction. Before proceeding, the polymer film needed to be prepared by either reducing the film or oxidizing it. Thus, initially the film is fully doped with cations (reduced) or doped with anions (oxidized). The oxidation applied potential was +1 V (from previous chapters it was proved that the oxidation potential of PEDOT is less than 1 V). On the other hand, the applied potential of the reduction was -1 V (also from previous chapters, the reduction was less negative than -1 V).

This step of "preparing" the polymer film is crucial for the whole process of the modelling, since initial conditions constitute the first building block of the numerical calculations of the problem. For the PEDOT film, cyclic voltammetry was also carried out by sweeping from 0 V to -1 V, and the resulting shape of the voltammogram was predicted.

N.B: All the voltages mentioned are *vs.* Ag/AgCl (3 mol L^{-1}) electrode.

4.3.2 Model descriptions

The geometry considered for the model is presented in figure 4.6. It consists of a film of polymer, PEDOT or PEDOT:PSS, sandwiched between an electrolyte solution to the left, and an electrode to the right. Two cases are demonstrated: a) The first case is when the voltage is negative, holes are evacuated from the film to the electrode and the cations are injected from the solution to the film. b) The second case is when the voltage is positive, cations are evacuated and replaced by holes.

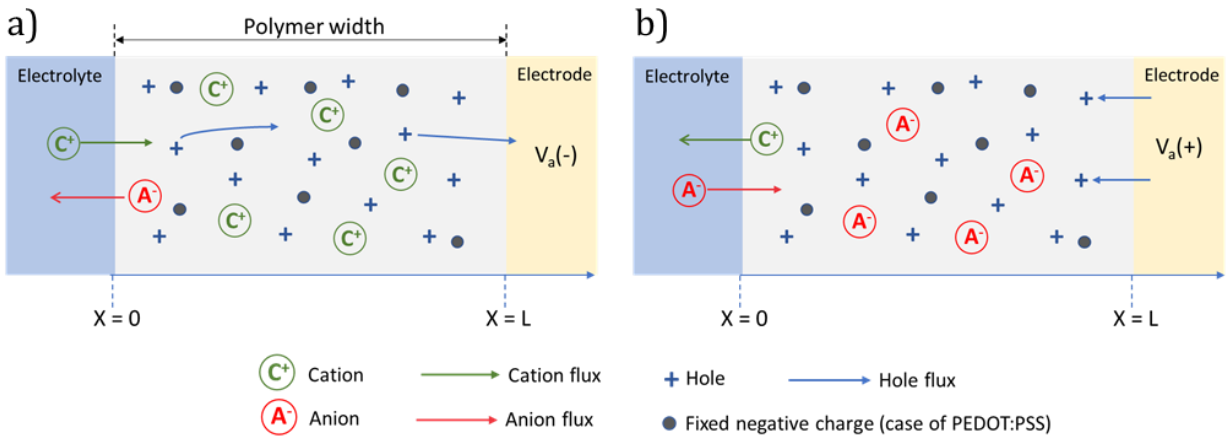

Figure 4.6. Schematic of the studied system showing the different species in the polymer film. **a,** the film is being reduced. **b,** the film is being oxidized

4.3.3 Assumptions

1) The transport of ions and holes through the PEDOT film or the PEDOT:PSS film is predominately one dimensional, occurring along the *x*-direction.

2) The diffusion coefficients of the cations and the anions through the polymer film are the same and independent from the electric field.

3) The transport of the ions and holes can be understood within the Nernst-Planck-Poisson mathematical model.

4) The solution is stagnant and without stirring thus the term of the convection transport is omitted in the Nernst-Planck equation.

5) No faradaic reactions are happening at the surface of the electrode.

4.3.4 Governing equations

Drift-diffusion equations:

The Nernst-Planck-Poisson approach is utilized to describe the transport of ions and holes in the polymer film. Their fluxes are given by the following equations (1, 2 and 3) **[4.3, 4.4]** where the first and the second terms between parenthesis are the contributions of diffusion and migration, respectively, to the total mass transfer.

Flux of cations:
$$J_c = -D_c\left(\frac{\partial C_c}{\partial x} - fC_c e\right) \quad (1)$$

Flux of anions:
$$J_a = -D_a\left(\frac{\partial C_a}{\partial x} + fC_a e\right) \quad (2)$$

Flux of holes:
$$J_h = -D_h\left(\frac{\partial C_h}{\partial x} - fC_h e\right) \quad (3)$$

where:

- D_c, D_a and D_h represent the diffusion coefficients of cations, anions and holes respectively.
- C_c, C_a and C_h represent the concentrations of cations, anions and holes respectively.
- $f\ is\ equal\ to\ \frac{F}{RT}$ and $e = -\frac{\partial V}{\partial x}$ representing the electric field along the *x* axis (V is the electric potential).

N.B: A hole is a term that emerged in the semiconductor's physics. It is a fictive positive charge assigned to the vacancy created when an electron is extracted for the semiconductor material (in this case from PEDOT or PEDOT:PSS).

Continuity equations:

For cations: $$\frac{\partial C_c}{\partial t} + \frac{\partial J_c}{\partial x} = 0 \quad (4)$$

For anions: $$\frac{\partial C_a}{\partial t} + \frac{\partial J_a}{\partial x} = 0 \quad (5)$$

For holes: $$\frac{\partial C_h}{\partial t} + \frac{\partial J_h}{\partial x} = 0 \quad (6)$$

where *t* is the time.

By joining the drift-diffusion equations (1,2 and 3) to the continuity equations (4,5 and 6), the following set of equations is obtained:

For cations: $$\frac{\partial C_c}{\partial t} = -\frac{\partial J_c}{\partial x} = D_c \frac{\partial}{\partial x}\left(\frac{\partial C_c}{\partial x} - f C_c e\right) \quad (7)$$

For anions: $$\frac{\partial C_a}{\partial t} = -\frac{\partial J_a}{\partial x} = D_a \frac{\partial}{\partial x}\left(\frac{\partial C_a}{\partial x} + f C_a e\right) \quad (8)$$

For holes: $$\frac{\partial C_h}{\partial t} = -\frac{\partial J_h}{\partial x} = D_h \frac{\partial}{\partial x}\left(\frac{\partial C_h}{\partial x} - f C_h e\right) \quad (9)$$

Poisson equations:

The Poisson equation relates the gradient of the electrical field inside the polymer to the net charge **[4.5]**, and it takes into account the fixed anions on the polymer backbone of PEDOT:PSS by adding or removing the C_{fixed} term from the equation as shown by (10) and (11):

For PEDOT:PSS : $$\epsilon \frac{\partial e}{\partial x} = F \times (C_c + C_h - C_a - \boldsymbol{C_{fixed}}) \quad (10)$$

For PEDOT : $$\epsilon \frac{\partial e}{\partial x} = F \times (C_c + C_h - C_a) \quad (11)$$

where ε is the permittivity of the film.

Set of PDE to solve:

As it was shown in equations (7), (8), (9), (10) and (11), the concentrations of holes and ions in the bulk of the polymer film link the set of the equations together, which implies their simultaneous resolution. Thus, the final partial differential equations (PDEs) to solve are the following:

$$\frac{\partial C_c}{\partial t} = D_c \frac{\partial}{\partial x}\left(\frac{\partial C_c}{\partial x} - f C_c e\right); \quad \frac{\partial C_a}{\partial t} = D_a \frac{\partial}{\partial x}\left(\frac{\partial C_a}{\partial x} + f C_a e\right)$$

$$and \quad \frac{\partial C_h}{\partial t} = D_h \frac{\partial}{\partial x}\left(\frac{\partial C_h}{\partial x} - f C_h e\right)$$

and,

$$\epsilon \frac{\partial e}{\partial x} = F \times (C_c + C_h - C_a - \boldsymbol{C_{fixed}}) \quad \text{or} \quad \epsilon \frac{\partial e}{\partial x} = F \times (C_c + C_h - C_a)$$

Initial and boundary conditions used:

The boundary conditions as well as the initial conditions used in the model are summarized in Table 4.2. Since in the previous assumptions it was stated that there are no faradaic reactions of the ions at the polymer/electrolyte interface, it results that there is no flux of ions ($J_c(L,t)$ and $J_a(L,t)$). Regarding the holes, at the electrolyte/polymer interface, its flux ($J_h(0,t)$) is equal to zero because the electrolyte does not conduct holes. Concerning the C_{fixed} term, it reflects the concentration of the accessible locations for the holes and ions. The electric potential V is time-independent and only vary at the boundaries $x=0$ and $x=L$. Another important fact is that the initial state of the polymer plays a decisive role for the simulation output. For instance, if the polymer film is totally oxidized, the full doping of the layer with anions should be considered. On another scenario, if the film is totally reduced, the full doping of the polymer layer with cations should also be considered. Thus, the initial conditions should be properly changed.

However, in some cases, it is not possible to set exactly the same initial conditions of the experiments because of the inability of the simulation to converge.

Table 4.2. Boundary and initial conditions used in the model

	$\boldsymbol{x = 0}$ (Electrolyte/Polymer)	$\boldsymbol{x = L}$ (Polymer/Electrode)	$\boldsymbol{t = 0}$
Cations	$C_c(0,t) = C_{fixed}$	$J_c(L,t) = 0$	$C_c(x,0) = 0$
Anions	$C_a(0,t) = C_{fixed}$	$J_a(L,t) = 0$	$C_a(x,0) = 0$
Holes	$J_h(0,t) = 0$	$C_h(L,t) = C_{fixed}$	$C_h(x,0) = C_{fixed}$
Potential	$V(0,t) = 0$	$V(L,t) = -V_a$	-

Dimensionless model:

The aim of the present model is to predict qualitatively the experimental responses of PEDOT and PEDOT:PSS, therefore, normalizing the model appears to be necessary to achieve this goal. In general, dimensionless parameters illustrate better the physical effects governing the studied system because the parameters are reduced to those that are truly independent. The process of the normalization consists in dividing (or multiplying) each variable by a characteristic scale of the system in hand.

- The concentrations of the ions and the holes are normalized by the fixed charge concentration C_{fixed}, which is the maximum concentration that could be reached:

$$\alpha_c = C_c/C_{fixed} \;\; ; \;\; \alpha_a = C_a/C_{fixed} \;\; ; \;\; \alpha_h = C_h/C_{fixed}$$

- The distance x is normalized by the width of the polymer film L:

$$\zeta = x/L$$

- The time t is normalized by the characteristic time t_D which is the time for cations to migrate across the film at a given voltage V_a:

$$\theta = t/t_D \;\; and \; t_D = \frac{L^2}{fV_aD_I}$$

  where D_I is the ionic diffusivity of the cations and the anions, $D_I = D_c = D_a$.

- The Diffusion coefficient of the holes is normalized by the ionic diffusivity D_I:

$$m = D_h/D_I = D_h/D_c = D_h/D_a$$

- The electric field e is normalized by the applied voltage divided by the polymer width:

$$\psi = e/(V_a/L)$$

- The applied overpotential of the electrode is normalized by the fixed voltage V_a:

$$\phi = V/V_a$$

- The fixed voltage of the electrode is multiplied by the thermal voltage f:

$$\vartheta = fV_a \quad and \quad f = \frac{F}{RT}$$

- For the Poisson equation (10) or (11), the normalization is made by introducing the term of Debye length λ_D which is defined as "the width of the screening layer adjacent to a charged surface, such as the polymer-electrolyte or polymer-cathode interfaces" **[4.3]**:

$$\varphi = \frac{\lambda_D}{L} \quad with\ \lambda_D = \sqrt{\frac{\epsilon RT}{2F^2 C_{fixed}}}$$

Replacing these unitless parameters in (7), (8), (9), (10) and (11) yields the following non-dimensional PDEs:

For cations:
$$\frac{\partial \alpha_c}{\partial \theta} = \frac{\partial}{\partial \zeta}\left(\frac{1}{\vartheta}\frac{\partial \alpha_c}{\partial \zeta} - \alpha_c \psi\right) \tag{12}$$

For anions:
$$\frac{\partial \alpha_a}{\partial \theta} = \frac{\partial}{\partial \zeta}\left(\frac{1}{\vartheta}\frac{\partial \alpha_a}{\partial \zeta} + \alpha_a \psi\right) \tag{13}$$

For holes:
$$\frac{\partial \alpha_h}{\partial \theta} = \frac{\partial}{\partial \zeta}\left(\frac{m}{\vartheta}\frac{\partial \alpha_h}{\partial \zeta} - m\alpha_h \psi\right) \tag{14}$$

Poisson equation for PEDOT:PSS:
$$\varphi^2 \vartheta \frac{\partial \psi}{\partial \theta} = \frac{1}{2}(\alpha_c + \alpha_h - \alpha_a - 1) \tag{15}$$

Poisson equation for PEDOT:
$$\varphi^2 \vartheta \frac{\partial \psi}{\partial \theta} = \frac{1}{2}(\alpha_c + \alpha_h - \alpha_a) \tag{16}$$

Table 4.3 shows the boundary and the initial conditions after normalization.

Table 4.3. Non-dimensional boundary and initial conditions.

	$\zeta = 0$ (Electrolyte/Polymer)	$\zeta = 1$ (Polymer/Electrode)	$\theta = 0$
Cations	$\alpha_c(0,\theta) = 1$	$\widetilde{J_c}(1,\theta) = 0$	$\alpha_c(\zeta,0) = 0$
Anions	$\alpha_a(0,\theta) = 1$	$\widetilde{J_a}(1,\theta) = 0$	$\alpha_a(\zeta,0) = 0$
Holes	$\widetilde{J_h}(0,\theta) = 0$	$\alpha_h(1,\theta) = 1$	$\alpha_h(\zeta,0) = 1$
Potential	$\phi(0,\theta) = 0$	$\phi(1,\theta) = -1$	-

where $\widetilde{J_c}$,$\widetilde{J_a}$ *and* $\widetilde{J_h}$ are respectively the normalized fluxes of the cations, anions and holes.

Cyclic voltammetry of PEDOT:

The previous equations (12) to (16), were used to model the ionic-electronic transport in PEDOT or PEDOT:PSS at fixed electric potential of the electrode. However, to simulate the cyclic voltammogram of PEDOT, it is obligatory to introduce a term that accounts for the time-changing voltage of the electrode. This was made by expressing the electrode potential in function of the scan rate and the time, and the boundary conditions become:

$$at\ \zeta = 0 \rightarrow \phi = 0$$

$$and\ at\ \zeta = 1 \rightarrow \phi = -f(t)$$

Hopping model:

The previous simulations can be made with the modified Nernst-Planck-Poisson equations, known as the hopping model which yields more accurate predictions about the ions and holes profiles. Thus, equations (7), (8) and (9) are changed and the set of the PDEs to be solved becomes (the Poisson equation is unchangeable) **[4.4]**:

For cations:
$$\frac{\partial C_c}{\partial t} = D_c \frac{\partial}{\partial x}\left(\frac{\partial C_c}{\partial x} - fC_c e + \frac{C_c}{C_{max} - (C_c + C_a)}\left(\frac{\partial C_c}{\partial x} + \frac{\partial C_a}{\partial x}\right)\right) \quad (17)$$

For anions:
$$\frac{\partial C_a}{\partial t} = D_a \frac{\partial}{\partial x}\left(\frac{\partial C_a}{\partial x} + fC_a e + \frac{C_a}{C_{max} - (C_c + C_a)}\left(\frac{\partial C_c}{\partial x} + \frac{\partial C_a}{\partial x}\right)\right) \quad (18)$$

For holes:
$$\frac{\partial C_h}{\partial t} = D_h \frac{\partial}{\partial x}\left(\frac{\partial C_h}{\partial x} - fC_h\left(1 - C_h/C_{fixed}\right)e\right) \quad (19)$$

And for the dimensionless equations (12), (13) and (14), they become:

For cations:
$$\frac{\partial \alpha_c}{\partial \theta} = \frac{\partial}{\partial \zeta}\left(\frac{1}{\vartheta}\frac{\partial \alpha_c}{\partial \zeta} - \alpha_c \psi + \frac{1}{\vartheta}\frac{\alpha_c}{\alpha_{max} - (\alpha_c + \alpha_a)}\left(\frac{\partial \alpha_c}{\partial \zeta} + \frac{\partial \alpha_a}{\partial \zeta}\right)\right) \quad (20)$$

For anions:
$$\frac{\partial \alpha_a}{\partial \theta} = \frac{\partial}{\partial \zeta}\left(\frac{1}{\vartheta}\frac{\partial \alpha_a}{\partial \zeta} + \alpha_a \psi + \frac{1}{\vartheta}\frac{\alpha_a}{\alpha_{max} - (\alpha_c + \alpha_a)}\left(\frac{\partial \alpha_c}{\partial \zeta} + \frac{\partial \alpha_a}{\partial \zeta}\right)\right) \quad (21)$$

For holes:
$$\frac{\partial \alpha_h}{\partial \theta} = \frac{\partial}{\partial \zeta}\left(\frac{m}{\vartheta}\frac{\partial \alpha_h}{\partial \zeta} - m\alpha_h(1 - \alpha_h)\psi\right) \quad (22)$$

4.3.5 Results

In this section, some of the main outputs of the simulation are shown and compared with the correspondent experimental data. The unitless set of PDEs (partial differential equations) were implemented in *MATLAB* and solved numerically by the *PDEPE* function. This latter allows to discretize the PDEs along the space into finite elements to form a mesh, and in each element the resulting ordinary differential equations (ODEs) were integrated in time. Throughout the simulations, three parameters influenced the results, which are the layer width of the film described by $\varphi = \frac{\lambda_D}{L}$, the relative diffusivity of holes to ions $m = D_h/D_I$ and the non-dimensional applied voltage $\vartheta = fV_a$.

N.B: The normalized current and fluxes shown in the results can be transformed into dimensional values using the equations provided in **Appendix F**.

4.3.5.1 Potentiostatic oxidation of PEDOT

Experimentally, the polymer film was initially reduced and then oxidized at +1 V *vs.* Ag/AgCl . Which means that holes were evacuated from the film and replaced by cations. Thus, it was logical to introduce this initial state of the film in the *MATLAB* script. However, a numerical problem occurred that consisted in the incapacity to run the simulation with a fully reduced film, thus a partially reduced polymer was employed. Figure 4.7 shows the current-time profiles on the electrode surface at different conditions of m and φ, with the fixed value of $\vartheta = 38.92$ (corresponds to 1 volt). The experimental curve shows a decreasing current along the time that indicates the discharge of the film: holes are getting inserted into the polymer. On the other hand, the predicted curves show different profiles but at $\theta = 0.6$ (normalized time), they start to converge to the same

current values as the experimental data. Although a well-fitting between the predicted and the experimental curves was not possible, it is possible to understand the influence of the modeling parameters on the results. For example, the effect of the modelling parameter m on the current-time profiles can be depicted by comparing the graphs of m=50, m=100, m=200 at φ=0.001. As m increases, which means the diffusivity of holes with respect to ions, the "bump" in the current-time curve increases. These bumps occurring between θ=0 and θ=0.3 signify that holes are getting extracted instead of being injected into the polymer film, and they are numerical errors.

For the other parameter, $\varphi = \frac{\lambda_D}{L}$, it reflects the influence of the polymer length (length and width are used interchangeably, and they mean the same thing) on the current profile and its effect can be extracted from the graphs of φ=0.001, φ=0.005 and φ=0.01 at m=100. As φ increases (L decreases), the discharge current (lowest point in the curve) becomes less and less intensive (from 1.5 to 0.5). This means that when the width of the polymer film decreases, the concentration of holes in the film will automatically decrease resulting in a lower discharge current.

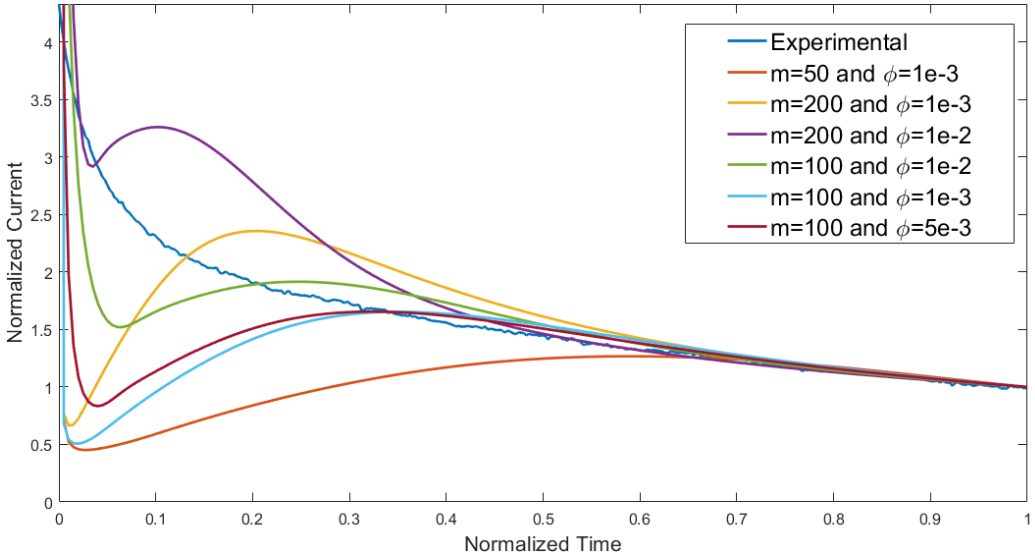

Figure 4.7. Current-time profiles for different m and φ at a constant ϑ plotted with the experimental profile.

4.3.5.2 Potentiostatic reduction of PEDOT

At a negative voltage (-1 V), the polymer film is reduced, cations invade it and the holes evacuate. Thus, an ionic flux is converted to an electronic signal. This latter is shown in the graphs of Figure 4.8. The predicted and experimental graphs show high agreement suggesting that the model was able to approximate the real data and the employed non-

dimensional parameters of m and φ could be used to estimate the diffusivity of the holes and the width of the polymer film. Such result induces to extract further information about the reduction of PEDOT, therefore, the concentrations profiles of ions and holes are plotted along time and space. Figure 4.9 and Figure 4.10 show respectively the variation of the concentrations of the holes and the cations. These concentrations appear to be opposite to each other: As cations invade the polymer film from the direction of the electrolyte (ζ=0), the holes are evacuated to the surface electrode (ζ=1). At the same time, Figure 4.11 shows the profile of anions which seems to play the role of a compensator of charges in the polymer. The invasion of cations at ζ=0 is also accompanied by an invasion of anions and then both the concentrations (of anions and cations) decrease simultaneously. Furthermore, when the hole concentration begins to build up, anion concentration increases simultaneously.

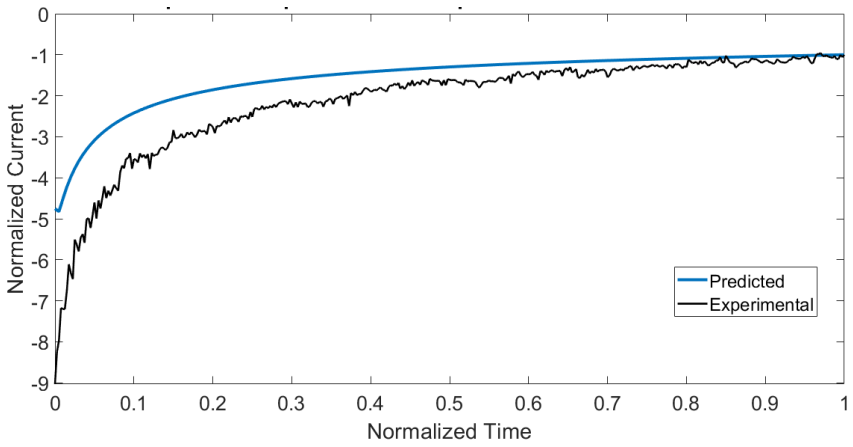

Figure 4.8. Current-time profiles of the reduction of PEODT: m=10 and φ=10^{-3}.

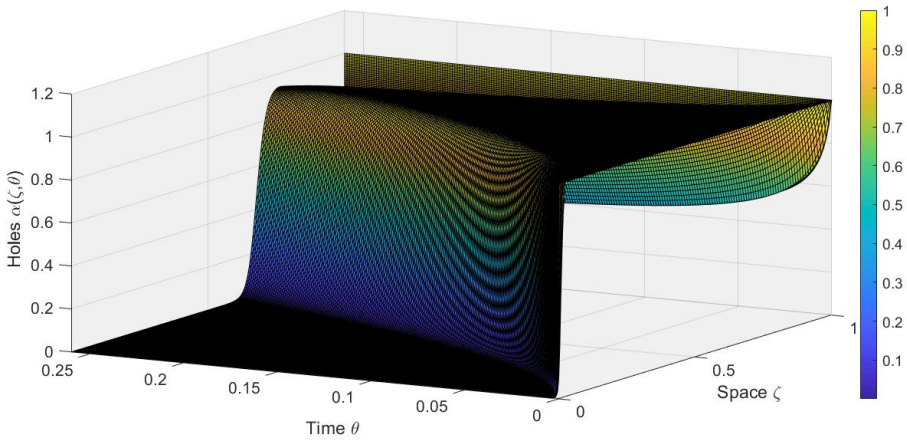

Figure 4.9 Profile of the hole for the reduction process of PEDOT: m=10 and φ=10^{-3}.

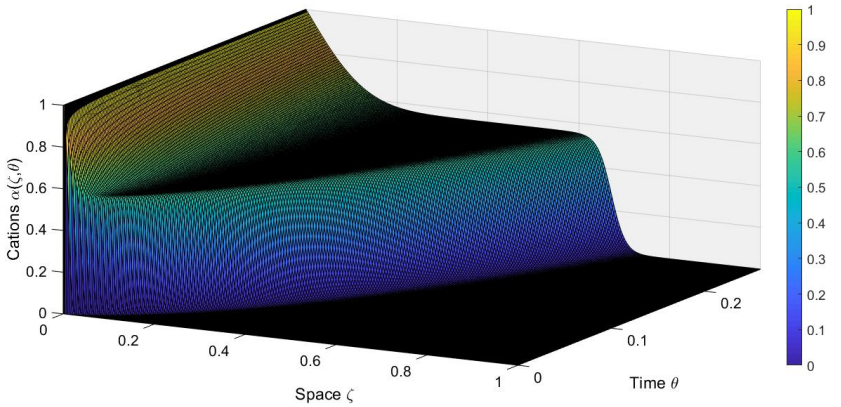

Figure 4.10 Profile of the cations for the reduction process of PEDOT: m=10 and φ=10^{-3}.

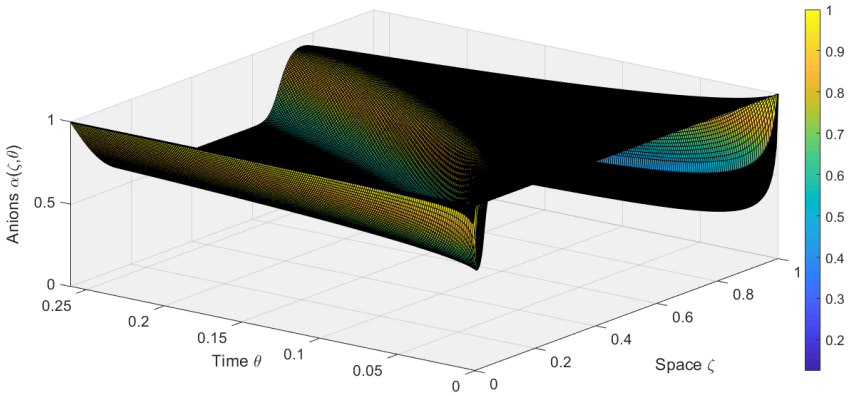

Figure 4.11 Profile of the anions for the reduction process of PEDOT: m=10 and φ=10^{-3}.

4.3.5.3 Potentiostatic oxidation of PEDOT:PSS

As shown in Figure 4.12, the predicted potentiostatic oxidation of the PEDOT:PSS film harmonizes with the experimental result indicating the ability of the model to approximate the real system. As in the case of the PEDOT reduction, it is possible to extract further information. However, to avoid redundancy, no further plots were shown for this simulation.

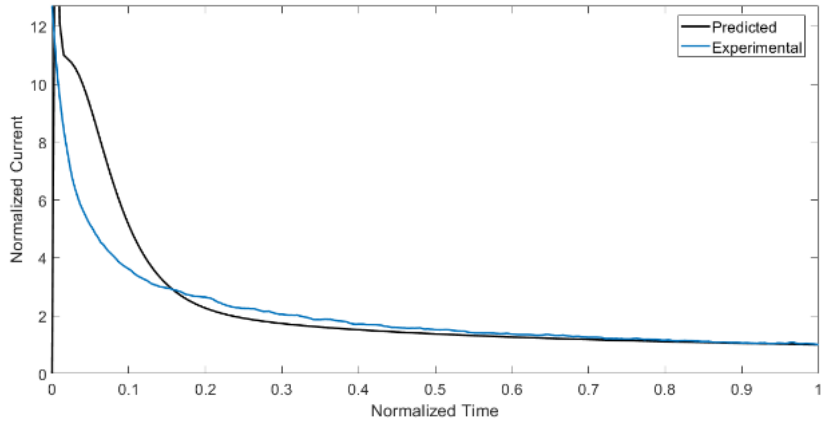

Figure 4.12. Current-time profile of the oxidation of PEDOT:PSS: m=1500, φ=0.01 and $\vartheta = 38.9$.

4.3.5.4 Potentiostatic reduction of PEDOT:PSS

The current-time graph of the reduction of PEDOT:PSS is shown in Figure 4.13, alongside the predicted current profile. Although at around θ=0.05 (normalized time) the two profiles don't match, the overall shapes agree. Both curves demonstrate an increase of current that stabilizes at θ=0.8. This current corresponds to the evacuation of holes from the PEDOT:PSS film , which is accompanied by ionic fluxes showed in Figure 4.14.

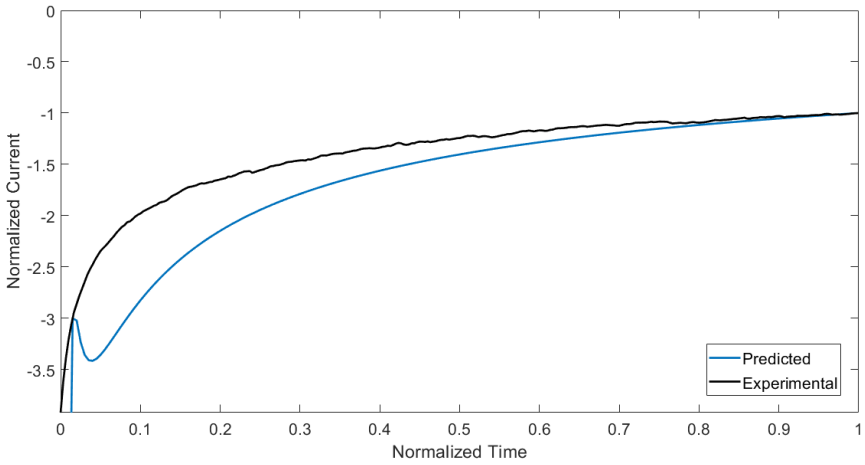

Figure 4.13. Current-time profile of the reduction of PEDOT:PSS: m=100, φ=0.01 and $\vartheta = 38.9$.

Regarding the concentrations of the holes and the cations (Fig. 4.14a and 4.14b), they exhibit the same behaviors as in the PEDOT experiment: when holes are extracted to the electrode, cations are injected into the film. Fig. 4.14c shows that at the electrolyte/polymer interface (ζ=0), the anion concentration is maximal, but at $\zeta > 0$, this concentration becomes equal to zero. This demonstrates that the anions are not interfering in the process of the cation's invasion or the hole's extraction, which agrees with the structure of PEDOT:PSS. This latter has fixed anionic charges (PSS^-) that compensate the holes and the cations, thus no anions are injected from the electrolyte to the polymer film.

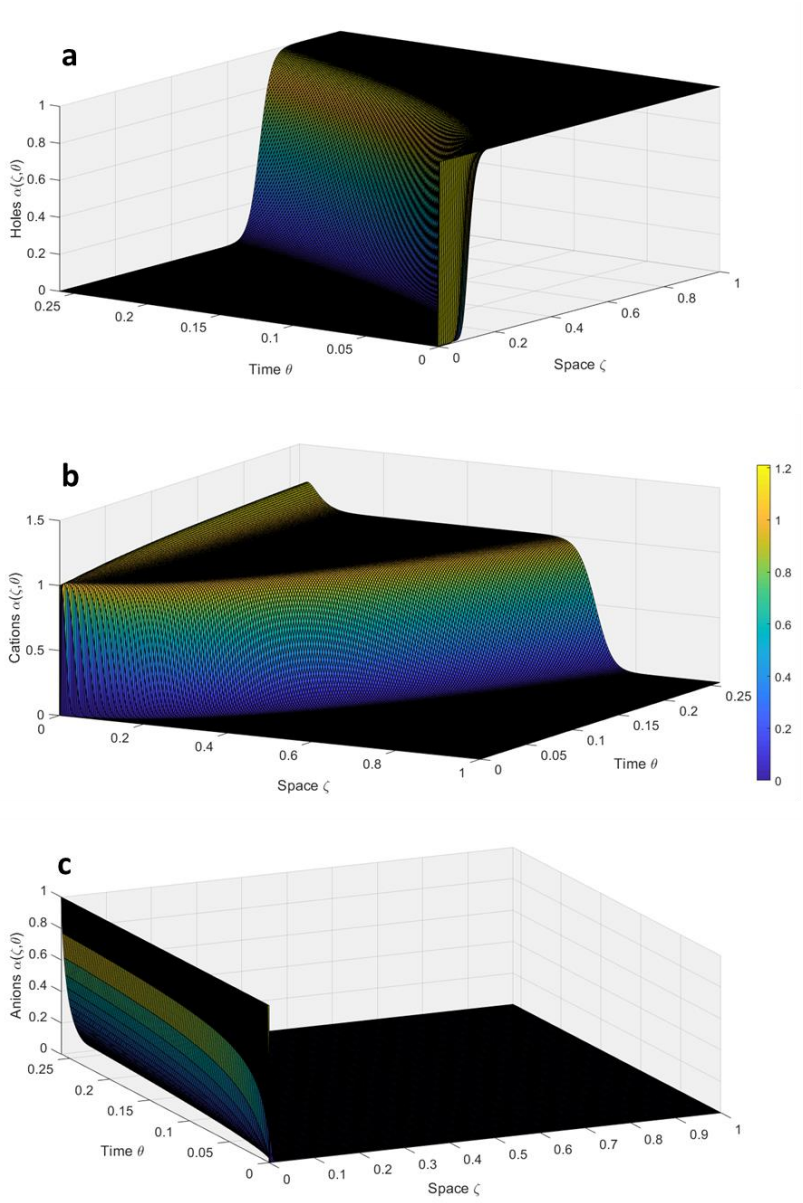

Figure 4.14. Ions and holes profiles for the reduction process of PEDOT:PSS: m=10 and φ=10^{-3}. **a,** holes profile. **b,** cations profile. **c,** anions profile.

4.3.5.5 Cyclic voltammetry of PEDOT

The shape of the different cyclic voltammograms (CVs) of PEDOT when swept from 0 V to -1 V were computed by *MATLAB* and plotted alongside the experimental CV in Figure 4.15. The idea consisted of changing the model parameters m, φ to see their influence on the CV. From the plotted CVs, interesting information can be drawn:

Effect of the hole mobility m: From the CVs at φ=0.01, and m={10, 50, 100, 300}, one can see that the area of the CV is increasing as m increases. When m reaches 100, a peak of reduction starts to appear, and at m=300, the reduction peak becomes expressed

between 0 and -0.2 V. Also, at even higher m values, the reduction peaks become more intense and less broad. These observations mean that as the mobility of holes increases (m increases), the reduction peak narrows indicating the fast holes evacuation from the polymer film during its reduction. Another point concerning the hole mobility can be obtained: The CV(m=10000, φ=0.04) and CV(m=1000, φ=0.04) show rectangular shapes between -0.4 V and -1 V representing capacitive currents. But the fact that they have very different values of m (10000 and 1000) and they exhibit practically the same shape is intriguing. Thus, one can hypothesize that the hole mobility cannot increase indefinitely, and at certain conditions, it reaches its maximum

Effect of the polymer width φ: By inspecting the CVs at m=300 and φ={0.01, 0.1, 0.3}, it is possible to see that as φ increases (L decreases), the peak of reduction becomes narrower. This means that during the polymer reduction, the cation injection is affected by the polymer width. In fact, as the polymer film grows, the cation injection into the film tends to occur over a larger interval of time (since there is larger distance to cover) which results in the broad peaks observed.

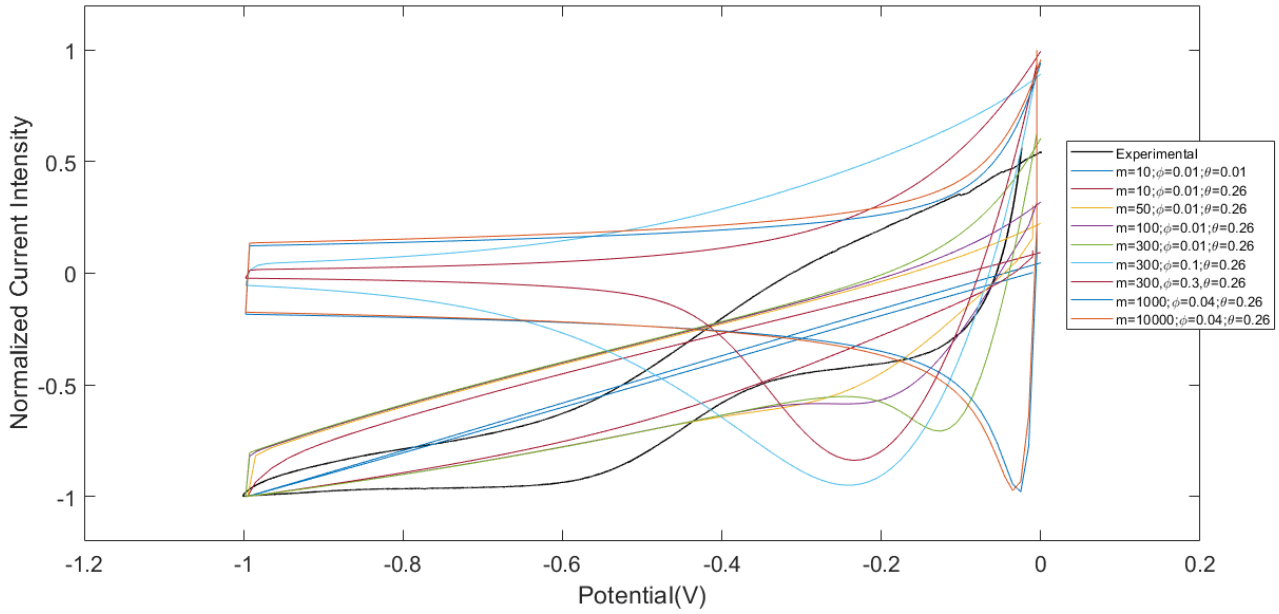

Figure 4.15. Predicted and experimental cyclic voltammograms of PEDOT.

4.4 Conclusions

In this chapter, a computational approach to understand the ionic-electronic conductivity within the polymers PEDOT and PEODT:PSS was realized through a model based on the Nernst-Planck-Poisson equations. The results obtained from the predictions, which were normalized by the characteristics of the system, agreed in many cases with the experimental data. This allowed to conclude that the polymer width promotes the delay of the ionic fluxes, since the time for the full doping or de-doping with cations increase by increasing the polymer width. Another conclusion is that the higher is the diffusivity of the holes, the faster is the doping/de-doping. However, the mobility of holes is always higher than the cations, so eventually the injection of holes or its evacuation can be limited by the cation's mobility inside the polymer. Although the results obtained from the modelling granted better vision of the ionic-electronic mechanisms inside the polymer, an exact match was not possible, especially in the case of the cyclic voltammetry of PEDOT and the oxidation of PEDOT. This output is expected, since the processes of the oxidation-reduction of conductive polymers are much more complicated than the model's assumptions and need to include the Butler-Volmer theory to approach the "real" phenomena occurring within the polymer film.

4.5 References

[4.1] Bard, A., & Faulkner, L. (**2000**). *Electrochemical methods and applications*. New York: Wiley-Interscience.

[4.2] Guidelli, R., Compton, R., Feliu, J., Gileadi, E., Lipkowski, J., Schmickler, W. and Trasatti, S. *Defining the transfer coefficient in electrochemistry: An assessment (IUPAC Technical Report)*. Pure and Applied Chemistry, **2014**, 86(2), pp.245-258.

[4.3] Feicht, S., Degen, G. and Khair, A. *Moving ion fronts in mixed ionic-electronic conducting polymer films*. AIChE Journal, **2015**, 61(4), pp.1447-1454.

[4.4] Volkov, A., Wijeratne, K., Mitraka, E., Ail, U., Zhao, D., Tybrandt, K., Andreasen, J., Berggren, M., Crispin, X. and Zozoulenko, I. *Understanding the Capacitance of PEDOT:PSS.* Advanced Functional Materials, **2017**, 27(28), p.1700329.

Chapter 5: Fabrication of based PEDOT DSSCs

5.1 Introduction

This chapter shows the application of the home-made poly(3,4-ethylenedioxythiophene) doped poly(styrene sulfonate) (PEDOT:PSS) in the construction of dye-sensitized solar cells (DSSCs). The fabrication and the assembly of the DSSCs were done in the Laboratory for Process Engineering, Environment Biotechnology and Energy (LEPABE) at the University of Porto. Subsequently, the photovoltaic performances of the DSSC were assessed in the same laboratory (LEPABE) laboratory.

5.2 Experimental section

5.2.1 Materials and instruments

Preparation of the PEDOT:PSS solutions:

Poly(4-styrenesulfonic acid) (PSS) 18% in water, sodium persulfate ($Na_2S_2O_8$) 98% and iron(III) sulfate hydrate ($Fe_2(SO_4)_3$) 97% were purchased from Sigma-Aldrich**.** The monomer 3,4-ethylenedioxythiophene (EDOT) 99% was purchased from Acros Organics. Dimethylsulfoxide (DMSO) 99.7% was purchased from Fisher. Ethylene glycol (EG) was purchased from Merck. Deionized water (DI) was used throughout the experiences and all the chemicals were used directly without further purification or treatment.

Fabrication of the DSSCs:

The assembly of the dye-sensitized solar cells were done in the LEPABE laboratory in Porto and the materials used were the following (consult Figure 5.1 for the chemical structures):

- Fluorine doped tin oxide (FTO) glass TEC7 with a sheet thickness of 2.2 mm provided by Greatcell Solar's.
- Transparent titanium oxide (TiO_2) paste 30NR-D with an average nanoparticle size of 30 nm provided by Greatcell Solar's.
- Reflecting layer WER2-O with an average nanoparticle size of 150-250 nm provided by Greatcell Solar's.
- Platinum nanoparticles Plastisol T/SP provided by Solaronix.
- Thermoplastic sealant Surlyn with 25 microns of thickness provided by Solaronix.

- The sensitizer was [5,15-bis(2,6-dioctoxyphenyl)-10-(bis(4-hexylphenyl)amino-20-4-carboxyphenyl ethynyl)porphyrinato]Zinc (II)] (YD2-o-C8), 95% purity, provided by Everlight Chemical.
- The electrolyte system was comprised of a redox system and additives. For the redox system, tris(2,2′-bipyridine-2N,N′) cobalt(III) tris(tetracyanoborate) (Co-300) and tris(2,2′-bipyridine-2N,N′) cobalt(II) bis(tetracyanoborate) (Co-200) were both 95% pure and were provided by Eversolar. For the additives, 4-tert-Butylpyridine (TBP) and lithium perchlorate were mixed with the redox system. The final composition of the electrolyte was 0.165 M of Co-200, 0.045 M of Co-300, 0.8 M TBP and 0.1 M $LiClO_4$.

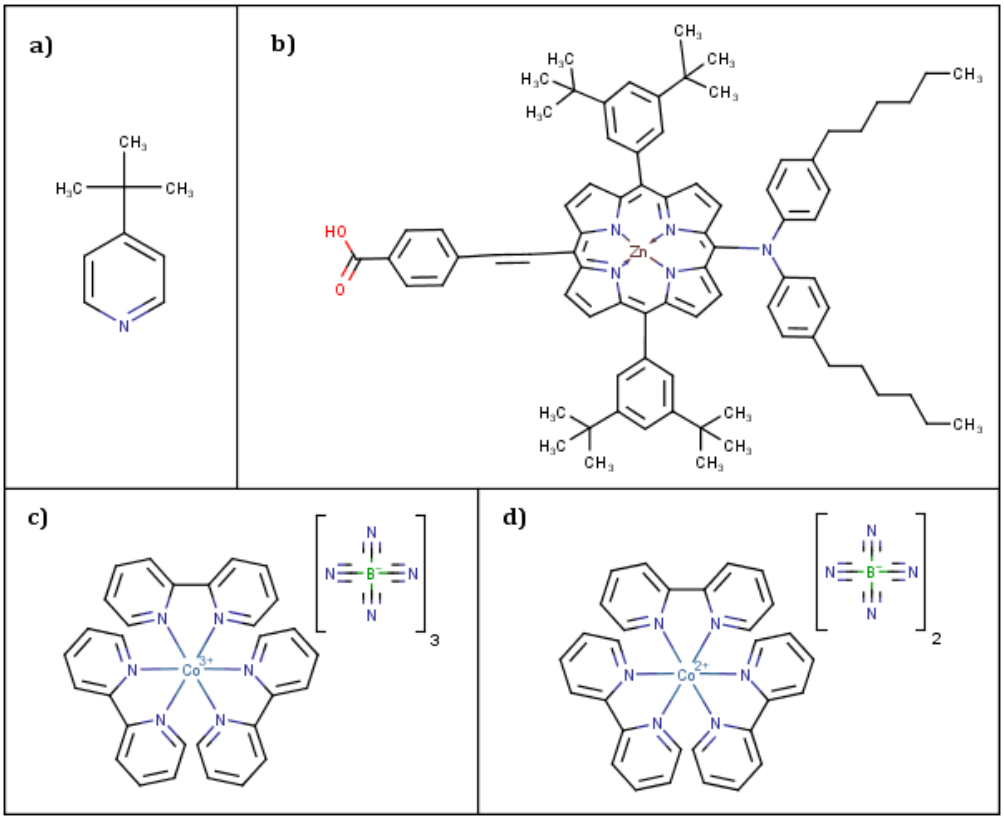

Figure 5.1. Structures of some chemicals used in the fabrication of the DSSCs: **a)** TBP, **b)** sensitizer (YD2-o-C8), **c)** Co-300 and **d)**Co-200 .

Characterization:

Electrochemical impedance spectroscopy (EIS) was used to characterize the DSSCs. The apparatus used was an Autolab, PGSTAT302N electrochemical station. The current *vs.* applied potential (J-V) responses of the cells was obtained under simulated solar light using a Solar Simulator MiniSol (LSH-7320, Newport). The J-V curves were collected with

and without a test mask (opaque sticker with a tailored aperture of a 3 mm diameter). The current-voltage tests of the fabricated solar cells with the PEDOT:PSS and the platinum nanoparticles were conducted under 1 insolation (1.5 air mass) which corresponds to 100 mW/cm^2 (standard incident solar energy at 25°C). To ensure the reproducibility of the results, two sets of measurements were done, the first one on the first day (day 0) of the fabrication of the DSSCs and the second set on the second day (day 1) after the fabrication of the DSSCs. To obtain correlated results, the measurements of the parameters of the DSSC were made 15 times, and standard deviation of each parameter was calculated.

5.2.2 PEDOT:PSS preparation

PEDOT:PSS solution was prepared through the chemical oxidative way. The solution was prepared in the ratio of 1:13 of EDOT to PSS using $Na_2S_2O_8$ and $Fe_2(SO_4)_3$ salts as oxidants for the EDOT monomer **[5.1]**.The solution kept under stirring for 42 hours to ensure the doping of the PEDOT by the PSS. Consequently, the solution was used directly to prepare three other solutions: One with 8% DMSO, one with 10% EG and a third one with only the prepared PEDOT:PSS.

5.2.3 Fabrication of the DSSCs

DSSCs were prepared using different counter electrodes based on the home-made solutions of PEDOT:PSS. Also, DSSCs using the platinum particles and the commercial PEDOT:PSS were fabricated to serve as a basis for comparison with the first DSSCs. The same protocol of the DSSCs fabrication was followed and it consists in:

1) Photoanodes preparation: Titanium dioxide (TiO_2) pastes and the dye were deposited on the FTO glass by screen printing technique.

2) Counter electrodes preparation:

- PEDOT:PSS counter electrodes: Home-made solutions of PEDOT:PSS and the commercial PEDOT:PSS were deposited on FTO glass sheets using the spin coating technique with 3000 rpm for 45 s. For some counter electrodes, more than one layer was deposited on the FTO glass sheets, thus, between each layer, the film was dried at 120°C for 15 min.
- Platinum counter electrodes: Platinum nanoparticles were deposited on FTO glass by doctor blading technique.

3) Sealing of the cell: The photoanode and the counter electrode were sandwiched together and separated by a sealant (a thermoplastic polymer) that prevents the leakage of the electrolyte. By virtue of a hot press of a 10 bar pressure and a 160°C temperature the sealant was melted.

4) Electrolyte injection: After sealing, the cell is left to cool down and then the electrolyte solution was injected through a hole.

5.3 Results and discussion

5.3.1 PEDOT:PSS solutions

Figure 5.2 shows the steps of the preparation of the PEDOT:PSS solution. As the reaction progresses, the color of the solution gets darker indicating the formation of PEDOT:PSS.

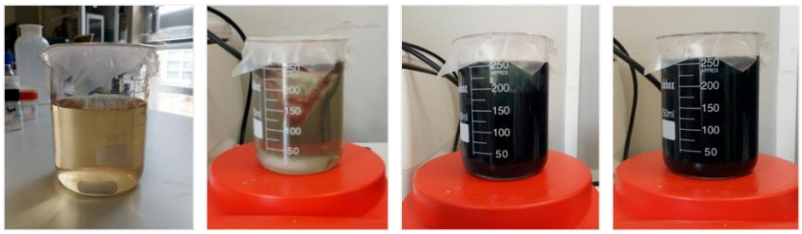

Figure 5.2. Progression of the polymerization of PEDOT:PSS (From left to right).

5.3.2 Photovoltaic performances of the based PEDOT:PSS electrodes DSSCs

The obtained DSSCs are shown Figure 5.3. The borders of the cells have metallic color due to the sputtering of silver that plays the role of contactor to the cells.

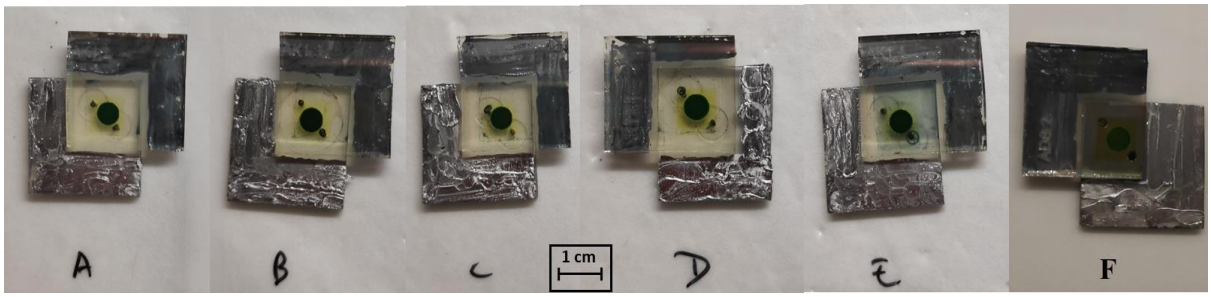

Figure 5.3. Dye-sensitized solar cells fabricated. **A**, PEDOT:PSS **B,** PEDOT:PSS-8%DMSO **C,** PEDOT:PSS-8%DMSO (4 layers) **D,** PEDOT:PSS-10% EG **E,** Commercial PEDOT:PSS F, Platinum nanoparticles.

5.3.2.1 J-V curves

5.3.2.1.1 Theoretical background

Current-voltage curves (J-V) allow to obtain the characteristic parameters that define a solar cell which are the open circuit voltage (*Voc* in volts), the short circuit current (*Jsc* in mA/cm^2), the fill factor (*FF* dimensionless), the maximum power point (*Mpp* in mW) and the power conversion efficiency (*PCE* in %). The following equations elucidate the relations between the different parameters:

$$FF = \frac{Mpp}{J_{sc}\, V_{oc}} \qquad \text{(a)}$$

$$PCE = \frac{Mpp}{Is} \times 100 = \frac{Jsc\ Voc\ FF}{Is} \times 100 \qquad \text{(b)}$$

Equation (a) describes the fill factor (*FF*) as the ratio of *Mpp* divided by *Jsc *Voc*. *Mpp* is the maximum power that can be delivered by the solar cell and it is the product of $J_{mp}*V_{mp}$, whereas the term of *Jsc*Voc* is purely theoretic and represents the ideal power delivered by an ideal solar cell that could never be attained. Hence, the *FF* parameter shows the aptitude of a solar cell to perform at its maximum capability **[5.2]**. Figure 5.4 illustrates the *FF* parameter.

Equation (b) **[5.3]** explains the efficiency of the solar cell. It is defined as the ratio of the maximum output of a solar cell (*Mpp*) to the incident sunlight power (*Is*).

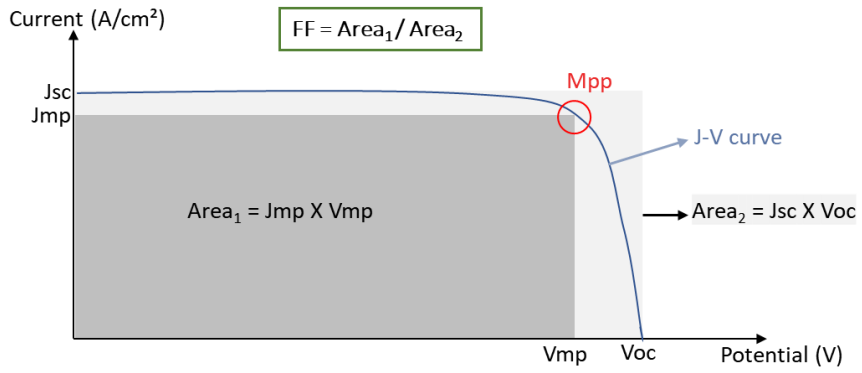

Figure 5.4. Fill factor illustration through the J-V curve of a solar cell.

5.3.2.1.2 Analyses of the J-V curves

The obtained figures were shown in Figure 5.7 and summarized in Table 5.1 and Table 5.2. The measured parameters were the *Voc*, *Jsc*, *FF*, *PCE* and the *Mpp*. As mentioned in the experimental section, for every fabricated DSSC, the parameters were measured 15

times, and the standard deviation was calculated to give an idea about the dispersion of the experiments.

By examining the data collected with and without the test cell mask, it appears that there are some differences in the obtained values. These dissimilarities in the efficiencies' values were expected because the test cell mask hides the non-active area of the cell and blocks any incident light coming from other sources (Figure 5.5) allowing only the illuminator's perpendicular light to be collected by the DSSC's active area which allows for unbiased measurements of the cells.

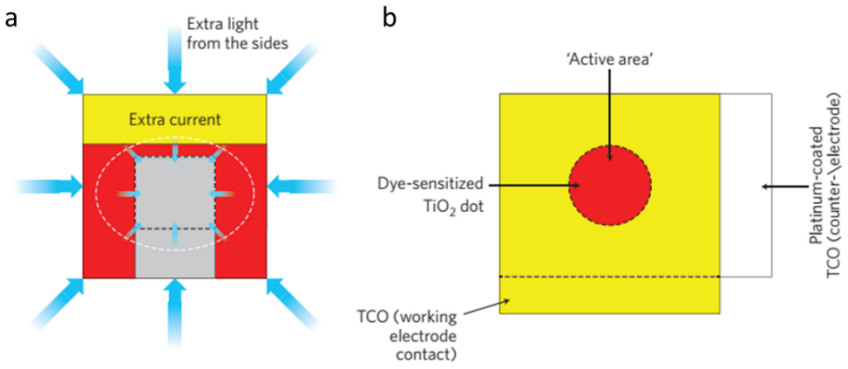

Figure 5.5. Errors that can result if masking is not employed. **a,** Divergent or reflected light can enter the glass substrate from the sides and additional photocurrent can be generated**. b,** DSSC scheme: If masking is not employed, divergent or scattered light can enter the sides which increases the measured photocurrent**[5.4].**

Thus, for the sake of precision, the comparison of the different DSSCs was made using the values obtained with the mask.

The PEDOT:PSS counter electrodes demonstrate efficiencies ranging from 7.256 % (to 8.534% on the first day (day 0) and from 6.994% to 8.79% on the second day (day 1). On the other hand, the efficiency of the counter electrode made with platinum particles has an efficiency of 6.301% on the first day and 6.371% on the second day. It is clear, that DSSCs based on PEDOT:PSS counter electrodes exhibit higher efficiencies than the platinum particles based DSSCs counter electrodes. Moreover, the fill factor (*FF*) values of the PEDOT:PSS counter electrodes are also higher than those of the platinum nanoparticles, both on the first and the second day. This infers that PEDOT:PSS is a better material for the counter electrodes used in DSSCs. They clearly offer higher catalytic activity for the reduction of the oxidant of the mediator, which implies faster reactions, and faster photo-generation of electric current.

The commercial PEDOT:PSS has an efficiency of 8.534% on the first day. This value surpasses those of the home-prepared PEDOT:PSS (7.539%), PEDOT:PSS-8% DMSO (7.501%), PEDOT:PSS-8% DMSO – 4 layers (7.799%) and PEDOT:PSS-10% EG (7.256%). Also, by comparing the values of the second day, the commercial PEDOT:PSS counter electrode still surpasses the home-prepared ones in terms of efficiency. It is clearly, that the commercial PEDOT:PSS yields better results than the home-made PEDOT:PSS. Its high values of efficiencies can be attributed to its purity, because the home-made solutions of PEDOT:PSS were not purified or washed. Another point is that the prepared PEDOT:PSS solutions showed lighter color than that of the commercial PEDOT:PSS indicating that the latter has higher concentration than the home-made ones (Figure 5.6). Therefore, the obtained results for the home-made PEDOT:PSS counter electrodes can be considered very promising since it is obvious that with further purification, product treatment and optimal concentration, the efficiency can go skyrocket.

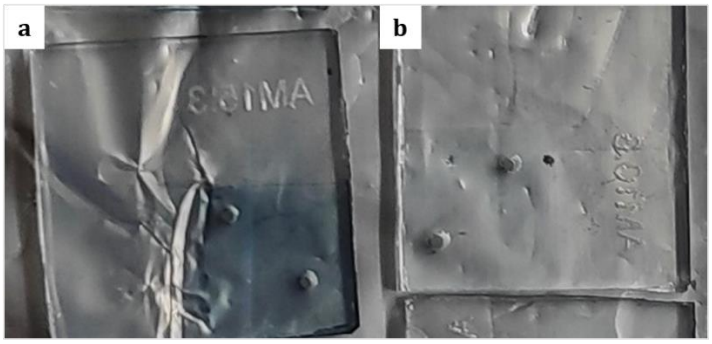

Figure 5.6. Concentration difference between **a,** the commercial PEDOT:PSS and **b,** the synthesized PEDOT:PSS.

Among the counter electrodes prepared with the home-made solutions, the most efficient ones seem to be made with PEDOT:PSS, PEDOT:PSS-8% DMSO and PEDOT:PSS-8% DMSO (4 layers). They respectively present efficiencies of 7.539% (day 0)/8.096% (day 1), 7.501% (day 0)/ 7.817% (day 1) and 7.799% (day 0)/7.963% (day 1). Evidently, increasing the layers of the deposition of PEDOT:PSS-8% DMSO on the FTO glass, results in higher efficiencies. Such a result suggests that the higher the PEDOT:PSS quantity is, the easier it is to collect holes and also the easier it is for the oxidant mediator to get reduced on the PEDOT:PSS. However, the PEDOT:PSS counter electrode has higher efficiency than the PEDOT:PSS-8% DMSO (one layer), which means that the DMSO didn't have an enhancement effect on the conductivity of PEDOT:PSS, but surprisingly the DMSO made it decrease.

It is noticeable from the four graphics in Figure 5.7 that the PEDOT:PSS-10% EG yielded the lowest J-V curve with an efficiency of 7.256% (day 0) and 6.994% (day 1). This suggests that the added EG didn't improve the performances of the PEDOT:PSS as in the case of DMSO. Adding DMSO and EG is known to increase the carrier mobility in PEDOT:PSS **[5.5]**. In fact, these additives separate the PEDOT:PSS chains into a PEDOT-rich grains and PSS-rich particles which creates better conducting pathways for the charges **[5.6]**.Thus, it is clear that the amount of PEDOT:PSS and the additives (EG or DMSO) should be adjusted until reaching the enhancement point.

Table 5.1. The photovoltaic performances of the DSSCs with different counter electrodes, measured on the first day (day 0).

Day 0										
A) PEDOT:PSS										
Mask presence	**PCE (%)**	**σ (±)**	**Voc (V)**	**σ (±)**	**Jsc (mA.cm^{-2})**	**σ (±)**	**FF**	**σ (±)**	**Mpp (mW)**	**σ (±)**
-	7.681	0.216	0.910	0.020	11.209	0.363	0.753	0.008	0.965	0.027
+	7.539	0.327	0.894	0.030	10.738	0.687	0.787	0.037	0.678	0.274
B) PEDOT:PSS - 8% DMSO										
	PCE (%)	**σ (±)**	**Voc (V)**	**σ (±)**	**Jsc (mA.cm^{-2})**	**σ (±)**	**FF**	**σ (±)**	**Mpp (mW)**	**σ (±)**
-	7.631	0.313	0.885	0.027	11.048	0.226	0.780	0.008	0.959	0.039
+	7.501	0.262	0.870	0.021	10.731	0.253	0.804	0.018	0.668	0.241
C) PEDOT:PSS - 8% DMSO (4 layers)										
	PCE (%)	**σ (±)**	**Voc (V)**	**σ (±)**	**Jsc (mA.cm^{-2})**	**σ (±)**	**FF**	**σ (±)**	**Mpp (mW)**	**σ (±)**
-	7.956	0.352	0.927	0.011	11.264	0.347	0.762	0.002	1.000	0.044
+	7.799	0.409	0.903	0.010	10.864	0.577	0.795	0.009	0.551	0.029
D) PEDOT:PSS - 10% Ethylene Glycol										
	PCE (%)	**σ (±)**	**Voc (V)**	**σ (±)**	**Jsc (mA.cm^{-2})**	**σ (±)**	**FF**	**σ (±)**	**Mpp (mW)**	**σ (±)**
-	6.949	0.289	0.922	0.003	9.876	0.287	0.763	0.007	0.873	0.036
+	7.256	0.042	0.901	0.002	10.053	0.113	0.801	0.006	0.513	0.003
E) PEDOT:PSS commercial										
	PCE (%)	**σ (±)**	**Voc (V)**	**σ (±)**	**Jsc (mA.cm^{-2})**	**σ (±)**	**FF**	**σ (±)**	**Mpp (mW)**	**σ (±)**
-	8.507	0.169	0.926	0.005	11.677	0.320	0.787	0.001	1.069	0.021
+	8.534	0.400	0.905	0.005	11.704	0.659	0.806	0.003	0.603	0.028
F) Platinum nanoparticles										
	PCE (%)	**σ (±)**	**Voc (V)**	**σ (±)**	**Jsc (mA.cm^{-2})**	**σ (±)**	**FF**	**σ (±)**	**Mpp (mW)**	**σ (±)**
-	6.300	0.650	0.922	0.017	10.253	0.354	0.666	0.064	0.733	0.152
+	6.301	0.397	0.904	0.014	9.417	1.001	0.743	0.051	0.568	0.239

Table 5.2. The photovoltaic performances of the DSSCs with different counter electrodes, measured on the second day (day 1).

Day 1										
A) PEDOT:PSS										
Mask presence	**PCE (%)**	**σ (±)**	**Voc (V)**	**σ (±)**	**Jsc (mA.cm^{-2})**	**σ (±)**	**FF**	**σ (±)**	**Mpp (mW)**	**σ (±)**
-	7.934	0.773	0.913	0.008	12.122	0.597	0.716	0.028	0.997	0.097
+	8.096	0.535	0.889	0.007	11.838	0.549	0.769	0.009	0.572	0.038
B) PEDOT:PSS - 8% DMSO										
	PCE (%)	**σ (±)**	**Voc (V)**	**σ (±)**	**Jsc (mA.cm^{-2})**	**σ (±)**	**FF**	**σ (±)**	**Mpp (mW)**	**σ (±)**
-	7.977	0.380	0.881	0.022	11.817	0.373	0.766	0.007	1.002	0.048
+	7.817	0.441	0.858	0.019	11.363	0.446	0.802	0.004	0.553	0.031
C) PEDOT:PSS - 8% DMSO (4 layers)										
	PCE (%)	**σ (±)**	**Voc (V)**	**σ (±)**	**Jsc (mA.cm^{-2})**	**σ (±)**	**FF**	**σ (±)**	**Mpp (mW)**	**σ (±)**
-	7.959	0.361	0.907	0.029	11.937	0.330	0.735	0.010	1.000	0.045
+	7.963	0.163	0.882	0.026	11.605	0.129	0.778	0.015	0.563	0.011
D) PEDOT:PSS - 10% Ethylene Glycol										
	PCE (%)	**σ (±)**	**Voc (V)**	**σ (±)**	**Jsc (mA.cm^{-2})**	**σ (±)**	**FF**	**σ (±)**	**Mpp (mW)**	**σ (±)**
-	6.502	0.425	0.908	0.013	9.796	0.460	0.731	0.003	0.817	0.053
+	6.994	0.390	0.887	0.012	10.090	0.372	0.781	0.004	0.494	0.028
E) PEDOT:PSS commercial										
	PCE (%)	**σ (±)**	**Voc (V)**	**σ (±)**	**Jsc (mA.cm^{-2})**	**σ (±)**	**FF**	**σ (±)**	**Mpp (mW)**	**σ (±)**
-	8.804	0.216	0.926	0.006	12.362	0.465	0.769	0.005	1.106	0.027
+	8.879	0.364	0.905	0.005	12.324	0.632	0.796	0.004	0.628	0.026
F) Platinum nanoparticles										
	PCE (%)	**σ (±)**	**Voc (V)**	**σ (±)**	**Jsc (mA.cm^{-2})**	**σ (±)**	**FF**	**σ (±)**	**Mpp (mW)**	**σ (±)**
-	6.310	0.254	0.922	0.015	10.609	0.415	0.647	0.062	0.793	0.032
+	6.371	0.603	0.905	0.013	9.693	1.040	0.727	0.020	0.571	0.227

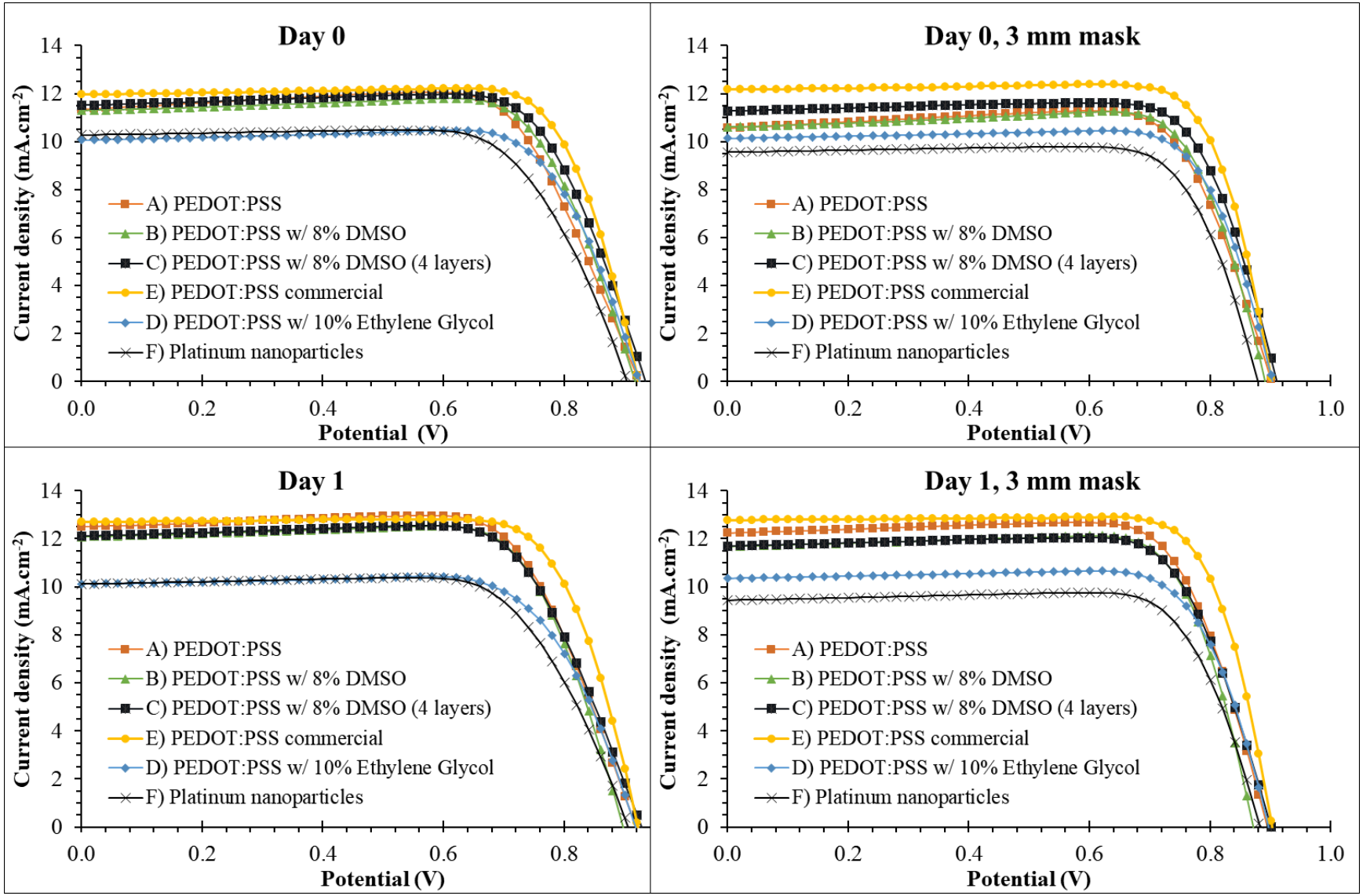

Figure 5.7. J-V curves of DSSCs with counter electrodes of PEDOT:PSS-8% DMSO, PEDOT:PSS-10% EG, commercial PEDOT:PSS and platinum nanoparticles. The measurements are collected between two days (day 0 and day 1) and with or without mask.

5.3.2.2 Electrochemical Impedance Spectroscopy (EIS)

5.3.2.2.1 Theoretical background

Impedance spectroscopy is a powerful method for characterizing the electrical properties of materials and their interfaces. When applied to an electrochemical system, like a dye-sensitized solar cell, it is often termed as electrochemical impedance spectroscopy (EIS) **[5.7]**.

Impedance is defined as the realistic resistance of an electrical element. It is the generalization of Ohm's law. The difference between the normal resistance and impedance is that the latter one includes other phenomena that influence the conductance of current like the capacitance and inductance.

The idea of EIS is to excite the cell by a small amplitude of a sinusoidal current. Hence the cell is considered as an impedance for the excitation and therefore assimilated to an equivalent electrical circuit of resistors and capacitors. Each part of this circuit describes a process occurring in the solar cell **[5.8]**.

5.3.2.2.2 Analysis of the EIS spectra

EIS measurements were carried out in the dark to avoid any perturbances caused by the photo-generation of current. The potential of the measurements was -0.85 V (close to Voc values obtained previously) in the frequency range of 0.05 Hz – 100 kHz. The resulting Nyquist spectra for each DSSC based on the prepared counter electrodes are given in Figure 5.8. Using Zview software for fitting the data, the series resistance (Rs), the charge transfer at the counter electrode/electrolyte interface (Rce), the electron recombination resistance at the photoanode (Rk) and the electron recombination lifetime (τ_n) were estimated and tabulated (Table 5.3).

Table 5.3. Electrochemical parameters of DSSCs with various counter electrodes.

DSSC	Rs ($\Omega \cdot cm^2$)	Rce ($\Omega \cdot cm^2$)	Rk ($\Omega \cdot cm^2$)	τ_n (ms)
A) PEDOT:PSS	0.8955	23.847	66.52	24.73
B) PEDOT:PSS w/ 8% DMSO	0.9980	12.800	46.60	17.93
C) PEDOT:PSS w/ 8% DMSO (4 layers)	1.0415	16.865	71.97	24.83
D) PEDOT:PSS w/ 10% Ethylene Glycol	1.076	12.2025	57.47	19.11
E) PEDOT:PSS commercial	1.0995	4.820	47.40	18.44
F) Platinum nanoparticles	1.5575	25.025	44.52	13.23

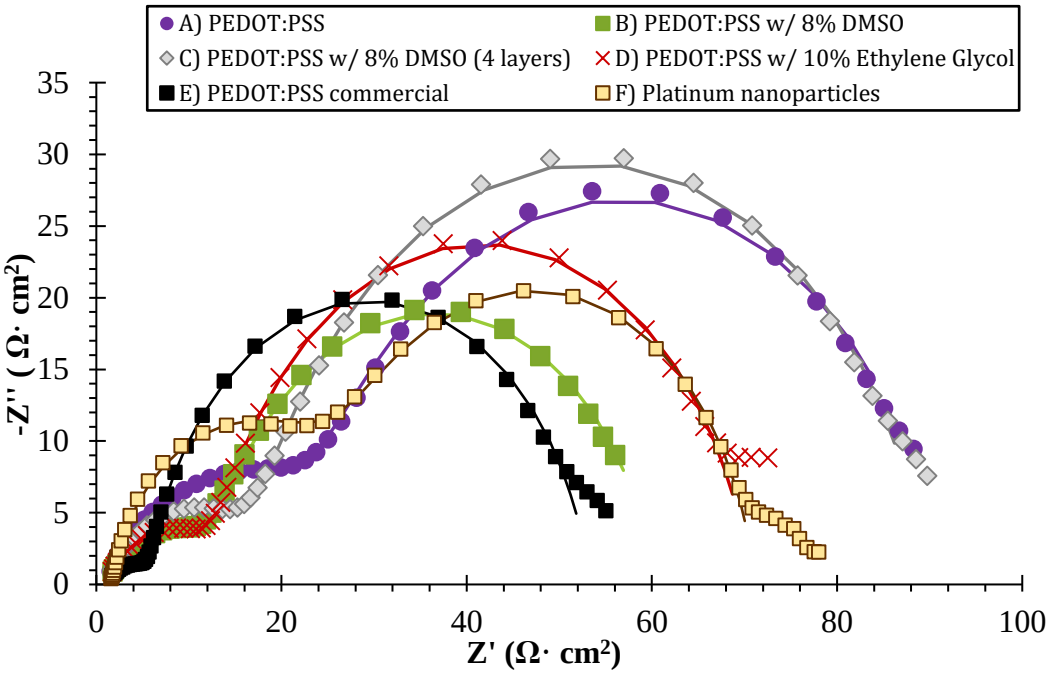

Figure 5.8. EIS of best DSSCs with different counter-electrodes, at -0.850 V under dark conditions.

Also the Randles equivalent circuit depicted for our DSSCs systems is shown in Figure 5.9. It consists of a series resistor (Rs), a counter electrode resistor (Rce) and a photoanode resistor (Rk). Each resistor has been attributed a constant phase element (CPE) in parallel. The CPE is an element that describes the double layer capacitance of electrodes, taking into account the deviation from an ideal capacitor **[5.9]**. The values of CPEce and CPEk were not shown in the table because of their irrelevance to the current work, however, they were shown in the equivalent circuit in Figure 5.9.

The first parameter that comes in sight is the series resistance (Rs). It represents the overall resistance generated by the solar cell, and when this parameter increases, it influences the fill factor of the solar cell. Thus, the lower is the value of Rs, the higher is the fill factor (and the efficiency) which means the better is the cell **[5.10]**. From Table 5.3, PEDOT:PSS based counter electrodes have lower values of Rs than the platinum nanoparticles based counter electrode, which corelates with the values of efficiencies discussed in the previous section. Furthermore, the DSSC prepared with the synthesized PEDOT:PSS (A), exhibits the lowest value of series resistance of 0.895 $\Omega \cdot cm^2$, indicating the good electrical behavior of the home-made PEDOT:PSS.

To go further in detail, the resistance at the photoanode/electrolyte interface (Rk) and the counter electrode/electrolyte interface (Rce) can be examined to evaluate the DSSCs.

The resistance of charge transfer at the counter electrode/electrolyte interface (Rce) is the most important parameter to analyze because the main purpose of this work is to assess the counter electrodes made with different solutions of PEDOT:PSS. Rce permits the evaluation of the electrons at the interface of the counter electrode and the electrolyte. From Table 5.3 it's shown that the highest value of Rce was recorded for the platinum nanoparticles counter electrode with a value of 25.025 $\Omega \cdot cm^2$. The lowest value was obtained for the commercial PEDOT:PSS counter electrode with a value of 4.82 $\Omega \cdot cm^2$. On the other hand, the counter electrodes prepared with the synthesized PEDOT:PSS (electrodes A, B, C and D) have values of Rce lower than the platinum nanoparticles, but higher than the commercial PEDOT:PSS. From the stated values of Rce. It can be concluded that PEDOT:PSS counter electrodes exhibit lower resistances to the charge transfer at the electrode/electrolyte interface, which means that PEDOT:PSS as a material, has higher electronic conductivity than platinum nanoparticles. Among the DSSCs prepared with the synthesized PEDOT:PSS, the one with PEDOT:PSS-10% EG has the best value of Rce, 12.205 $\Omega \cdot cm^2$. Compared to the DSSC base on PEDOT:PSS (electrode A) that has 23.847 $\Omega \cdot cm^2$, one can see that the addition of ethylene glycol (EG) enhanced the electronic conductivity of PEDOT:PSS by reducing the resistance to the charge transfer from the counter electrode to the electrolyte. Also, the DSSCs with based PEDOT:PSS-DMSO counter electrodes exhibit lower Rce values (12.8 $\Omega \cdot cm^2$ and 16.865 $\Omega \cdot cm^2$) than the sole PEDOT:PSS. Therefore, it is safe to say that the addition of DMSO to the PEDOT:PSS has also increased its conductivity. Such results agree with the fact that additives like DMSO and EG are good conductivity enhancers. Through J-V analysis, the effect of these additives was not very well expressed, but through a precise technique like the EIS, it was possible to view the positive effect of the additives (DMSO and EG) on the conductivity of PEDOT:PSS.

The electron recombination lifetime (τ_n) is an indicator of the survivability of electrons after being generated in the anodic layer. In fact, as the dye absorbs light, electrons excite and transfer to the photoanode. As the electrons survive for longer (τ_n increases), less recombination takes place (Rk increases). Electrode C, PEDOT:PSS w/ 8% DMSO (4 layers), has the highest τ_n, which means that this material contributes in the preventing of the recombination of the electron, which leads to more efficient cells.

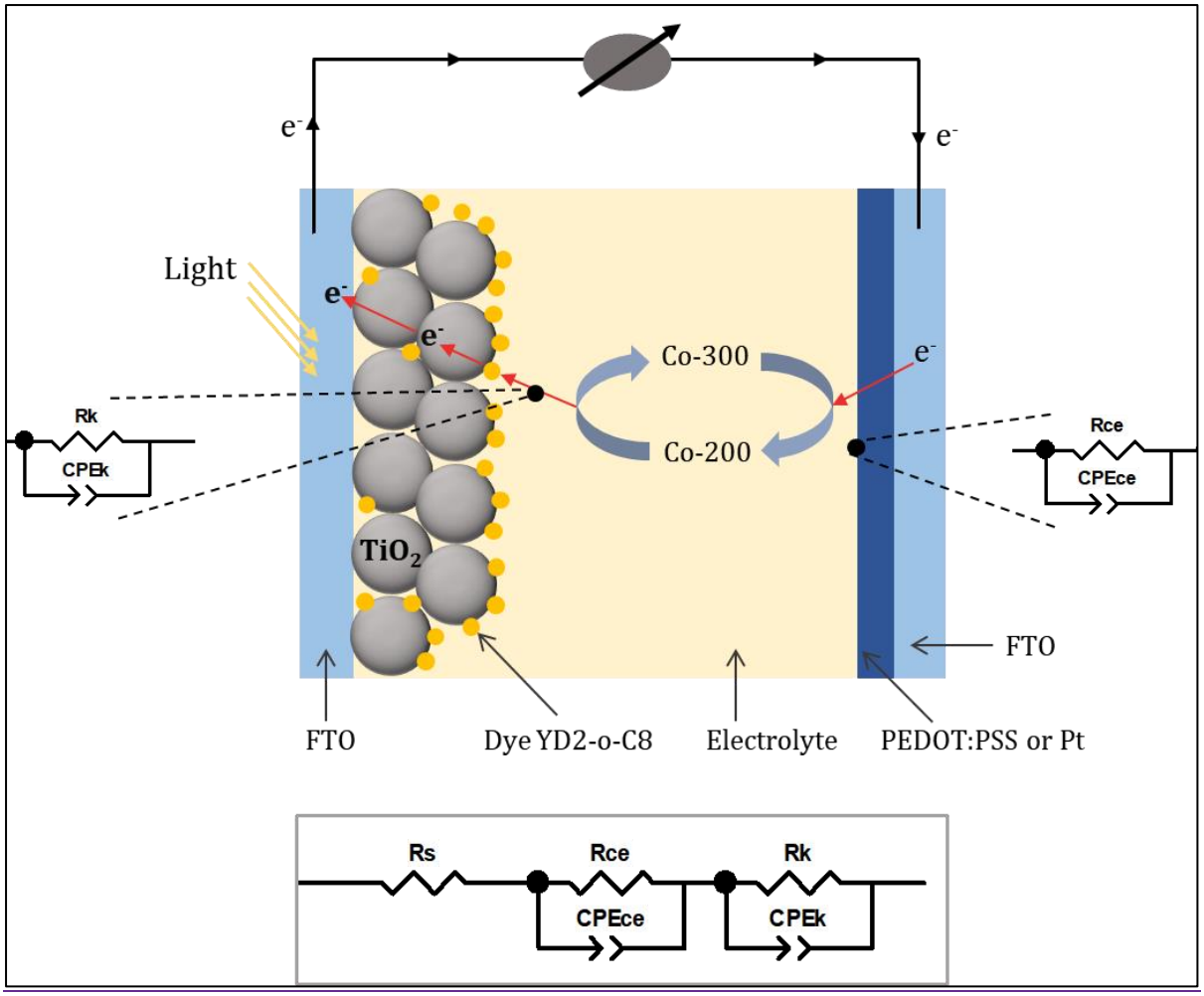

Figure 5.9. Equivalent electrical circuit of the assessed DSSCs

5.4 Conclusions

In this chapter, the poly(3,4-ethylenedioxythiophene) doped poly(styrene sulfonate) (PEDOT:PSS) was synthesized through chemical oxidative polymerization. Subsequently, the PEDOT:PSS was utilized to fabricate counter electrodes that were used in the building of dye-sensitized solar cells (DSSCs). At the same time, two other DSSCs were built based on platinum counter electrode and commercial PEDOT:PSS. The cells were characterized by electrochemical impedance spectroscopy (EIS) and current-voltage curves (J-V). The results proved that PEDOT:PSS was a more efficient material than the platinum for the use as counter electrodes in dye-sensitized solar cells (DSSCs). The cells based on PEDOT:PSS exhibited higher fill factor compared to the based platinum DSSC. Also, through EIS analysis, PEDOT:PSS counter electrodes demonstrated higher electronic

conductivity than the platinum counter electrode. It is important to point out that the synthesized PEDOT:PSS had values of fill factors that approached or exceeded the fill factor obtained for a DSSC based on the commercial PEDOT:PSS. In addition, with the synthesized PEDOT:PSS solutions, an efficiency that ranged from 7% to over than 8% was achieved (compared to 8.4% with commercial PEDOT:PSS). This difference in efficiencies is due to the impurities which can be easily overcome to obtain a better synthesized PEDOT:PSS.

It was also shown that adding high boiling solvents (ethylene glycol and DMSO) modify the characteristics of the DSSC, by either increasing or diminishing the PEDOT:PSS conductivity which demonstrates that this polymer can be tailored as desired by changing the conditions of the synthesis and the additives.

As a conclusion, PEDOT:PSS is a reliable, cheap material that can be embedded in the DSSCs to reduce their cost and to improve their efficiencies. Thanks to its high conductivity, PEDOT:PSS can be used as a cathode for fuel batteries, and even in other electronic devices.

5.5 References

[1] Sakunpongpitiporn, P., Phasuksom, K., Paradee, N., & Sirivat, A. *Facile synthesis of highly conductive PEDOT:PSS via surfactant templates*. RSC Advances, **2019,** 9(11), , 6363-6378.

[2] Kumavat, P., Sonar, P., & Dalal, D. *An overview on basics of organic and dye sensitized solar cells, their mechanism and recent improvements.* Renewable And Sustainable Energy Reviews, **2017**,*78*, 1262-1287.

[3] Elumalai, N., & Uddin, A. *Open circuit voltage of organic solar cells: an in-depth review*. Energy & Environmental Science, **2016**, 9(2), 391-410.

[4] Snaith, H. J. (**2012**). *The perils of solar cell efficiency measurements. Nature Photonics, 6(6), 337 340.*

[5] Liu, C., Jiang, F., Huang, M., Yue, R., Lu, B., Xu, J., & Liu, G. *Thermoelectric Performance of Poly(3,4-Ethylenedioxy-thiophene)/Poly(Styrenesulfonate) Pellets and Films*. Journal Of Electronic Materials, **2011**, *40*(5), 648-651.

[6] Pasha, A., Khasim, S., Al-Hartomy, O., Lakshmi, M., & Manjunatha, K. *Highly sensitive ethylene glycol-doped PEDOT–PSS organic thin films for LPG sensing*. RSC Advances,**2018**, *8*(32), 18074-18083.

[7] Sarker, S., Ahammad, A., Seo, H., & Kim, D. *Electrochemical Impedance Spectra of Dye-Sensitized Solar Cells: Fundamentals and Spreadsheet Calculation*. (**2019**).

[8] Bard, A., & Faulkner, L. (**2000**). *Electrochemical methods and applications*. New York: Wiley-Interscience.

[9] J. R. Macdonald and W. B. Johnson, Impedance Spectroscopy, John Wiley & Sons, New York, NY, USA, **2005**

[10] Mali, S., Betty, C., Bhosale, P., & Patil, P. *Eosin-Y and N3-Dye sensitized solar cells (DSSCs) based on novel nanocoral TiO2: A comparative study.* Electrochimica Acta, **2012**, *59*, 113-120.

Conclusions - Outlook

The work presented in this thesis provided a contribution to the understanding of the ionic-electronic properties of the poly(3,4-ethylenedioxythiophene) (PEDOT) as a substitute material for the expensive platinum in the engineering of novel dye-sensitized solar cells (DSSCs). The main objective of the study was to demonstrate that the hybrid ionic and electronic conductivity of PEDOT endows this material with high affinity to collect electrons from the external load of the DSSCs and to catalyze the redox mediator used in the cells.

Both experimental and computational methods were used to investigate the mechanisms of the ionic-electronic conductivity of PEDOT and the output results of the simulation agreed to a certain extent with the experiments.
Nevertheless, there are some hindrances encountered during the modelling of the ionic-electronic transport of PEDOT. The first obstacle was the numerical approach used in the *MATLAB* codes, since defining boundary conditions of a real system is not very intuitive to perform and can cause many dissimilarities with the reality. The second hindrance is related the phenomenological equations used to describe the simulated system. To solve the numerical handling of the equations, it is possible to use a more developed simulation software like *COMSOL* that has predisposed models. However, this feature of ready-made models is a double-edged sword because unlike *MATLAB*, *COMSOL* is a "black box" where it is not possible to manipulate and "touch" the equations. Also, among the solutions that can alleviate the modelling processes is the use of proper theories that can describe the observed phenomena in a more accurate way. In fact, PEDOT response under electrochemical analyses, combines both faradaic and non-faradaic currents which impose the necessity for a more developed theories that can account for both currents.

Another point that was highlighted in this work, is the capacitive behavior of the PEDOT material. Through simple, yet effective experiments, it was possible to relate the capacitive behavior of PEDOT to the intercalation/de-intercalation of cations. Clearly, more developed experiments can be conducted with more time and tools. The capacitance of PEDOT polymers can be harnessed to manufacture supercapacitors that can be integrated in various electronic devices with a low-cost price. It can substitute the

lithium ion batteries with novel batteries based on solid-state electrolytes that have better cycling life and with zero risks.

Alongside the capacitive feature, the conductivity of PEDOT can be exploited to detect different molecules. It can be used as a biosensor for medical use, or even a sensor for gases (e.g. CO_2).

In addition, the electrochromic aspect of PEDOT (switching colors from dark blue to light blue) can be utilized as a material in electronic devices' screens or even in windows to render them switchable between dark and light depending on the furnished current.

Furthermore, PEDOT is a tailorable polymer, there are many methods to enhance its ionic-electric conductivity. Principally the tailoring is divided into two categories: Pre-treatment and post-treatment of the product. The former includes the quantities used of reagents like the monomer to dopant ratio or the oxidant quantity. The latter includes the processes employed to modify the characteristic of PEDOT after its synthesis and consists of the second doping (adding a molecule that improves conductivity like the DMSO), annealing of the product and its purification. Thus, through these methods, the possibilities to modify the PEDOT are endless.

Appendix

A. Voltammograms of the PEDOT/graphite electrodes at different scan rates

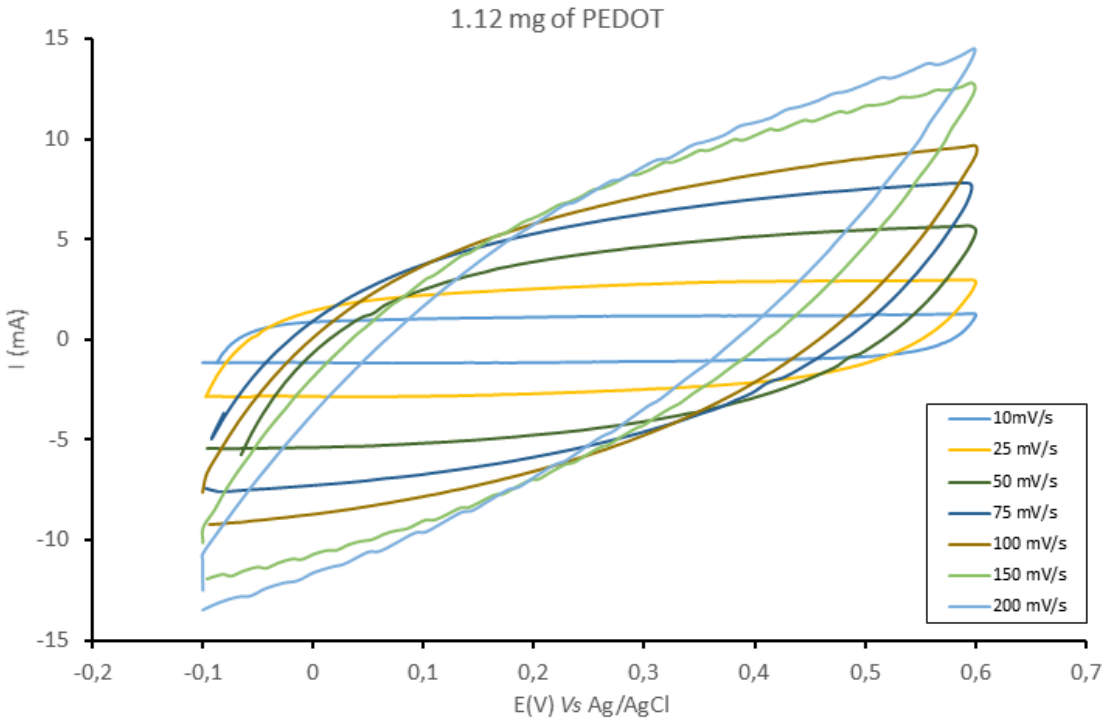

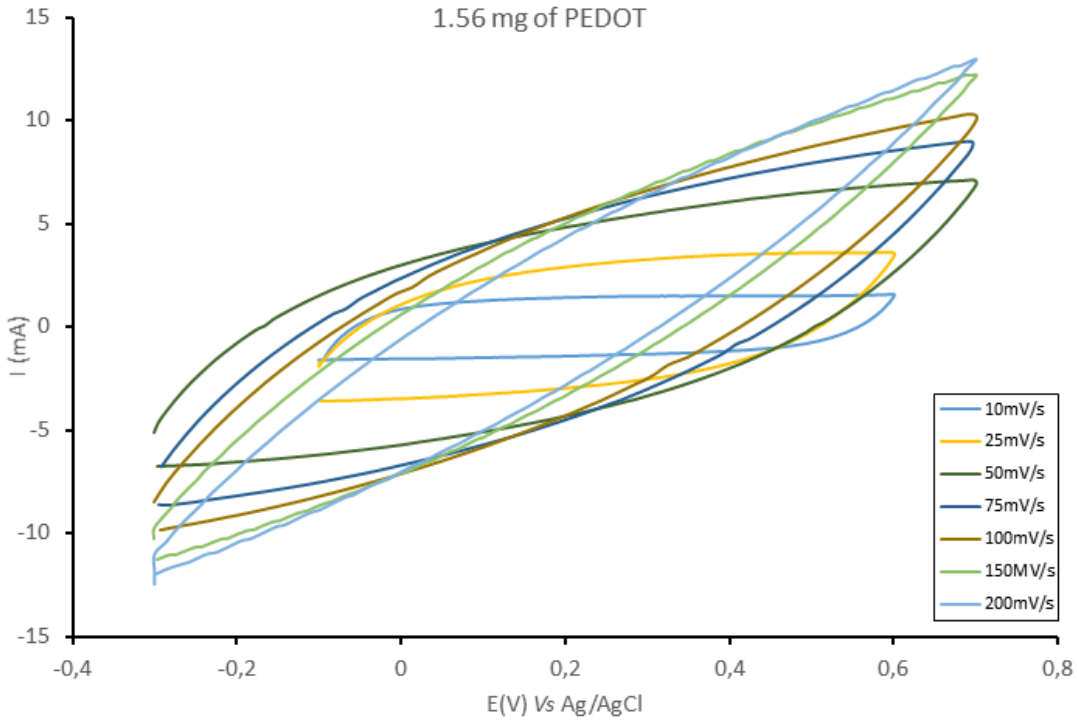

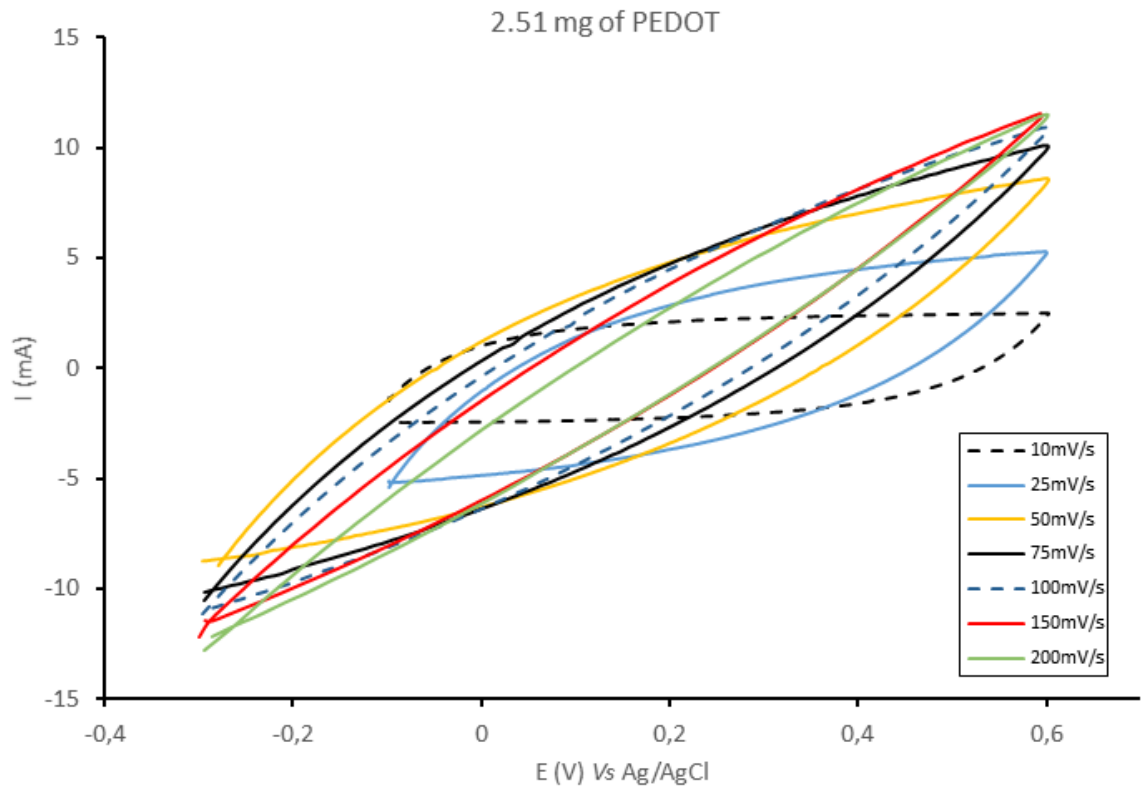
2.51 mg of PEDOT
15
10
5
0
-5
-10
-15
I (mA)
-0,4
-0,2
0
0,2
0,4
0,6
E (V) Vs Ag/AgCl
10mV/s
25mV/s
50mV/s
75mV/s
100mV/s
150mV/s
200mV/s

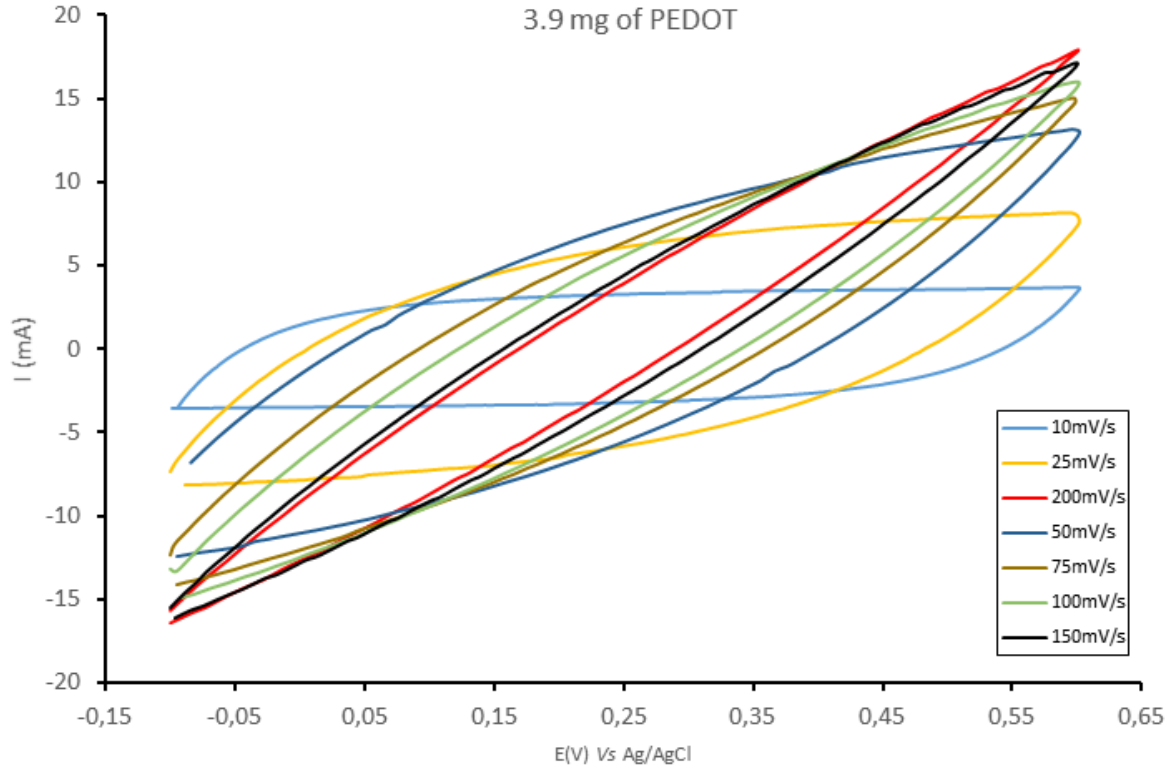
3.9 mg of PEDOT
20
15
10
5
0
-5
-10
-15
-20
I (mA)
-0,15
-0,05
0,05
0,15
0,25
0,35
0,45
0,55
0,65
E(V) Vs Ag/AgCl
10mV/s
25mV/s
200mV/s
50mV/s
75mV/s
100mV/s
150mV/s

Appendix B. Determination of the oxidation peaks of EDOT in different salts

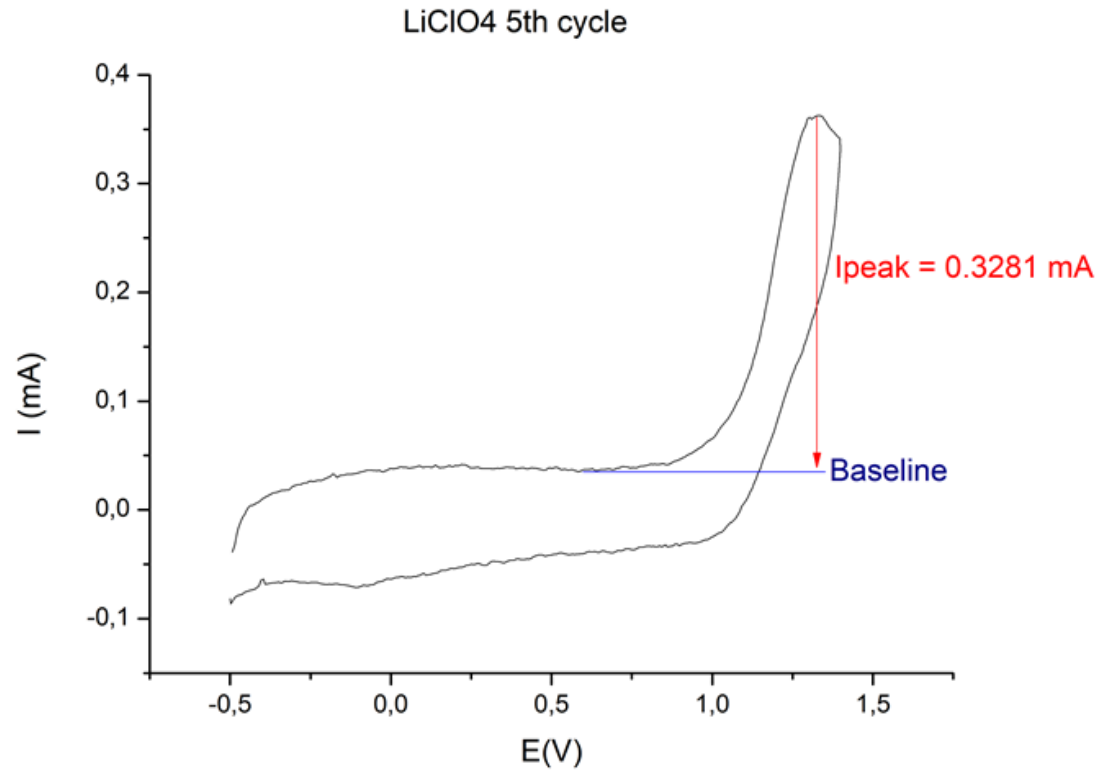

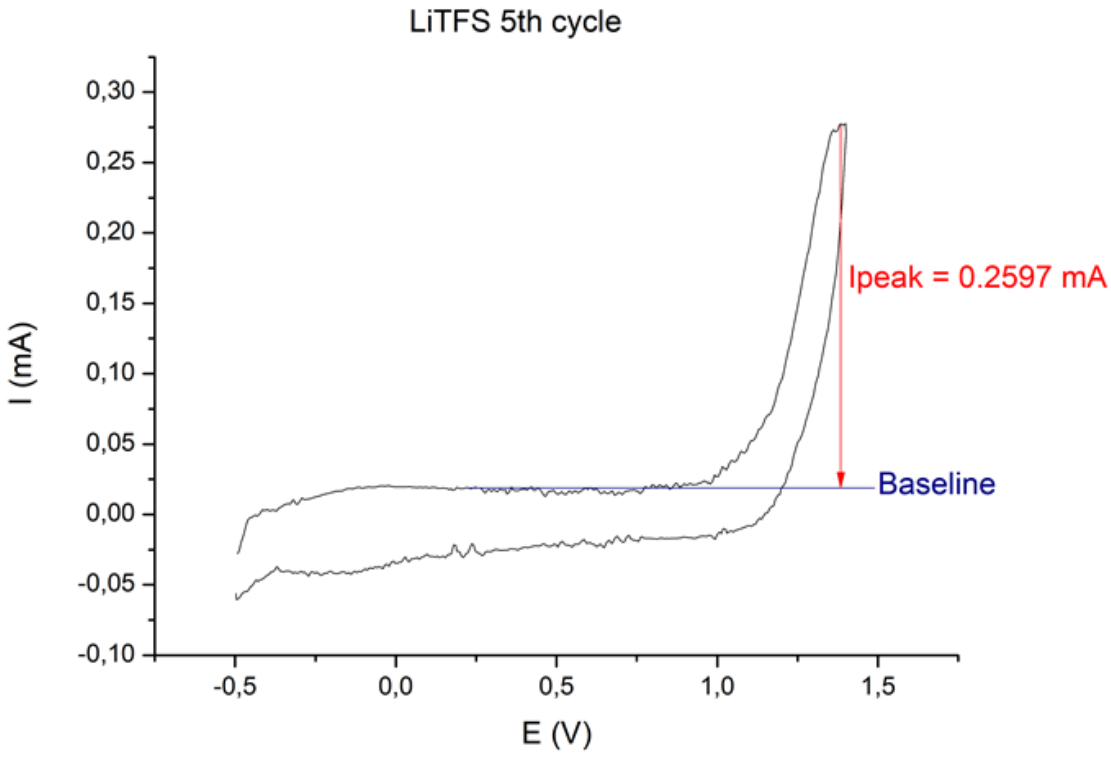

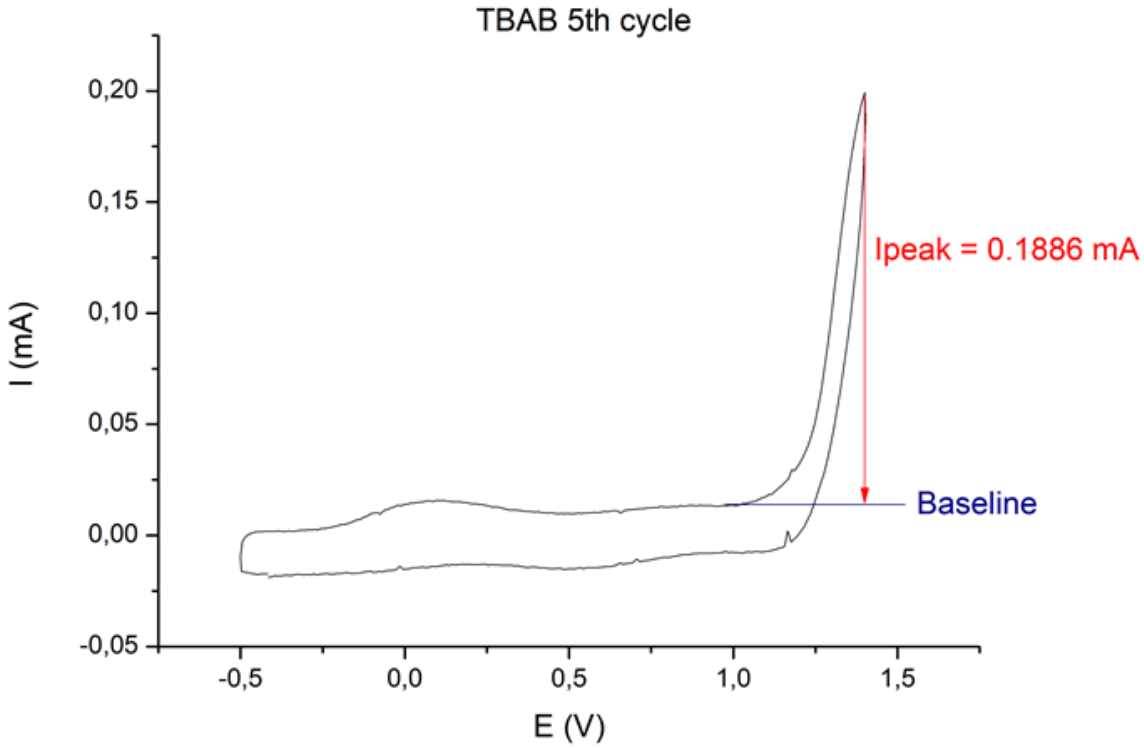
TBAB 5th cycle
I (mA)
E (V)
Ipeak = 0.1886 mA
Baseline
0,20
0,15
0,10
0,05
0,00
-0,05
-0,5
0,0
0,5
1,0
1,5

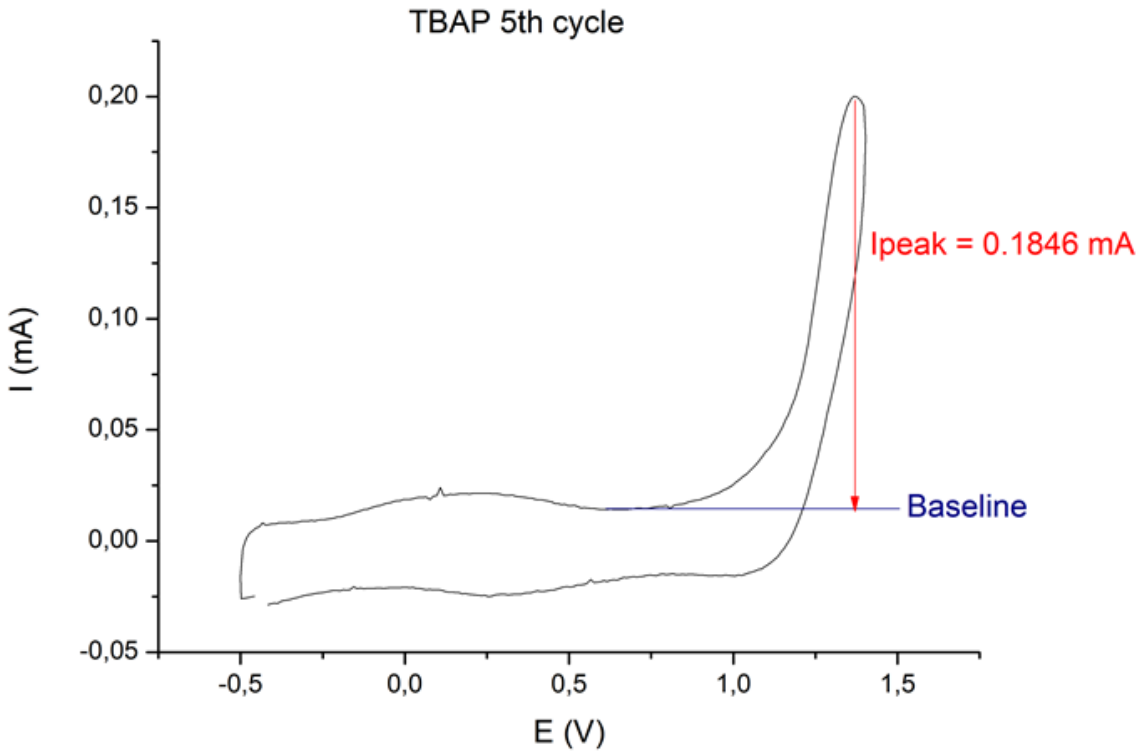
TBAP 5th cycle
I (mA)
E (V)
Ipeak = 0.1846 mA
Baseline
0,20
0,15
0,10
0,05
0,00
-0,05
-0,5
0,0
0,5
1,0
1,5

Appendix C. Determination of the oxidation potentials of EDOT in different salts

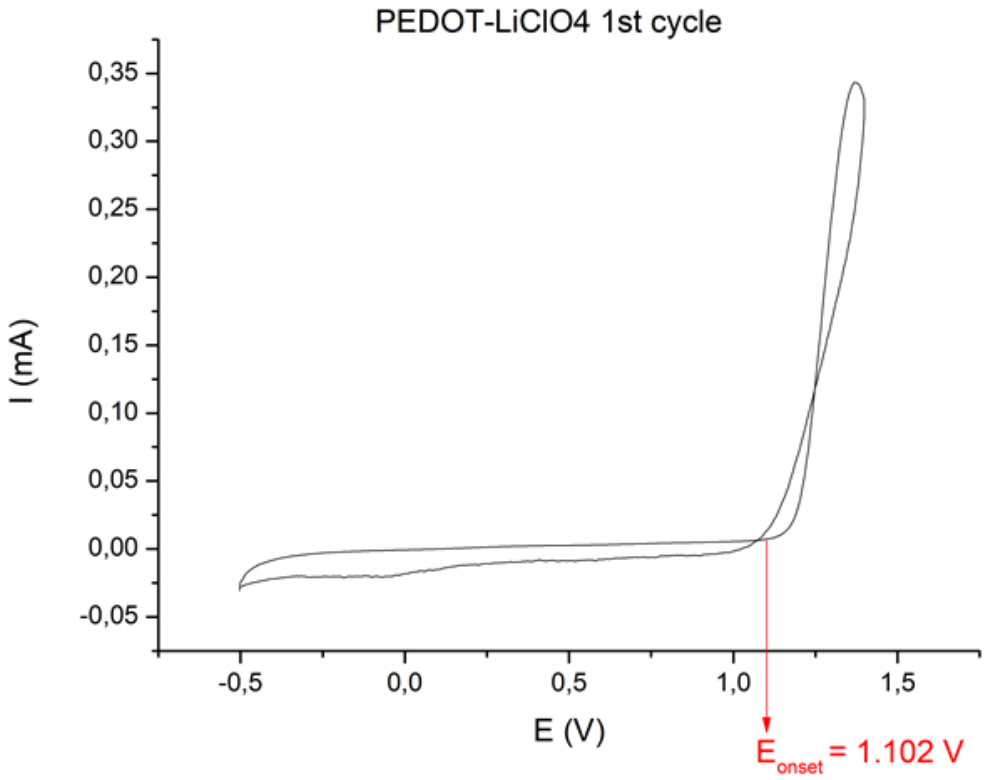

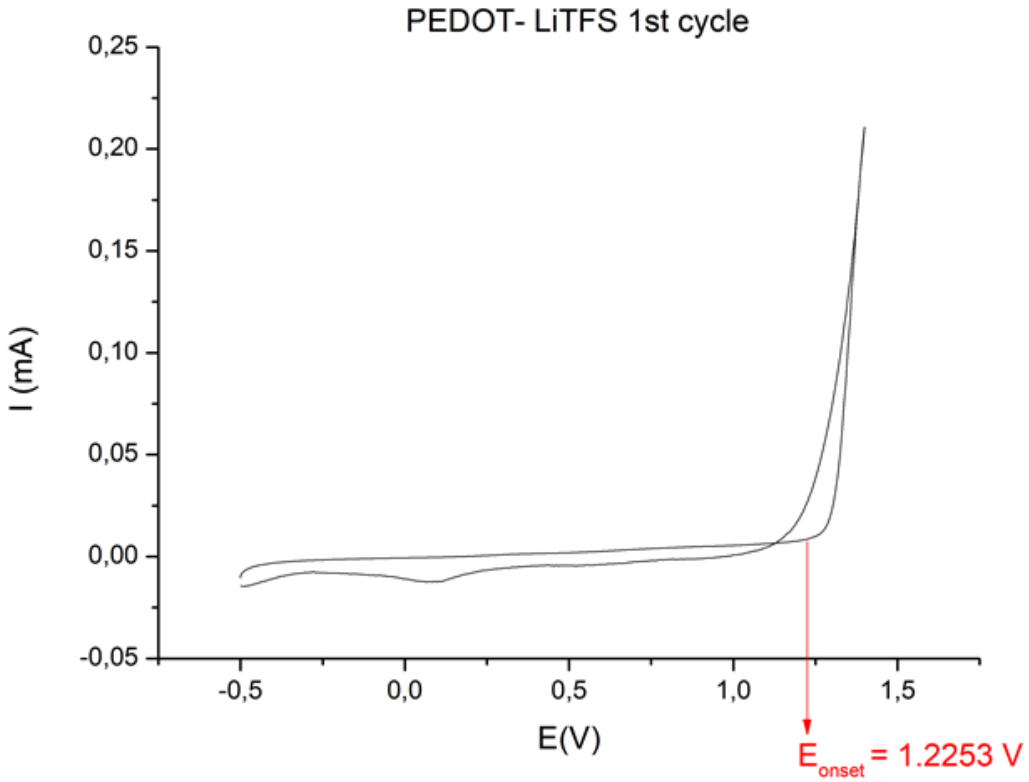

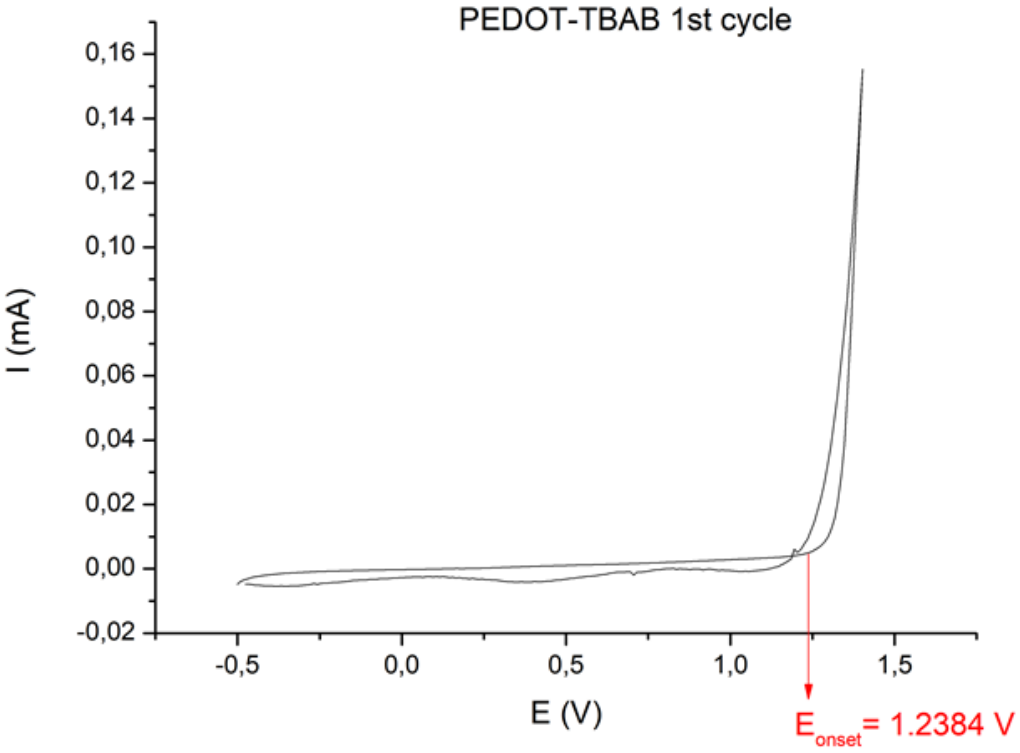
PEDOT-TBAB 1st cycle
I (mA)
0,16
0,14
0,12
0,10
0,08
0,06
0,04
0,02
0,00
-0,02
-0,5
0,0
0,5
1,0
1,5
E (V)
E onset = 1.2384 V

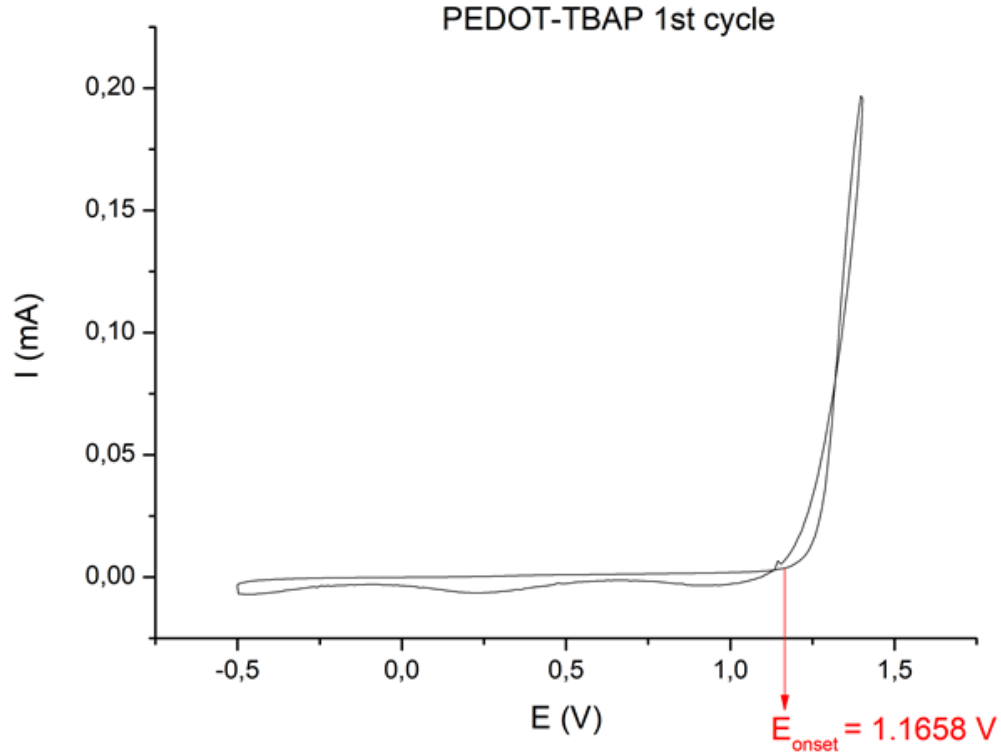
PEDOT-TBAP 1st cycle
I (mA)
0,20
0,15
0,10
0,05
0,00
-0,5
0,0
0,5
1,0
1,5
E (V)
E onset = 1.1658 V

Appendix D. Voltammograms of the different PEDOT films in the triiodide/iodide system at different scan rates

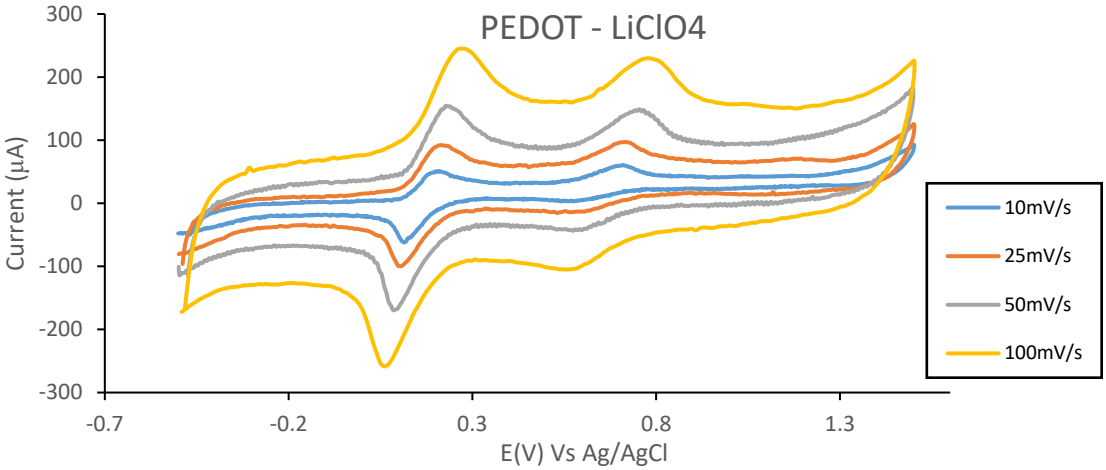

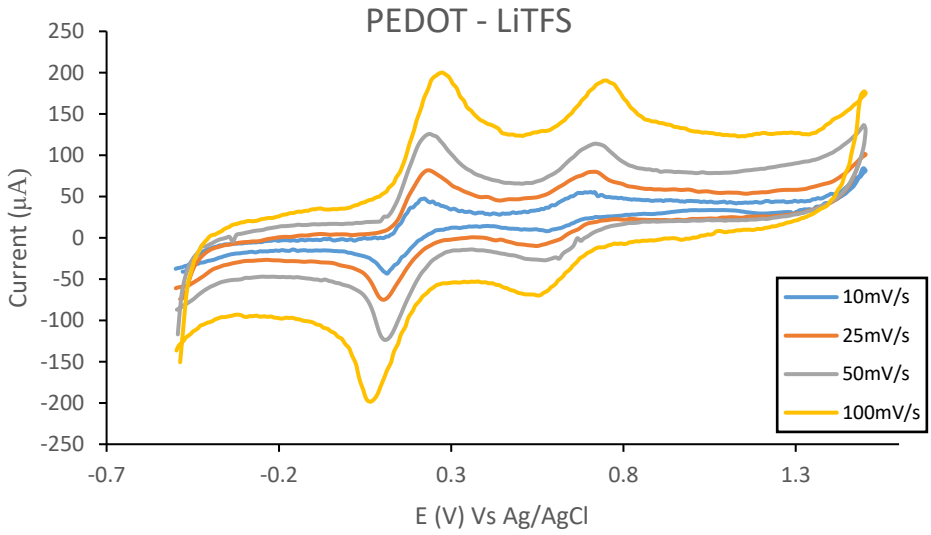

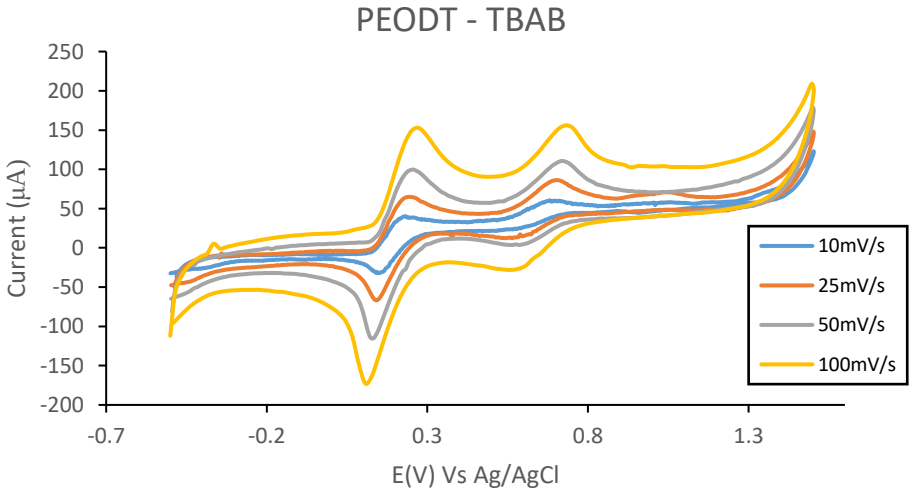

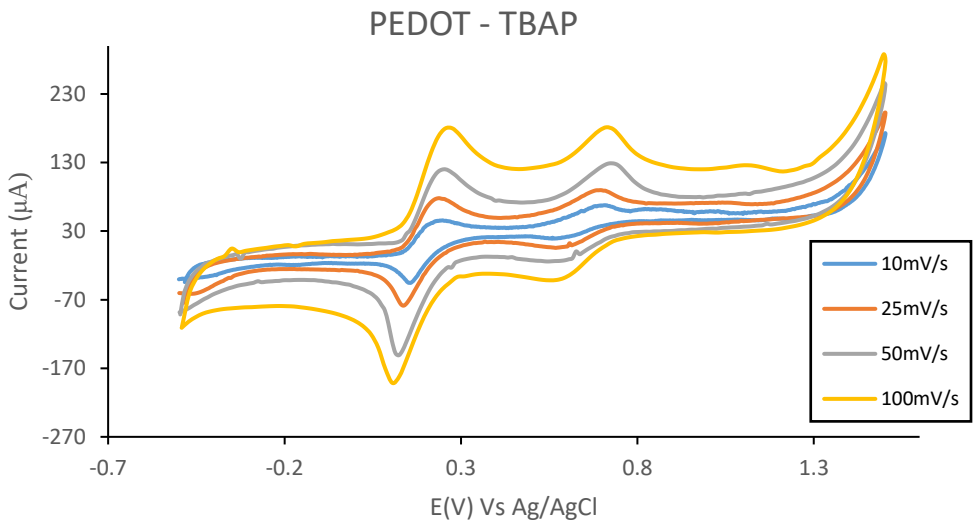

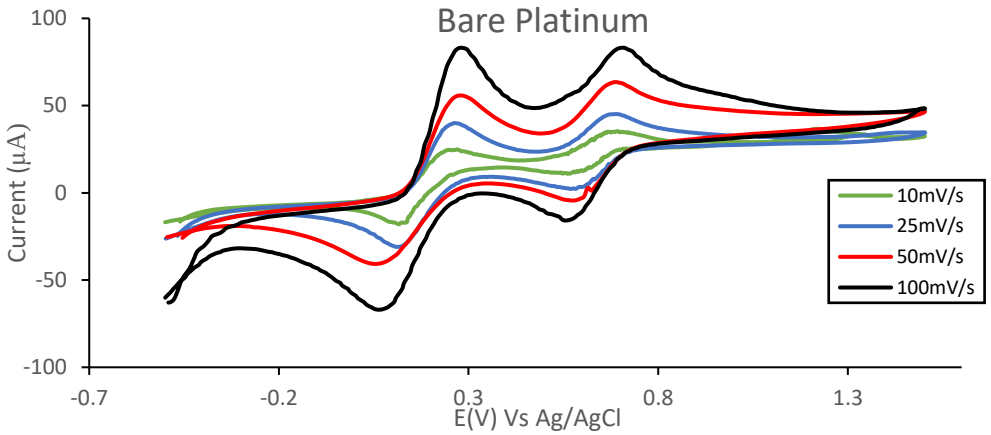

Appendix E. Data extraction from a cyclic voltammogram

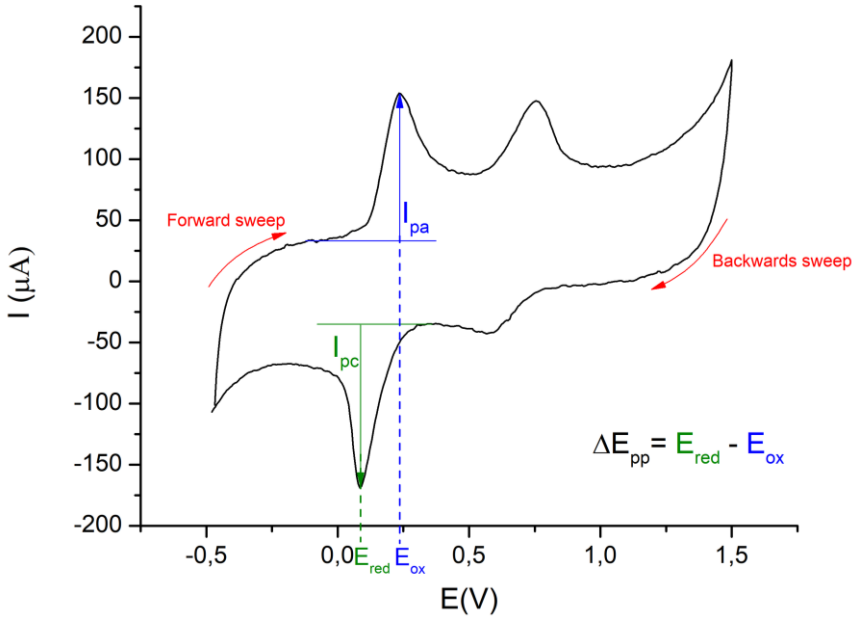

Appendix F. Transformation from dimensionless current to dimensional current

From the flux of holes, the current can be calculated by:

$$J_h(dimensional) = \frac{fV_a D_I C_{fixed}}{L} \times J_h(non\text{-}dimensional)$$

Current calculation using dimensional flux of Holes:

$$I = F \times J_h(x = L)$$

Note that the following expression should be equivalent:

$$I = F \times \int_0^L -\frac{\partial C_h}{\partial t} dx = F \times \int_0^L \frac{\partial J_h}{\partial x} dx \sim F \times \sum_{i=1}^{N} \Delta J_h$$

$$= F \times [J_h(2) - J_h(1) + J_h(3) - J_h(2) + \cdots + J_h(N-1) - J_h(N-2) + J_h(N) - J_h(N-1)]$$

$$= \quad F \times [J_h(N) - J_h(1)]$$

$$= F \times J_h(N)$$

$$= F \times J_h(x = L)$$